The Influence Of Soil Organic Matter (SOM) In Soils From Long-Term Experiments: Measurements Of Compression Properties, Water Release Curves, Thermogravimetry, Acoustical Impedance And Neutron Tomography

Thesis

The influence of soil organic matter (SOM) in soils from long-term experiments: measurements of compression properties, water release curves, thermogravimetry, acoustical impedance and neutron tomography

Thesis Submitted By

Kamrun Nahar Suravi

For the Degree of
Doctor of Philosophy

April 2022

School of Engineering & Innovation
Faculty of Science, Technology, Engineering and Mathematics
The Open University
Milton Keynes, United Kingdom

Certificate of Originality

Faculty of Science, Technology, Engineering & Mathematics

School of Engineering and Innovation

The Open University Walton Hall

Milton Keynes

MK7 6AA. United Kingdom.

Tel +44 (0) 1908 653686

This is to certify that this thesis paper is entirely my own investigation and I am responsible for the work submitted in this thesis, except as specified in acknowledgements, in text or in references, and that neither the thesis nor the original work contained therein has been submitted to this or any other university or institution for a degree.

The thesis has been submitted on May 2020 for examination and resubmitted on April 2022.

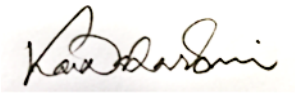

_____ (Signature)

_____11th April 2022 ____ (Date)

Supervisors

Professor Keith Attenborough
Emeritus Professor
School of Engineering & Innovation
The Open University
Milton Keynes, United Kingdom

Dr Shahram Taherzadeh
Associate Professor
School of Engineering & Innovation
The Open University
Milton Keynes, United Kingdom

Dr Richard Whalley
Soil Scientist
Soil Physics Group
Department of Sustainable Agriculture Sciences
Rothamsted Research
Harpenden, United Kingdom

Publications

K. N. Suravi, K. Attenborough, S. Taherzadeh, A. J. Macdonald, D. S. Powlson, R. W. Ashton, W. R. Whalley (2021), 'The effect of organic carbon content on soil compression characteristics', *Soil Till. Res*, *209*, 104975.

K. N. Suravi, H. C. Shin, K. Attenborough, S. Taherzadeh, W. R. Whalley (2019), 'The influence of organic matter on acoustical properties of soil', *Proceedings of the 23rd International Congress on Acoustic,* Aachen, Germany.

Awards

CSIA Travel Fellowship, 2017

Abstract

Soil Organic matter (SOM) is a very important factor in soil productivity and health. As SOM is the basis of nutrient cycling in soil, it has important consequences for both plant growth and the development of the root system. Also, organic matter influences the physical and mechanical properties of soils by improving soil structure and changing the soil pore system. Soil physical properties determine soil health and regulate plant growth by controlling root development and maintaining the availability of water and nutrients to plants. The effect of soil organic carbon (SOC) on the consolidation behaviour of soil from two long-term field experiments at Rothamsted (the Broadbalk winter wheat experiment and Hoosfield spring barley) has been investigated. These experiments are located on soil with similar particle size distributions, but with SOC contents ranging from approximately 1 to 3.5 g/100g. Soils taken from plots with contrasting SOC contents were compressed and deformed in a triaxial cell and the normal consolidation and critical state lines were determined. It has been found that the compression index was independent of SOC, but the void ratio at any given effective stress was highly correlated with organic carbon content. By comparison with uniaxial compression data, the apparent influence of SOC on the compression index is likely to be due to its effect on soil hydraulic properties rather than any intrinsic effects on strength. The plastic limit test appears to be a useful, simple and direct way of comparing soil physical behaviour and expected soil density. Thermogravimetric analysis (TG) has been used to deduce the organic matter content and its composition. Water release characteristics, and soil strength have been measured with the suction plate method and indirect tension method, respectively. As well the traditional measurements, the application of two relatively novel methods including neutron scattering by thin soil slices and non-invasive acoustical reflection from samples in an impedance tube is reported. The neutron scattering data has not proved useful as a result of the difficulties in obtaining and using soil samples in the required form. However, impedance tube measurements show that

(a) the sound absorption of the surfaces of sand and soil samples decreases with increasing water content and (b) changes in absorption coefficient spectra deduced from impedance tube measurements on soil samples extracted from the long-term agriculture experiments, involving different organic matter content but similar water content, are consistent with the predicted effects of changes in porosity and permeability in rigid-porous air-filled media. The increase in bulk porosity with organic matter increase suggested by the acoustic measurements agrees with the results of the water retention and compression tests.

Acknowledgements

I wish to express all my devotion and reverence to the most merciful beneficent creator, God Almighty. I would like to express my deepest gratitude and indebtedness to my supervisors, Professor Keith Attenborough, Dr Shahram Taherzadeh and Dr Richard Whalley for their support, guidance and patience throughout this PhD project. It has been an honor to work alongside such esteemed and knowledgeable supervisors. I especially appreciate the patience in times of personal difficulty.

I would like to extend thanks to Lawes Agricultural Trust (LAT) for their part-funding of this PhD project and the Centre for Sustainable intensification of Agriculture (CSIA) to fund my work in CAU, Beijing, China.

The assistance from the support staff at Rothamsted Research specially Rhys Ashton, Steve Freeman, Sally Murdoch and the academic staff at the Open University has been greatly appreciated. The supply of materials and organization of conferences and workshops has provided invaluable knowledge and experience.

I would like to express my sincere appreciation and profound regards to my mentor Dr Alice Milne from Rothamsted Research, Professor Tusheng Ren and his team at CAU and David Powlson, Andy Macdonald, Andy Gregory, Ho-Chul Shin from Rothamsted Research for their cordial co-operation at different stages for accomplishing this project. I also wish to express my gratitude to Dr Winfried Kockelmann from ISIS facility, STFC, Rutherford Appleton Laboratory, UK for his kind support and co-operation in Neutron Imaging work in IMAT.

I would like to further extend my appreciation to my husband and my family without whom I would never have finished the thesis. The unwavering support has kept me going and thus I dedicate this thesis to them.

Table of Contents

List of Figures

List of Tables

Chapter 1. Introduction

Increasing global food demand and the need for global food security poses huge challenges for the sustainability of agriculture and the environment [1]. Intensive agriculture for maximum food production may threaten the sustainability of the soil ecosystem. As soil is a limited resource, agricultural production depends on improving soil quality. But intensive use of soil throughout history has led to depletion in soil quality, leading in turn to reduced yields because of the consequent reduced organic matter [2]. For high crop production and sustainable soil ecosystem, soil structural stability is a very important issue. Though root penetration, plant support, drainage, aeration, retention of moisture, and plant nutrients are linked with the physical condition of the soil [3]. Present management practices to improve soil physical conditions and to make farming more sustainable include the application of organic manure (organic farming) and the lowering of tillage intensity [4]. Soil properties as well as soil quality are highly influenced by agricultural practices. Cultivation and fertilisation (manure and inorganic fertiliser application) have great impact on soil physical and mechanical stability [5, 6, 7].

For instance, compaction of an agricultural soil reduces its permeability, modifies biological activity in it and can restrict root growth [8]. Furthermore, bulk density increases, reducing the volume of soil macro pores which in turn affects soil physical properties: air permeability, porosity (void ratio), pore size distribution, hydraulic conductivity, and penetration resistance [9, 10, 11]. According to Zhang *et al.* [12], SOM forms a complex structure with soil particles and acts as a spring against compression and mechanical deformation of soil. Increased SOM content also increases physical stability and mechanical resilience [13], thus inhibiting destruction of pore structures, and making the soil less susceptible to compaction, by providing mechanical resistance to consolidation and shear deformation [12, 14, 15, 16]. Poor structural condition of soil (compaction, degradation) can

restrict plant growth and affect crop yield. While it is very important in agricultural research to have reliable information and knowledge regarding physical properties and structural stability of soil [17], there are too few data that allow an understanding of how the management of soil organic matter can affect the physical conditions of soil including the critical state parameters and hydraulic properties. More studies regarding the influence of SOM are essential and this thesis offers such a study.

The long-term experiments at Rothamsted *i.e.*, Broadbalk wheat experiment and Hoosfield spring barley experiment, provide a source of soils with very different soil organic matter contents, but with a similar soil texture. These long-term experiments provide the best opportunity to investigate the changes in soil properties and processes over time and thereby, investigate the long-term sustainability of agricultural systems. This should help to formulate future strategies for maintaining soil health [18,19].

The objectives of this study were to observe the changing pattern of soil physical properties including pore-related properties, water retention and mechanical properties of long-term agricultural soils and therefore identify the impact of organic matter (*i.e.*, soil organic carbon) and nitrogen applications on soil structure-related properties. To achieve these objectives, along with measurements involving compression and water release, relatively novel methods including thermogravimetry (TG), neutron imaging and acoustic reflection are used to determine soil properties.

The research presented in this thesis seeks to answer three questions.

1. How do long-term management practices i.e., fertilisation with farmyard manure and nitrogen, alter organic matter content, and thereby, affect soil physical properties?
2. To what extent do data from triaxial cell testing, thermogravimetric analysis, neutron tomography and impedance tube (acoustic analysis) tests give information about the influence of organic matter on soil properties?

3. What additional information about soil physical behaviour to that obtained from traditional methods is yielded by the relatively novel methods mentioned above?

A series of classical tests including water release characteristics, compression tests (both uniaxial and triaxial), indirect tensile test, thermogravimetric analysis, neutron tomography and impedance tube measurements were carried out on arable soil samples from long-term agricultural experiments in connection with the following research questions 1 and 2. But further work will be needed to address research question 3 to a better extent.

Chapter two of this thesis is a review of soil physical properties and their relationship to soil organic matter. Also, it describes the extent to which techniques such as physical and mechanical analysis of soils including compression test, measurement of soil strength and water retention along with relatively novel methods including neutron tomography, thermogravimetric analysis and acoustical absorption measurement can be used to give information about the influence of organic matter. Chapter three offers brief descriptions of the sampling sites and sampling methods. Chapters four to seven describe the different measurements and their results in turn. Chapter four details the measurements of soil particle density, consistency limits (plastic and liquid limits), soil carbon content and soil organic matter composition. Measurements of soil water release properties are described in chapter five. Chapter six is about measurements of soil mechanical properties. Chapter seven describes measurements of acoustical absorption by soil surfaces. A discussion of the overall results obtained from this study together with conclusions and recommendations for further work are in chapter eight.

Chapter 2. Literature review

2.1 Soil organic matter (SOM)

Soil is an essential medium for plant growth, composed of a complex combination of solid particles, liquid and gas with a diverse community of living organisms. The solid phase of soil can be described as mineral material and organic matter which bind together to make the soil productive [20]. Soil organic matter (SOM) is one of the most complex and heterogeneous components of soils which is a mixture of particulate organics, humus, fine plant roots and living microbial biomass [21]. Conceptually, SOM can be divided into different components based on their rate of decomposition. Active, labile, or microbial components decompose rapidly. Intermediate and unprotected components decompose slowly and passive, recalcitrant, and protected components do not decompose [3].

Soil organic matter (SOM) content influences the amount of plant residues returned to the soil, and the rate of residues and SOM decomposition, can be measured by the balance between inputs (*i.e.*, plant residues, organic amendments, manure) and outputs (*i.e.*, harvesting of above-ground biomass, oxidation following cultivation) from an arable soil [22]. Application of manure such as farmyard manure (FYM), increases SOM quantity, nutrient availability, soil aggregation and other soil functions [23, 24]. Soil carbon to nitrogen ratio (C: N) which is an influencing factor for SOM decomposition can be affected by management practices such as fertilisation and crop rotation. [25, 26].

2.1.1 Importance of SOM

SOM is very important for controlling soil and ecosystem functions by improving biological, chemical and physical soil properties. It enhances nutrient supply to plants, improves water retention and infiltration, provides buffering of pollutants and contaminants, and improves soil structure, thus, providing stability against erosion [27]. Many studies have recognized SOM as a main indicator of soil quality and health [27, 28, 29]. Soil organic matter (SOM) and derivatives from organic matter decomposition have a great impact on

soil aggregation [30]. Organic matter can increase microbial activity in soil as microorganism breakdown organic materials and increase the uptake of carbon. Increased microbial activity stimulates microbial secretion in soil which enhances aggregate stability [31].

SOM has a positive impact on soil water characteristics by improving the hydraulic conductivity. Also, it increases the equilibrium water retention of soil at any water potential [32]. Blair *et al.* [10] and Watts *et al.* [33] state that a small increment of soil organic carbon (SOC) can have great influence on aggregate stability, water infiltration and the energy required for tillage. Soil organic carbon (SOC) content along with its composition are the key soil factors that affect soil physical stability which is strongly influenced by management practices [34]. Moreover, increasing the SOC content minimises the proportion of mechanically dispersed clay thus promotes the stability of soil macro-structure improving soil friability [33, 35] and having a significant influence on the relationship between soil strength and water status [36]. SOM in cultivated arable systems is nevertheless important to fulfil the primary function of sustaining better crop yields [37, 38]. Storage of organic matter in soil has an important role in the global carbon (C) cycle and in combating climate change [3]. Thus, information about the proportion of the different components of SOM is very crucial not only for C storage in soil but also to explain the effects of SOM on soil and its properties.

2.1.2 Composition of SOM

Soil organic matter consists of a continuum of components ranging from labile compounds that mineralize rapidly during the first stage of decomposition to more recalcitrant residues (difficult to degrade) that accumulate as they are deposited during advanced stages of decomposition as microbial by-products [39]. SOM includes a complex mixture of living organisms, dead organic debris, and anthropogenic inputs [40]. During the decay of plants, a major part of plant carbon (~99%) is biodegraded and recycled to the atmosphere as CO_2. The organic matter remaining in soils is thus a C pool exhibiting high resistance

to biodegradation. Also, some SOM may be in the minor classes, such as carbohydrates, amino acids, lipids and phenols [41].

The different proportions of SOM *i.e.*, labile (less stable) and recalcitrant (stable or fixed) organic matter can be strongly influenced by management practices in arable soil [42]. Lal [43] found a close relation between the stability of SOM and the quality of soil. Moreover, there are indications that the physical stability of soil is closely related to the young and active (labile) soil organic matter (SOM) fraction [44, 45, 229]. So, it is very important to quantify different fractions of SOM and to relate them to the changes in soil physical properties. To study stability and quantity of SOM, thermal analysis like thermogravimetric analysis (TG), can be a very useful technique [46].

Unlike compositions, distribution of SOM in soil is also very important to study the effect of soil C.

2.1.3 Distribution of SOM in soil

The supply of water, air and nutrients, and the ability for roots to penetrate soil are largely determined by soil structure – the spatial arrangement of soil particles in aggregated units and the surrounding pore network – which itself is determined by the spatial distribution of SOM. Simultaneously, soil structure affects the spatial distribution of SOM and controls its stability against microbial decomposition thus affecting C sequestration [21]. As soil management practices are known to affect the content of SOM, so it may also affect its spatial distribution in arable soil [22]. While it is a challenge to map the spatial distribution of SOM in soil, modern imaging technology, such as X-ray imaging and neutron imaging can be useful.

2.1.3.1 Neutron Tomography (NT)

Tomography and radiography, well known for their uses in medical sciences and material sciences [47] and have been applied to soil analysis. Neutron Tomography (NT) is a non-destructive technique that provides a three-dimensional map of the neutron attenuation

coefficient within an object [48]. In contrast to medical imaging, the samples are rotated instead of the beam line.

Computed tomography (CT) is a method to acquire three-dimensional information about the structure inside a sample. Recently, X-ray CT has also become quite a useful technique to study soil matrix, like soil-root interaction, root distributions and pore geometry. [49, 50].

2.1.3.2 Theory behind neutron imaging

The electrical neutrality of a neutron is a property that makes it useful in neutron imaging applications. Also, neutrons can respond to external magnetic fields and interact with the magnetic moments of unpaired electrons in matter. Neutron imaging is similar to X-ray imaging but in most cases the mechanisms of neutron interaction with matter provide an image contrast that is complementary to that of X-rays. For example, in comparison with 100 keV X-rays (a typical value for commercial X-ray scanners), neutrons have a much higher penetration depth in most metals due to their zero charge [51]. X-rays interact with the electrons via electromagnetic effects: the photoelectric effect, Compton scattering (corresponding roughly to absorption and scattering with neutrons, respectively), and electron positron pair production. These interactions correlate strongly with the atomic number of the atoms present [52]. This means that X-rays are relatively insensitive to light elements such as hydrogen, while heavier elements such as lead prove difficult to penetrate (even high energy X-rays (100-300 keV) can only penetrate several millimetres of lead) [53]. Conversely, since it is electrically neutral, a neutron can interact strongly with nuclei, can be highly penetrating and therefore is well able to investigate the interior of large materials non-invasively [54]. Atomic nuclei are ~10^5 times smaller than outer electron orbits and, as a result, neutrons pass through matter much more easily than X-rays can [55]. Due to different interactions with matter, neutrons attenuation of light elements such as hydrogen (and its compounds such as water and hydrocarbons) and lithium is several orders of magnitude higher than their X-ray attenuation. Furthermore, metals such as aluminium and titanium are far more transparent to neutrons than to X-rays [56].

Neutrons are produced either by fission in nuclear reactors or by spallation. In spallation a high-energy proton beam strikes a heavy metal target and neutrons are ejected from the resulting excited nuclei (Figure 2.1). In both phenomena, the neutrons have high energy spectrums that are too high to use for neutron scattering or imaging. Moderators are used to cool the neutron spectrum to lower energy levels which basically rely on the temperature of the moderating medium, often hydrogen or hydrogenous materials [54].

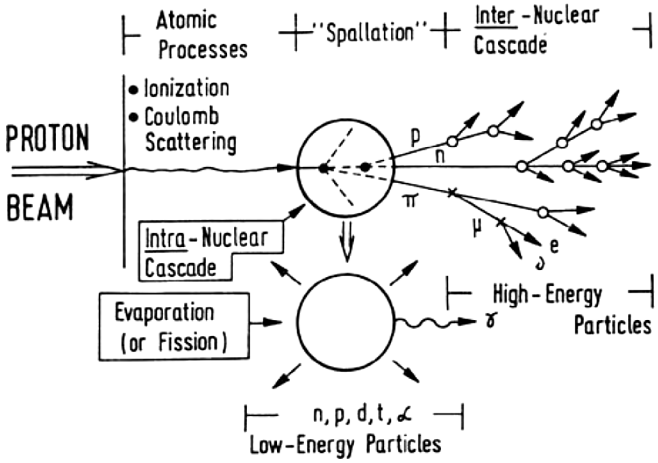

Figure 2.1 *Nuclear spallation by high-energy proton bombardment [57].*

Neutrons can be removed from the incident beam by absorption or by a change in direction (scattering) as they interact with material in the beam. So, a neutron may interact with a nucleus by either scattering or absorption (Figure 2.2). The scattering processes attenuate the incident neutron beam and give rise to contrast, which can be used for real-space imaging. On the other hand, in a neutron absorption process, a neutron is absorbed by a nucleus, often resulting in an unstable, radioactive nucleus that will decay with a half-life. The half-life is the time required for the radioactivity in radioactive matter to decay to half of its original value. As the radioactive nucleus decays it may emit a variety of secondary radiation, including an α particle, which is identical to a helium nucleus and carries two units of positive charge; a β particle, which is an energetic electron or positron; γ rays, which are high-energy photons originating in the nucleus. Normally the α particle interacts strongly with matter and can be attenuated rapidly, whereas the other two radiations can penetrate relatively deeply into matter [54].

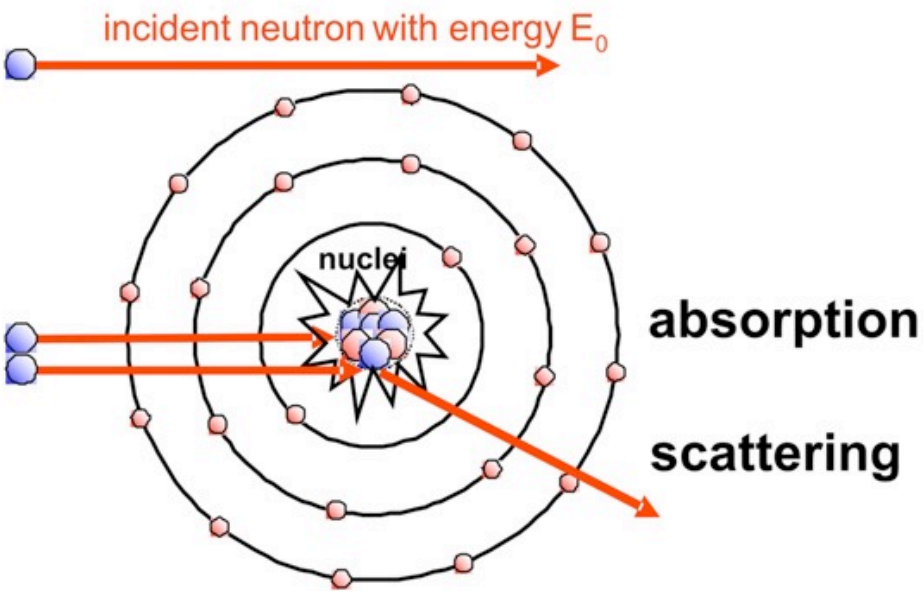

Figure 2.2 *Interaction of matter with neutrons [47].*

2.1.3.3 Fundamentals of neutron tomography (NT)

Typically, neutron tomography (NT) creates a large set of radiographs of an object at different orientations and which are used to construct virtual 3D images offline [54]. It uses radiographic projection images from many views to reconstruct the distribution of materials in the sample. Mostly, the projections are acquired with equiangular steps over either 180° or 360° to cover the whole sample. The projection images are acquired using a combination of a scintillator to convert the neutrons to visible light and a CCD camera. Transformation of the projection data into a three-dimensional image is a computationally intensive task handled by special reconstruction software [58]. The reconstruction of projection images can be done by applying Filtered Back-Projection (FBP) algorithm (the widely used analytical reconstruction method) [59, 47]. During the reconstruction process, slices perpendicular to the rotation axis are produced. When these slices are stacked in a sequence, they form a three-dimensional volume image of the sample. The reconstructed volume data can be visualised using three-dimensional rendering graphics software. Using such tools, regions can be segmented based on their attenuation coefficients and geometry. This can be used to reveal details inside the sample in three dimensions [58].

2.1.3.4 NT in soils

Neutrons form a highly penetrating radiation passing through matter without damaging or structurally modifying it, a property that makes them the ideal tool for many kinds of complementary material investigations. Moreover, the strong interaction of neutrons with hydrogen (H) and their ability to distinguish between hydrogen (H) and deuterium (^{2}H) with no radiation damage make neutrons a good probe for imaging in life sciences [60].

Soil is a heterogeneous system with biotic, abiotic and structural interactions [61]. There is a need to improve understanding of the interactive mechanisms involved in root growth and soil microstructural changes [62]. The spatial response of soil conditions in the rhizosphere (root zone) plays a critical role in understanding the dynamics of the whole soil systems. However, X-rays are not well-suited to characterisation of water distribution, since the contrast ratios between water, plant roots, and other soil constituents are poor [60]. Several studies reported that the high neutron attenuation coefficient of hydrogen (H) makes neutron radiography and tomography very attractive techniques for measuring water dynamics in plant-soil systems [63, 64, 65] and mapping the water content distribution in soils [66, 67]. Moreover, most of organic compounds in soil contain H, including carbohydrates, proteins and lignin. The use of neutron tomography offers a timely opportunity to 'map' the three-dimensional spatial distribution of H. In other words, the technique uses neutron transmission to map the fine-scale (30-60 μm) distribution of H^+ ions in a sample in three dimensions non-destructively. By using air-dried soil samples (*i.e.*, with virtually no water-based H), the H^+ ions should predominantly be contained in organic materials, and hence, NT can be expected to yield a spatial 'map' of SOM. NT measurements on long-term experiment soil samples are reported in Appendix 3.

The remainder of this chapter describes physical and mechanical analyses of soils including compression test, measurement of soil strength, soil density, consistency measurement and measurement of water retention characteristics.

2.2 Soil physical properties

Soil physical properties can be defined by its texture, structural characteristics, liquid and gaseous movement in soil, soil density, water holding capacity and mechanical characteristics. Previous studies showed that several soil physical properties including structural stability, porosity (void ratio), bulk density, water retention may serve as indicators of soil health [68, 69, 70, 71, 72]. As some properties such as soil texture and depth are inherent to a particular soil type, they are not affected by soil management. Others, however, can be reversed and improved through the adoption of proper soil management strategies [73].

Plant growth in soil can be greatly affected by soil physical properties [73]. For optimal plant growth, stabilisation of soil aggregate is a very important. Soil stabilisation can be described in terms of aggregate stability, moisture retention characterises, hydraulic conductivity and mechanical strength of the soil. Formation of soil structure and stabilisation of aggregated structure are very important and can be considered as the most desirable soil criterion for sustaining agricultural productivity and for preserving environmental quality [74]. The rhizosphere can be defined as the zone of high biological activity around the living roots [75]. Plant roots have a great impact on aggregate stability of soil along the zone of the rhizosphere. Plant roots can prohibit degradation of soil caused by different physical and mechanical forces and stabilize the soil [76]. Biological actions in rhizosphere soil include root exudation and other secretion by microbial activities, microbial colonization, and microbial decomposition [75]. Decomposition is a biological process that includes the physical breakdown and biochemical transformation (*i.e.*, mineralisation and humification) of complex organic molecules of dead material into simpler organic and inorganic molecules. In the decomposition process, different products are released including carbon dioxide (CO2), energy, water, plant nutrients and resynthesized organic carbon compounds found in rhizosphere soil [77]. Root exudation can accelerate the biological activity in the rhizosphere as different exudates increase the nutrient concentration for microbial growth

[78]. Root exudates along with the compounds released from microbial activities creates an adhesive environment that binds soil particles together to form micro and macro aggregates and stabilize the soil [79]. Biological exudations are mostly composed of different organic compounds which act as binding materials for soil particles to form a rhizosheath [80]. Czarnes *et al.* [79] state that binding mechanisms between soil particles in the rhizosphere enhance root-soil interactions and as a result increase soil stability. Organic exudates released from plant root and microbial degradation of organic matter such as mucilage possess high adhesive forces that increase the stability of soil in the rhizosphere. The chemical nature of root mucilage results in a higher cementing capacity of this compound [76]. Czarnes *et al.* [81] suggest that the addition of organic matter especially biological exudates increases the bond energy between the soil particles and aggregates. According to Oades [82], root or fungal hyphae are not persistent for stable aggregates whereas mucilage or other polysaccharides shows more stable binding properties within the macro aggregates. Soil structure can be defined in terms of stability [83]. Soil aggregate stability explains soil physical stability against slaking (the breakdown of soil aggregates due to the entrapped air compression during wetting) and mechanical stresses [84]. Primary soil particles are bound together into micro aggregate mostly by different organic binding materials (microbial derivatives, humified organic matter or organo-metal complexes) and these micro aggregates are bound together into macro aggregates by plant root or fungal hyphae or cementing agents (root or microbial exudates) [30, 85]. Micro-structural stabilization depends on texture and clay mineralogy, ionic forces, iron oxides and soil organic matter [86].

Plant growth and soil quality are very much dependent on soil physical properties which can be regulated by SOM content, so, it is very important to investigate the influence of SOM on physical and mechanical characteristics of agricultural soils and the relationship between them in more detail.

2.2.1 Water infiltration in soil

Sorptivity and repellency are important measures to predict soil water infiltration capacity. Sorptivity is mainly an indicator of the capacity of soil to absorb water or any liquid. It is the tendency of a soil to absorb and transmit water or any other liquid by capillary action of soil pores [87]. According to Philip [88], sorptivity can be determined from horizontal infiltration where water is transmitted by capillary action.

$$I = S\sqrt{t} \tag{2.1}$$

where I is cumulative infiltration at time, t and S is the sorptivity.

Both hydraulic conductivity and sorptivity are controlled by the shape, volume and tortuosity of pores. Generally, a soil with larger pores has a greater hydraulic conductivity but smaller sorptivity, while a soil with smaller pores exhibits higher sorptivity as it is controlled by capillarity [89, 90]. Sorptivity also depends on initial water content can regulate the preliminary stage of infiltration process [87]. For instance, a dry soil typically has a much greater sorptivity than a wet soil [89].

In agricultural soils, hydrophobic behaviour is generally associated with lower clay content where organic molecules are adsorbed to the charged clay surfaces or with biological waxes adsorbed to siliceous sands [91, 92]. Hallett [90] reported that the water repellency of soil is mainly regulated by the hydrophobic coating of organic compound in soil aggregates. Soil repels water when soil particles are bonded together with hydrophobic organic compounds or waxy compounds produced by plant root exudates, certain fungal species, surface waxes from plant leaves and decomposing soil organic matter [89]. According to the intrinsic sorptivity method developed by Tillman *et al*. [93], an index of water repellency can be measured by comparing the sorptivity of water (influenced by repellency) to the sorptivity of ethanol (not influenced by repellency). The water repellency parameter can be determined from sorptivity of soil as-

$$R = 1.95\left(\frac{S_e}{S_w}\right) \tag{2.2}$$

Where, R is water repellency index, S_w, sorptivity of pure water and S_e is sorptivity of ethanol (95%) [81].

If soil is highly water repellent the sorptivity and capillary rise of soil will be zero [89]. According to Tilman *et al*. [93], most soils are more or less water repellent, where water infiltration will be slower than expected. When a highly water repellent soil dries to less than a critical water content, it exhibits non-wettable behaviour [94]. Several studies reported that water repellent soils can regain its wettability after prolonged wetting [95]; by increasing populations of wax-degrading bacteria that consume hydrophobic compounds [96]; and by removing hydrophobic coatings from soil surfaces by tillage [97].

2.2.2 Soil water retention characteristics (SWRC)

Soil water retention characteristics (SWRC) can be considered as the most important indicator of soil structural stability [98]. Soil water retention characteristics indicate the relationship between volumetric water content of soil (θ) and matric head (h) in drying soil. In standard conditions, the water release characteristic of a soil can be divided into the three stages shown in Figure 2.3.

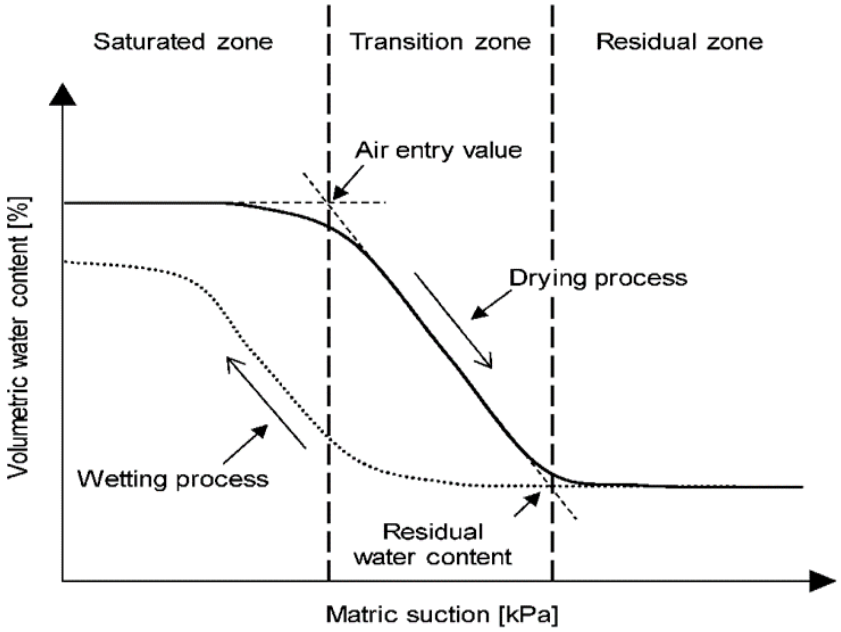

Figure 2.3 *Schematic diagram of water release curve describing different phases of water content in soil [99].*

As the matric potential (a negative hydrostatic pressure in equilibrium with the soil water) begins to decrease from zero, initially no water will drain, and the soil condition can be described as saturated. Eventually, as the matric potential becomes more negative, the water in the pores starts to drain and air invades the soil matrix at the air entry point and this stage is said to be the capillary fringe. At very low matric potentials, the water menisci made by London-van der Waals force become disconnected and the soil is said to be at the residual water content [100]. Figure 2.4 shows the angles involved in interfacial tensions between soil and water at the air–soil–water interface.

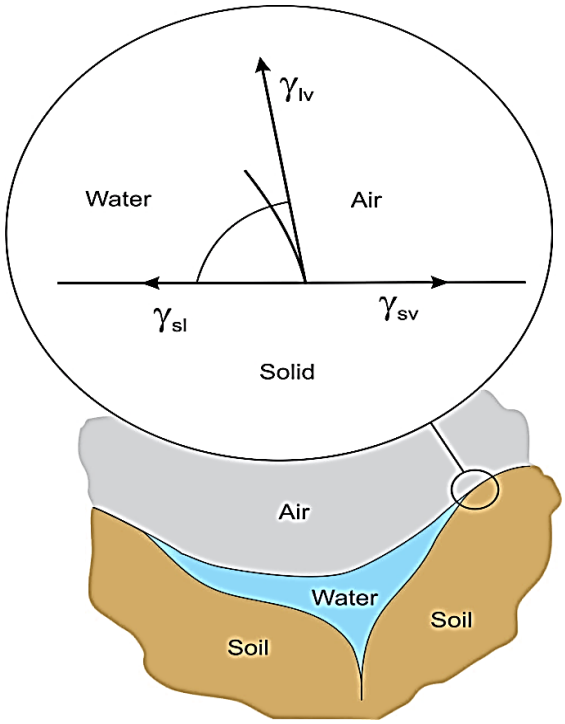

Figure 2.4 *Interfacial tensions of a partly saturated soil pore representing the angle of contact between the water and soil [101].*

2.2.2.1 Factors governing SWRC

The soil water release characteristic is an important soil physical property controlled by the soil pore geometry [102]. Pore size distribution can regulate macroscale behaviour of soils, including infiltration and conductivity [103]. Generally, soil with high organic carbon can possess a more stable structure, be less prone to runoff, erosion or surface capping and have a greater water infiltration rate and have a greater water retention as a result of greater

hydraulic conductivity and greater bulk porosity than soil with low organic carbon [104, 105, 106, 107]. Soil water release characteristics can be regulated by the soil type, particle size distribution, clay mineralogy, organic matter content, initial void ratio, bulk density, plasticity index [108]. Soil water retention at low suction (0-100 kPa) strongly depends on pore size distribution (capillary effect) and organic matter [99, 108]. Moreover, SOM increases the equilibrium water retention of soil at any water potential [19]. Deformation or alteration of the structure and distribution of soil pores caused by external perturbations, such as compaction or shear, will affect water retention [109, 110, 111, 112].

2.2.2.2 Van Genuchten model

Many models have been devised to demonstrate the relationship between water content and matric potentials of soil matrix. The most widely used model for SWRC was developed by van Genuchten [113]. The water release characteristic is often sigmoidal, highly non-linear, and generally fitted to the van Genuchten function' for most arable soils [101]. Fitted parameters can be used to estimate the relative conductivity of unsaturated soil in this particular function. Van Genuchten Model for water release can be expressed as

$$\theta = (\theta_s - \theta_r)[1 + (\alpha h)^n]^{-m} + \theta_r,\ m = 1 - \frac{1}{n} \qquad (2.3)$$

where θ is water content at water potential h; θ_s and θ_r are saturated and residual water contents respectively. α, n and m are empirical coefficients (α is inversely related to the air-entry pressure, n is dimensionless, related to the pore size distribution). According to van Genuchten [113], these four independent parameters (α, n, θ_s and θ_r) can be estimated from the soil water retention curve. Of these four, the saturated water content (θ_s) is probably always available as it is easily obtained experimentally. The residual water content (θ_r) may be measured experimentally, for example, by determining the water content on very dry soil. Unfortunately, θ_r measurements are not always made routinely, in which case they should be estimated by extrapolating available soil water retention data towards lower water contents. The contribution of agricultural management to soil water retention could also be

quantitatively characterized by the parameters derived from the van Genuchten model [113] (*i.e.*, α and n, the location of the inflection point and the steepness of its slope), because changes in α and n are considered to be closely related to pore size distribution and therefore to aggregate and particle size distribution [114, 115].

2.2.2.3 Methods used for SWRC

Different methods (both direct and indirect measurement) are used to measure the total suction and matric potentials of soils. The direct measurement techniques which are costly and time consuming, can be described as Tensiometers (water-filled tensiometer, osmotic tensiometer). The indirect measurement methods are Conductivity/ porous matrix Sensors, Pressure Plate Extractors, sand suction tables, suction plate method and Filter Paper Method [101].

2.2.2.4 Importance of SWRC

Soil water release curves are used to explore the modality of soil pore size distributions, water storage capacity, enable estimation of plant available water in soil, indicate the hydraulic conductivity and aeration status of soil, and can be used for the characterization and modelling of water flow and solute transport in soil [116, 117]. For instance, a minor change in water release curve may cause drastic change in hydraulic conductivity functions [108, 118, 119]. The differences of soil water retention and transmission characteristics can be considered as a fundamental property describing soil structure [117]. Mechanical characteristics of unsaturated soil including the shear strength and tensile strength can be interpreted from soil water release curves [99, 120]. Vanapalli *et al.* [121] have established an analytical model using the soil water retention curve and the effective shear strength parameters to predict mechanical behaviour of unsaturated soil.

2.2.3 Soil strength (Tensile strength)

The mechanical strength of soils is important for plant root growth and soil management, *i.e.*, tillage [122]. Tensile strength of soil can also be considered as an important factor for describing soil mechanical stability. For instance, tensile strength is remarkably sensitive to

the soil microstructure, and this makes it an important parameter to measure in research into the structure and behaviour of soil [123]. According to Dexter and Kroesbergen [124], tensile strength is the most useful measure of soil strength because it is a very sensitive indicator of the condition of a soil. Tensile failure is the desired mode of soil failure in tillage, as the soil breaks down into smaller fragments without disturbing soil microstructure [125]. The tensile strength of soil depends on its structure and how strongly the soil particles are bound together. The higher the bonding energy of soil particles the greater the tensile strength of soil [81]. Also, the tensile strength of soil is one of the governing factors which affect the cracking of soil. An applied stress is concentrated at crack tips and the crack propagates if the stress exceeds the strength in the crack tip, which may lead to catastrophic failure of the sample. The stress concentration increases with increased length and narrowness of the crack's tips. Therefore, stress concentration is expected to increase with increased pore continuity and to decrease with increased pore tortuosity [125].

Moreover, soil water content, clay content, organic matter content and aggregate size have an influence on the tensile strength of soil aggregates [120, 122]. Organic matter incorporation in soil including farmyard manure (FYM) can influence soil tensile strength. Czarnes *et al.* [81] report that addition of organic compounds increases soil stability by increasing bond energy between the soil particles and aggregates. Another study shows that aggregates in arable soil have greater tensile strengths than those in bulk soil [126].

Tensile strength can be measured by direct and indirect tension tests (Figure 2.8). The indirect test is also known as Brazilian (disc) test. Both methods are used to measure tensile strength in the lab. Indirect measure of tensile strength is more cost-effective and repeatable than the direct test [127]. In the direct tension test, the specimen can be pulled apart by a tensile force while in the indirect tension test, a compressive force is applied across the diameter of specimen until failure [123]. From the direct test, the peak tensile load applied to the sample is recorded as uniaxial tensile strength [127]. In the Brazilian method, a compressive load is applied to the soil sample and the tensile strength can be described as

stress applied per unit area at the failure of a soil disc under tension. The stress (σ) on the soil disc can be determined as

$$\sigma = 2F/\pi DL \quad (2.4)$$

here F is the applied load at failure, D is the diameter of soil disc and L is length of soil disc [81].

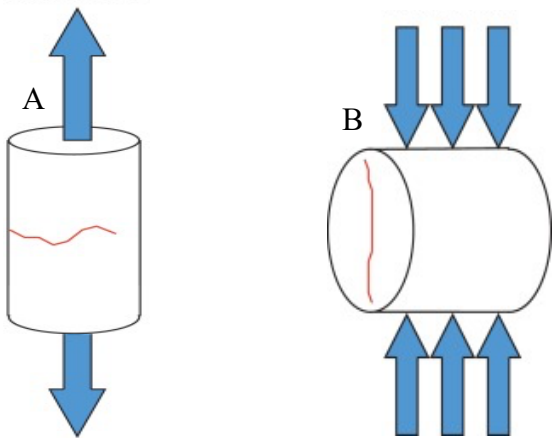

Figure 2.5 *Direct (A) and indirect (B) methods for the measurement of tensile strength.*

2.2.4 Mechanical stresses and soil compaction

Farming practices cause compaction and consolidation. Soil compaction increases bulk density, preferentially reducing the soil macro pores, thereby affecting air permeability, porosity, pore size distribution, hydraulic conductivity, and biological activities, but enhances mechanical strength which finally impacts on plant growth, especially root growth [128]. In an agronomic context, a soil is compacted when the air-filled porosity decreases to a point where it restricts aeration, and the soil is so dense that it inhibits root proliferation. According to Petersen [129], the changes in the soil stress-strain properties with moisture content can be a most important issue for agricultural soil mechanics.

2.1.4.1 Triaxial compression and shear stress

In triaxial compression, soil porosity (void ratio) decreases with increasing confining pressure. According to critical state theory, while a soil undergoes shear stresses, and finally it achieves a critical state, after that the void ratio, mean normal stress and deviatoric stress.

remain unchanged [129]. Whalley *et al.* [128] have demonstrated a linear relationship between the void ratio of soil and the logarithm of applied stress which can be described as the normal consolidation line (NCL). The NCL is obtained under isotropic stress which illustrates irreversible plastic deformation in the absence of shear. Sometimes this can also be designated as the isotropic consolidation line (ICL) or the virgin compression line (VCL). When the normally consolidated soil is sheared to reach a critical state condition (shear deformation) under constant radial stress, it possesses constant bulk density or void ratio. That unique behaviour of remoulded soil can be explained by means of the critical state line (CSL) [11, 128]. Figure 2.6 shows the schematic diagram representing consolidation and critical states of soil during shear deformation. According to O'Sullivan and Robertson [130], the critical state characteristics of soil (NCL and CSL) can be predicted from

$$e = N + \lambda \log(\sigma) \quad \text{in case of NCL} \tag{2.5}$$

$$e = N' + \lambda' \log(\sigma) \quad \text{in case of CSL} \tag{2.6}$$

here e is void ratio, σ is mean effective stress, N and N' are constants and λ and λ' are slopes of NCL and CSL respectively. λ is also described as compression index.

The triaxial compaction test is normally carried out on a cylindrical specimen in a triaxial cell (Figure 2.7) where (i) both the radial and axial stresses applied to the soil are controlled and (ii) the pore water pressure is usually either controlled or measured [11]. First, the specimen is subject to a confining pressure and after that an additional axial stress is applied to the specimen [131]. The test is performed by considering the field moisture and drainage condition, this test can be done by three different ways:

1. consolidated- drained test (CD-test),
2. consolidated-undrained test (CU-test) and
3. unconsolidated-undrained test (UU-test).

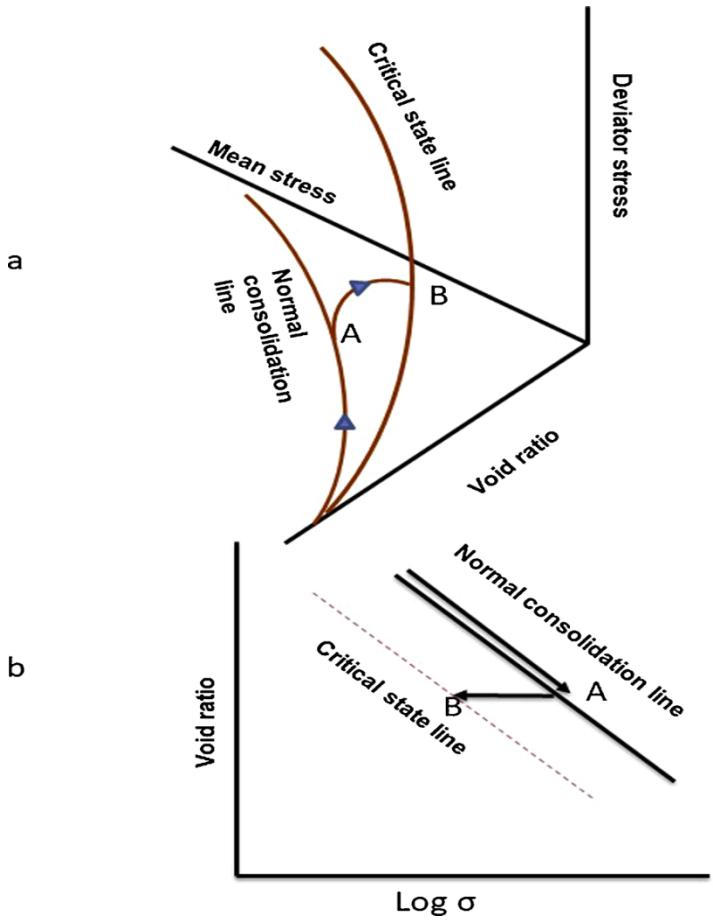

Figure 2.6 *The critical state model of soil deformation. (a) describes consolidation and shear deformation of soil and (b) illustrates the normal consolidation line (NCL) and the critical state line (CSL) on the void ratio vs log mean stress plane. In both cases, route A represents the normal consolidation when soil undergoes isotopic stress and route B represents the shear deformation of undrained soil during which the void ratio remains constant [132].*

The total measurement process can be divided in two major steps: i) consolidation of specimen and ii) shearing at a constant volume. The cylindrical soil specimen should be saturated prior to consolidation. Saturation of the soil specimen is required to make the measurement of pore water pressure and volume change more reliable. In an undrained test, the build-up of pore pressure depends on the saturation. But in a drained test, the volume change can be restricted because of saturation [131]. Soil compaction depends on the degree of saturation or the moisture content of soil [128]. After the specimen is fully saturated, isotropic pressures (σ_2, σ_3; $\sigma_2=\sigma_3$ in triaxial compression) are applied to consolidate the specimen (isotropic compression) for sufficient time to establish a base for evaluation of the

test. In the shearing stage of the test, an additional stress (σ_1) is applied in the axial direction to reach peak failure.

$$\sigma_1 = \sigma_d + \sigma_3 \tag{2.7}$$

here σ_d is the additional stress difference (deviator stress). Normally three principal stresses σ_1, σ_2 and σ_3 act on the soil in the field condition. In a triaxial apparatus, the cell pressure (hydrostatic) acts as the isotropic confining stress (minor principal stress, σ_3). The major principal stress (σ_1) is applied through a piston in the axial direction [131].

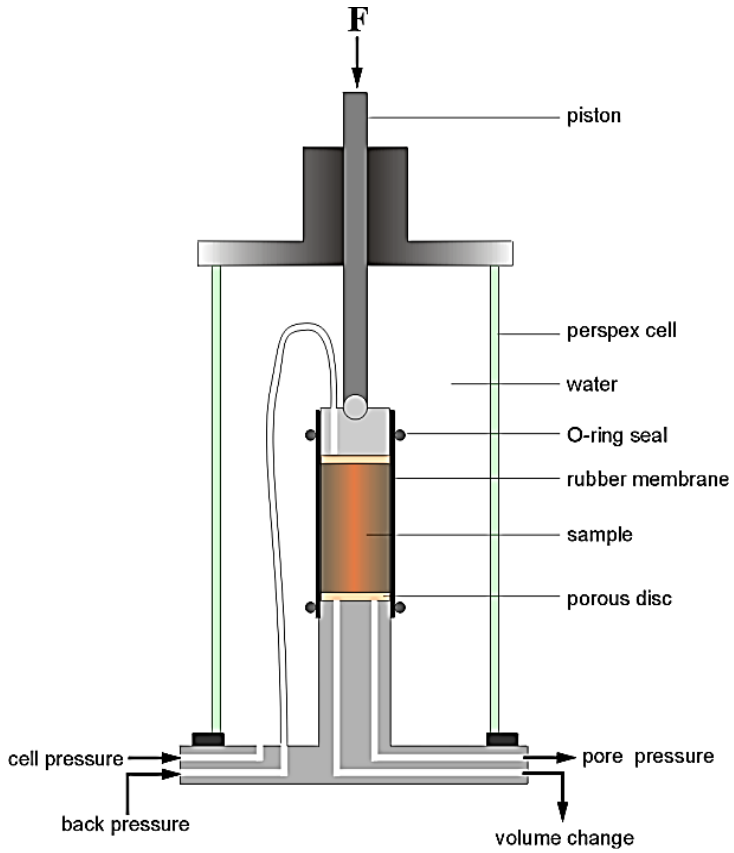

Figure 2.7 *Typical Triaxial cell arrangement [133].*

The soil physical properties can be measured by different traditional methods as described earlier sections. This study also focused on a novel technique which can be used for studying soil physical characteristics i.e., acoustical impedance measurements.

2.3 Acoustical probing of soils

Soil is a complex porous elastic medium. Acoustic wave propagation measurements provide an alternative to the classical methods used in soil physics and can be utilized to describe properties of porous materials including soils [17, 134, 135, 136, 137]. Sound propagation in any porous medium is influenced by its texture, structure, roughness, degree of compaction and the moisture content [134, 136, 138, 141, 142]. A suspended loudspeaker propagating acoustic energy onto soil, the response of which is quantified by measure the total pressure above the soil surface been used to study the formation of surface crusts [143]. Sound wave propagation through a soil is a mechanical phenomenon causing relatively small perturbations without altering its fabric [138]. Sound can penetrate through the pores in soils filled with air or partially filled with water. Attenborough *et al*. [139] found that sound can penetrate through soil due to surface porosity and associated air permeability and thus be absorbed and undergo phase change through friction and thermal exchanges between the pore fluid and the surrounding solid.

The pore structure and tortuosity around soil particle aggregates have an influence on sound penetration [140]. Connelly and Hodgson [144] investigated the variation of the diffuse field absorption with organic content and plant species in substrate materials used for green roofs. They found that the diffuse field absorption coefficient of compacted substrate at wilting capacity increased with the percentage of organic matter.

While acoustical methods can be used to study soils *in situ* [134, 136 - 139], in keeping with the laboratory-based activities in the rest of the thesis, results of using a laboratory method i.e., an impedance tube are reported here. This method has been used previously to study effects of moisture content [140].

The impedance tube study reported here, differs from the work by Connelly and Hodgson [144] in the use of normal incidence on repacked soils in the laboratory rather than diffuse

or free field absorption coefficient *in situ* and measurements on long-term cultivated soils rather than on the substrates used for green roofs.

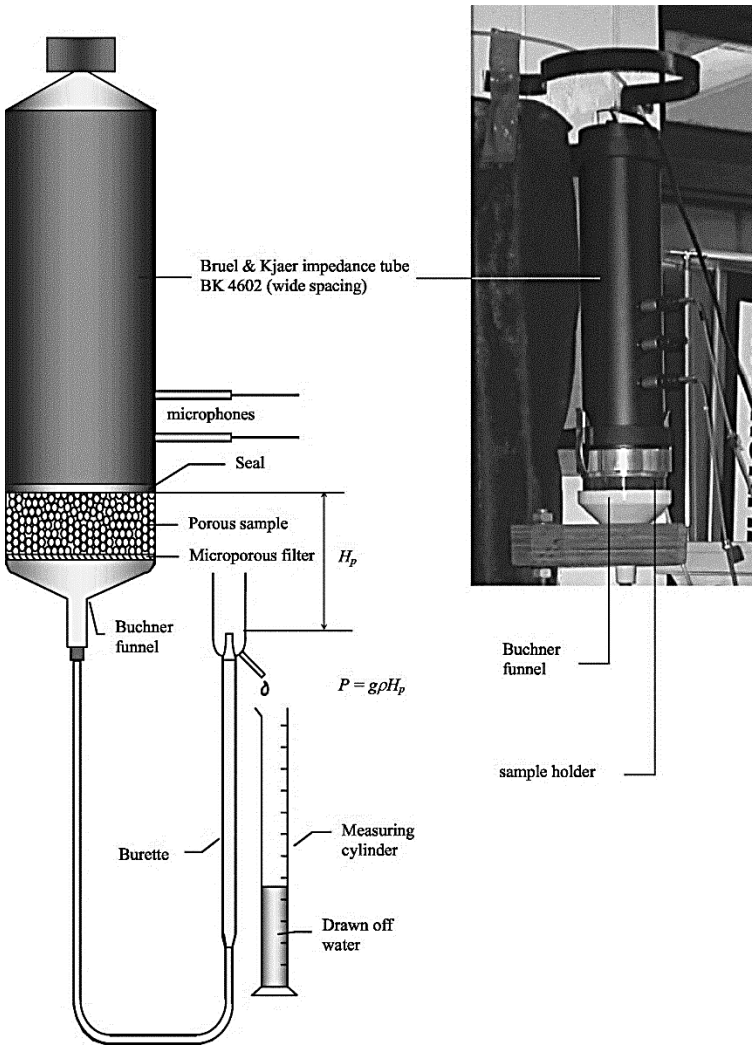

Figure 2.8 *The assembly of impedance tube for simultaneous measurement of the pore size distribution and acoustic surface impedance of water saturated porous samples [140].*

2.3.1 Sound propagation in porous and elastic materials

Classical Biot theory for a porous and elastic medium [145, 146] predicts the existence of three wave types in the porous medium: two types of dilatational or compressional waves (1st and 2nd kind) and one rotational or shear wave. In a soil consisting of a dense solid frame with a low-density fluid, such as air saturating the pores, the first kind of dilatational wave, often called the 'fast' wave which is characterized by particle motion in phase with fluid motion, has a velocity very similar to the "P" wave in geophysics travelling in the drained frame. However, the attenuation of the first dilatational wave

type is higher than that of the P wave in the drained frame. The extra attenuation comes from the viscous forces in the pore fluid acting on the pore walls. This first dilatational wave has negligible dispersion and its attenuation is proportional to the square of the frequency, as is the case also for the rotational wave. If the fast waves are excited predominantly, viscous coupling at pore walls means that some of their energy is carried in the pore fluid as the second type of dilatational wave or 'slow' wave. In air-saturated soils, the second dilatational wave, often called the 'slow' wave, has a much lower velocity than the first. The attenuation of the 'slow' wave stems not only from viscous forces at the pore walls but from thermal exchange with the pore walls. In the rigid-frame limit, theory predicts a single wave which is the same as that predicted in simpler theories for the acoustical properties of rigid-framed porous solids. It is the wave type responsible for the acoustical properties of sound absorbing materials [147]. In his work in 1956, Biot [146] introduced the concepts of tortuosity (sinuosity factor ξ) and the structural factor δ (deviation from cylinders with constant circular cross section) characterizing the complexity of the pore geometry at high frequencies. Attenborough [148] has offered an alternative definition for the tortuosity (q) and proposed a description of acoustical properties in terms of static and dynamic shape factors.

2.3.2 Johnson-Champoux-Allard (JCA) model

In measurements made using the reflection of sound at a soil surface, an air-filled soil may be regarded as having a rigid frame. Allard and Champoux [149] have proposed a semi-phenomenological model for sound propagation in rigid-framed porous materials based on Biot's theory. According to their theory, the reflection of sound from soil surfaces may be considered to depend on five non acoustical parameters that describe the acoustical properties of porous materials with rigid frames. These parameters include porosity, Ω, (the ratio of the volume taken up by connected pores to the total volume of the material), tortuosity, T, (a measure of pore or streamline curvature), characteristic viscous length, Λ,

(a geometrical parameter determined by the viscous interactions between fluid and structure and indicative of the narrowest pore dimensions), characteristic thermal length, Λ', (a geometrical parameter similar to hydraulic radius that can be determined from the internal surface area per unit volume), and flow resistivity, R_s, (the ratio of the static pressure gradient across the sample to the resulting air flow velocity). The Johnson-Champoux-Allard (JCA) Model [149, 151] uses the following expressions for the complex density and compressibility in a rigid porous material:

$$\rho_b(\omega) = T\rho_0\left[1 + \frac{iR_S\Omega}{\omega\rho_0 T}G(\Lambda)\right], \tag{2.8}$$

where $G(\Lambda) = \sqrt{\left(1 - \frac{4iT\eta\rho_0\omega}{{R_S}^2\Lambda^2\Omega^2}\right)}$, $\Lambda = s_\rho\sqrt{\left(\frac{8T\eta}{\Omega R_S}\right)}$

and

$$C_b(\omega) = (\gamma P_0)^{-1}\left[\gamma - (\gamma - 1)\left[1 + \frac{iR_S\Omega}{\omega\rho_0 T N_{PR}}G'(\Lambda')\right]^{-1}\right] \tag{2.9},$$

where $G'(\Lambda') = \sqrt{\left(1 - \frac{4iT\eta\rho_0\omega N_{PR}}{{R_S}^2\Lambda'^2\Omega^2}\right)}$, $\Lambda' = s_C\sqrt{\left(\frac{8T\eta}{\Omega R_S}\right)}$.

g is the ratio of specific heats in air, ρ_0 is the density of air, ω is the angular frequency, $i = \sqrt{(-1)}$ and η is the dynamic viscosity coefficient in air.

The surface impedance of a hard-backed layer of material of thickness, d, is given by

$$Z(d) = Z_c\coth(-ikd) \tag{2.10}$$

where normalised characteristic impedance $Z_c(\omega) = [1/(\rho_0 c_0)]\sqrt{(T/\Omega^2)(\rho(\omega)/C(\omega))}$.

The (complex) normal incidence plane wave reflection coefficient, R_p, is

$$R_p = \frac{Z(d)-1}{Z(d)+1} \tag{2.11}$$

and the normal incidence absorption coefficient is given by

$$A = \left|1 - {R_p}^2\right| \tag{2.12}$$

Attenborough [150] has shown how tortuosity and the other parameters are related to the complexity of the pore geometry at high frequencies.

2.3.3 Impedance tube measurement

The sound absorption coefficient can be measured by using an acoustic impedance tube or standing wave tube [152]. In an impedance tube measurement, a loudspeaker at one end of the tube is used to excite the sample at the other end (which is closed by a rigid termination) with sound. The variation of sound pressure in the resulting standing wave is measured using one or more microphones. Horoshenkov and Mohamed [140] used the two-microphone Bruel & Kjaer impedance tube (Type BK 4206) shown in Figure 2.8, to measure the variation of normal incidence absorption coefficient spectra with varying moisture content in sands. Absorption coefficient is related to acoustic surface impedance.

Acoustic impedance is the response of a passive system to a harmonic excitation. The specific acoustic impedance, *Z*, is defined as the ratio of the acoustical pressure and the particle velocity at a given point in the frequency domain. It is a complex quantity. For plane waves in tubes, the acoustic impedance at any cross-section of the tube is the ratio of mean pressure *P* and volume velocity, *U*, over the cross section [152]:

$$Z = {}^{P}/_{U} \tag{2.13}$$

2.3.4 Different methods for impedance measurement

2.3.4.1 Two microphone method (TMM)

In the two-microphone method, the impedance of a sample material is determined from the measurement of the transfer function between two microphones located at different positions along a waveguide connected to that sample. A loudspeaker emits white noise, in the waveguide over a time duration adequate to reduce variance in the results, as computed with a modified average periodogram. This measurement method is based on the mathematical theory of one-dimensional wave propagation in a cylindrical duct which can be expressed by the following equation

$$P_{(x,y)} = P_{+(x,f)} + P_{-(x,f)} = Ae^{-\Gamma x} + Be^{\Gamma x} \tag{2.14}$$

where *A* and *B* are the complex frequency-dependent amplitudes of the progressive and

regressive traveling-wave components. The propagation parameter (Γ) can be defined as the given formula, $\Gamma = \alpha + i\omega/v_\varphi$, where α is the attenuation and v_φ the phase velocity [153]. According to Lefebvre [153], the impedance (Z) can be calculated from the above equation as

$$Z = \frac{Z}{Z_c} = \frac{H\sinh(\Gamma x_1) - \sinh(\Gamma x_2)}{H\cosh(\Gamma x_1) - \cosh(\Gamma x_2)} \qquad (2.15)$$

here H is the transfer function between the two microphones and Z_c is the characteristic impedance.

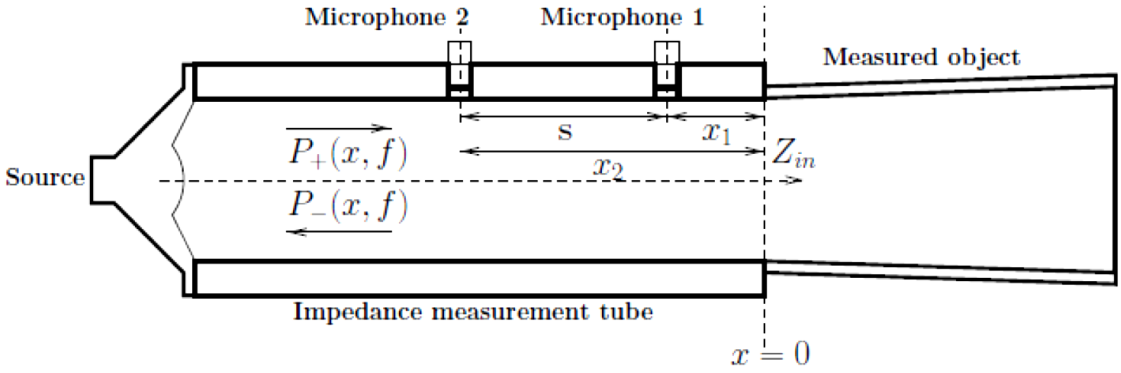

Figure 2.9 *Schematic diagram of the two-microphone measurement tube showing the positions of microphones, distance between two microphones (S) and position of sample measured (x=0) [153].*

Prior to the measurement, a relative calibration of microphones pairs is used to eliminate frequency and phase response differences between them. Ideally, this calibration is made in anechoic conditions and with microphones located at the same reference plane and exposed to a broadband noise signal [154, 155].

The two-microphone method does not give satisfactory values for surface impedance and therefore absorption coefficient if the distance between the two microphones is too small or close to a multiple of the half wavelength. According to Dalmont [152], this problem can be resolved by using more than two microphones.

2.3.4.2 Single microphone method (SMM)

Given the need for matched microphones in the two-microphone method, some studies have shown that use of only one microphone in two different positions or measurements can be

preferable to the use of two microphones since this although more laborious is equivalent to a two-microphone method [156].

The principle of the method is to measure the transfer function *H* of the acoustic pressure between two different positions in the measurement tube with the same microphone. Then the reflection coefficient *R* of the reference plane is estimated from the transfer function. Finally, the impedance *Z* is calculated from the reflection coefficient [157].

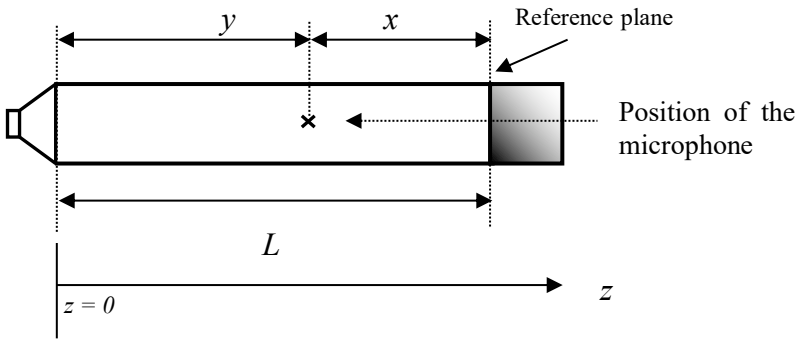

Figure 2.10 *Diagram of the standing wave tube for impedance measurement showing y is the distance between the position of the microphone and the loudspeaker; x is the distance between the position of the microphone and the reference plane; L is length of the tube; and z is the axis of propagation of the sound wave [157].*

In the case of plane wave propagation (below the cut-off frequency of the tube), the acoustic pressure can be calculated as [157]

$$p = Ae^{-jky} + RAe^{jk(y-2L)} \tag{2.16}$$

where the first term contains waves travelling in the direction *z* increasing, and the second term represents waves travelling in the direction *z* decreasing. *R* is the complex reflection coefficient of the sample in the plane $z = L$. *A* is a complex factor representing the amplitude of all the reflections in the tube.

This expression can be rewritten in terms of *x*, the distance of the microphone from the sample, as:

$$p = A\left(e^{-jk(L-x)} + R.e^{jk(L-x-2L)}\right) = Ae^{-jkL}(e^{-jkx} + R.e^{-jkx}) \tag{2.17}$$

If the pressure is measured at two different positions $x = x_1$ and $x = x_2$ $(x_1 < x_2)$ with the same microphone, the transfer function is given by:

$$H = \frac{p_1}{p_2} = \frac{A_2 e^{-jkL}(e^{-jkx_2} + R.e^{-jkx_2})}{A_1 e^{-jkL}(e^{-jkx_1} + R.e^{-jkx_1})} \tag{2.18}$$

But $A_1 = A_2$ (same source and same microphone in a standing wave tube in steady state), so:

$$H = \frac{(e^{-jkx_2} + R.e^{-jkx_2})}{(e^{-jkx_1} + R.e^{-jkx_1})} \tag{2.19}$$

It follows that: $$R = \frac{(e^{-jkx_2} + He^{-jkx_2})}{(e^{-jkx_1} + He^{-jkx_1})} \tag{2.20}$$

Normalised impedance in normal incidence is determined by:

$$\frac{Z}{\rho_0 c_0} = \frac{1+R}{1-R} \tag{2.21}$$

where the air density $\rho_0 = 1.293$ kg m^{-3} and c_0 in m s^{-1}, is the speed of sound in air-

$$c_0 = 331.6\sqrt{1 + (^T/_{273})} \tag{2.22}$$

where T is the temperature in degree Celsius. In normal conditions, $c_0 \approx 340 ms^{-1}$.

It follows that

$$\frac{Z}{\rho_0 c_0} = \frac{1 + \frac{e^{jkx_2} - He^{jkx_1}}{He^{-jkx_1} - e^{-jkx_2}}}{1 - \frac{e^{jkx_2} - He^{jkx_1}}{He^{-jkx_1} - e^{-jkx_2}}} = \frac{He^{-jkx_1} - e^{-jkx_2} + e^{jkx_2} - He^{jkx_1}}{He^{-jkx_1} - e^{-jkx_2} - e^{jkx_2} + He^{jkx_1}} \tag{2.23}$$

where $j = \sqrt{-1}$. If the transfer function is written: $H = H.e^{j\Phi}$ then the equation (2.23) can be rearranged as-

$$\frac{Z}{\rho_0 c_0} = \frac{\tilde{H} \sin kx_1 \sin \Phi + j\left[\sin kx_2 - \tilde{H} \sin kx_1 \cos \Phi\right]}{\tilde{H} \cos kx_1 \cos \Phi - \cos kx_2 + j\left[\tilde{H} \cos kx_1 \sin \Phi\right]} \tag{2.24}$$

If the source is far enough from the microphone the incoming and outcoming wave can be separated in the time domain giving two separate signals. After a Fourier transform the impedance is obtained [152].

2.3.5 Application of acoustics to soil strength measurement

The classical method to measure soil mechanical strength is invasive and laborious as it

requires manually pushing a penetrometer through the soil [158]. A previous study [137] has shown the feasibility of using a wave propagation model as a non-invasive alternative to the use of penetrometer. In another study, Shin *et al.* [158] reported that an acoustic-seismic (A–S) coupling technique can be effective in measuring the depth profile of the soil strength non-invasively with crops present.

2.3.6 Limitations of impedance tube investigations in a laboratory

The impedance tube technique has some limitations-

- Soil samples have to be repacked from extracted cores,
- The impedance tube needs to be aligned vertically to make measurements on soil samples.

2.4 Summary of the research contributions in this thesis

Food production along with soil health depend on soil physical properties which are regulated by SOM content, so, it is very important to investigate the influence of SOM on physical and mechanical characteristics of agricultural soils in more detail.

This chapter has reviewed the past research on SOM including its composition and distribution to identify their impact on soil physical properties i.e., soil water retention and soil strengths. As well as soil water holding capacity and soil mechanical strength, it is also important to explore consolidation behaviour of soil, especially for agricultural soil. This thesis presents some novel research on soil compaction due to long-term fertilisation management and the impacts of SOM on soil consolidation characteristics.

More techniques are now available to study soil mechanical and structural properties, for example pore size distribution, than have been used traditionally. So, in this thesis, two relatively novel methods of neutron diffraction and acoustic reflection are used. Although, acoustical methods can be used to study soil mechanical properties and pore size distribution simultaneously, this thesis only reports measurements on SOM effects that relate to pore structure. To an extent, the thesis explores what additional or corroborative information can be deduced from such relatively new methods.

Chapter 3. Methods: soils and sampling

3.1 Introduction

The aim of this study was to observe the impact of agricultural managements on soil physical behaviours. Long-term agricultural experiments provide a great opportunity to study long-term management effects on soil behaviour for arable soil. Thus, two long-term agricultural experiment sites in Rothamsted research were chosen to collect soil samples for pursuing the objectives of this study. The Broadbalk winter wheat experiment is the world's oldest continuous long-term agricultural experiment (in operation for more than 175 years), and the Hoosfield spring barley experiment represents more than 150 years of continuous arable use. As an important hypothesis of this study is that the SOM influences soil physical properties, plots with a significant variation of SOM content from long-term experiments are chosen to be studied and sampled.

For any kind of research in soil science, proper sampling of soils is very important factor. Soil sampling involves extraction of cores from a soil to give information on the soil properties, including its nutrient status, composition and other characteristics which are important to plant growth. An unrepresentative soil sample may be misleading and may result in over or under application of fertilizer [159]. So, the method of soil sample collection is extremely important in the accuracy and repeatability of a soil test. Moreover, collecting and handling soil samples properly is very important. This chapter gives a brief description of the soils collected for this study, a short review of the sites chosen for sampling and the methods of soil sampling.

3.2 Sampling sites

Continuous agriculture over many growing seasons can provide much useful information regarding its soils and environment. For this reason, soil samples were collected from two long-term arable field experiments at Rothamsted Research near Harpenden, Herts,

including the Broadbalk winter wheat experiment and the Hoosfield spring barley experiment.

3.2.1 Broadbalk winter wheat experiment

Broadbalk is the world's oldest continuous long-term agricultural experiment started by Sir John Bennet Lawes and Sir Joseph Henry Gilbert in 1843[160]. According to John Lawes [161], the Broadbalk soil is capable of giving high wheat yield if well manured. The Broadbalk soil is classified as Batcombe soil series according to the Soil Survey of England & Wales (SSWE) [162] with Clay loam to silty clay loam soil texture over clay-with flints. Every year wheat has been sown and harvested throughout the field. The strips along the length of the experiment are the different treatment plots (see Figures 3.1 and 3.2). The aim of establishing this experiment was to test the effects of different combinations of inorganic inputs including N, P, K, Mg containing fertilisers applied in different plots and organic manure applications such as farmyard manure (FYM), on the yield of winter wheat. There is a control treatment plot which has not received any organic or inorganic inputs since 1843. Broadbalk is tilled by a tractor-mounted five furrow reversible plough nowadays, but in early years the field was ploughed by a cattle-drawn plough. Herbicides have been introduced in the experiment to control weeds since 1964, except on section 8 (occasionally left fallow). Chalk has been applied sporadically since 1950s to buffer the soil and maintain the pH at a suitable range for optimal crop growth.

The quadrilateral experimental field is further divided into 10 (0-9) different sections along its width (see Figures 3.1 and 3.2). Sections labelled 0,1, 8 and 9 have only been growing wheat except that, since herbicides have not been applied, in section 8 has been left occasional fallow to control weeds. Initially the remaining 6 sections went into 3 course rotations but in 1978 section 6 reverted to continuous wheat and other 5 sections went into a 5-course rotation viz.: fallow, potatoes, wheat, wheat, wheat until 1997 and oats, forage maize, wheat, wheat, wheat from 1997 to 2017. In 2018, the rotation on these 5 sections changed to wheat, wheat, oats, wheat, beans [163].

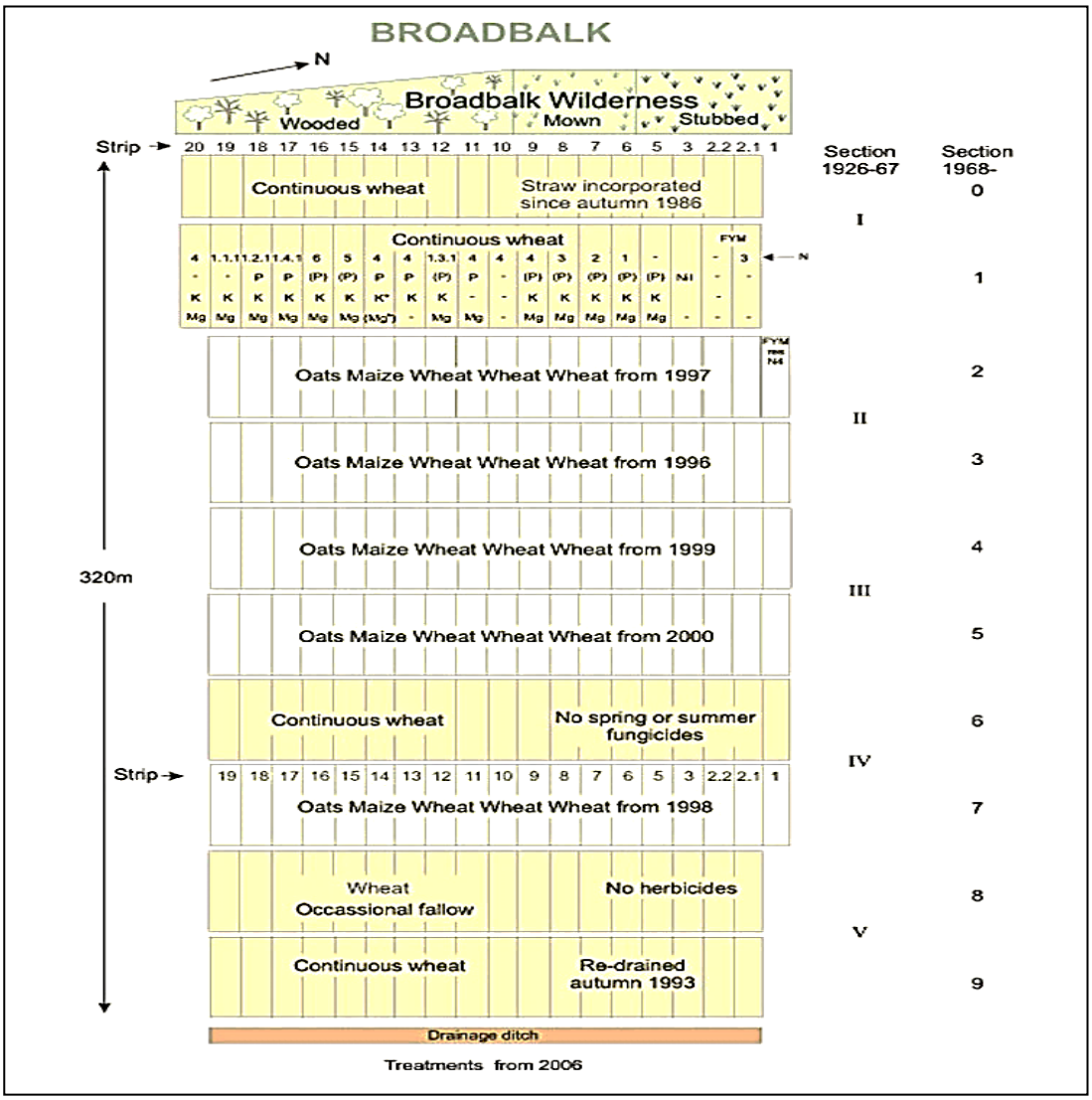

Figure 3.1 *Layout of Broadbalk wheat experiment showing that the strips along the length of the field are different treatments plots and the sections along its width are cropping patterns [164].*

Figure 3.2 *Aerial view of Broadbalk wheat experiment in present days. The plots used for sampling are highlighted with the red rectangle.*

3.2.2 Hoosfield spring barley experiment

The Hoosfield barley experiment was started by Lawes and Gilbert in 1852. Since then, spring barley has been grown continuously in this experimental field. Soil is clay loam to silty clay loam textured topsoil over clay-with flints and classified as Batcombe soil series according to Soil survey of England and Wales [162]. This experiment was established to observe the effects of different inorganic fertilisers (nitrogen (N), phosphorous (P), potassium (K), magnesium (Mg) and sodium silicate) and farmyard manure (FYM) on the yield of spring barley. The Hoosfield site has been fallowed only four times since 1852 to control weeds because it is spring sown. The experimental design is factorial in nature (Figures 3.3 and 3.4) with 1-4 strips for testing four different combination of nutrients (0 v P v KMgNa v PKMgNa) crossed by 4 series (O, A, AA and C) with different levels and forms of nitrogen (N). Nitrogen (48 kg N per ha) has been applied on four series. On series "O" no nitrogen has been applied. Series "A" has received ammonium sulphate, series "AA" sodium nitrate, and series "C" castor bean meal. An additional four plots on the south side have been used to test different residual inputs like unmanured (plot 61), ash (see RRes booklet [227]) applied from 1852 to 1932 (plot 62), FYM (35 t per annum) applied from

1852 to 1871 (plot 71) and FYM (35 t per annum) applied since 1852 (plot 72). In 2001, two new plots were introduced *i.e.*, P2KMg (plot 63), FYM (35 t per annum) applied since 2001 (plot 73). Strip 5 was introduced to test other different combinations of N, P, K and Mg [163].

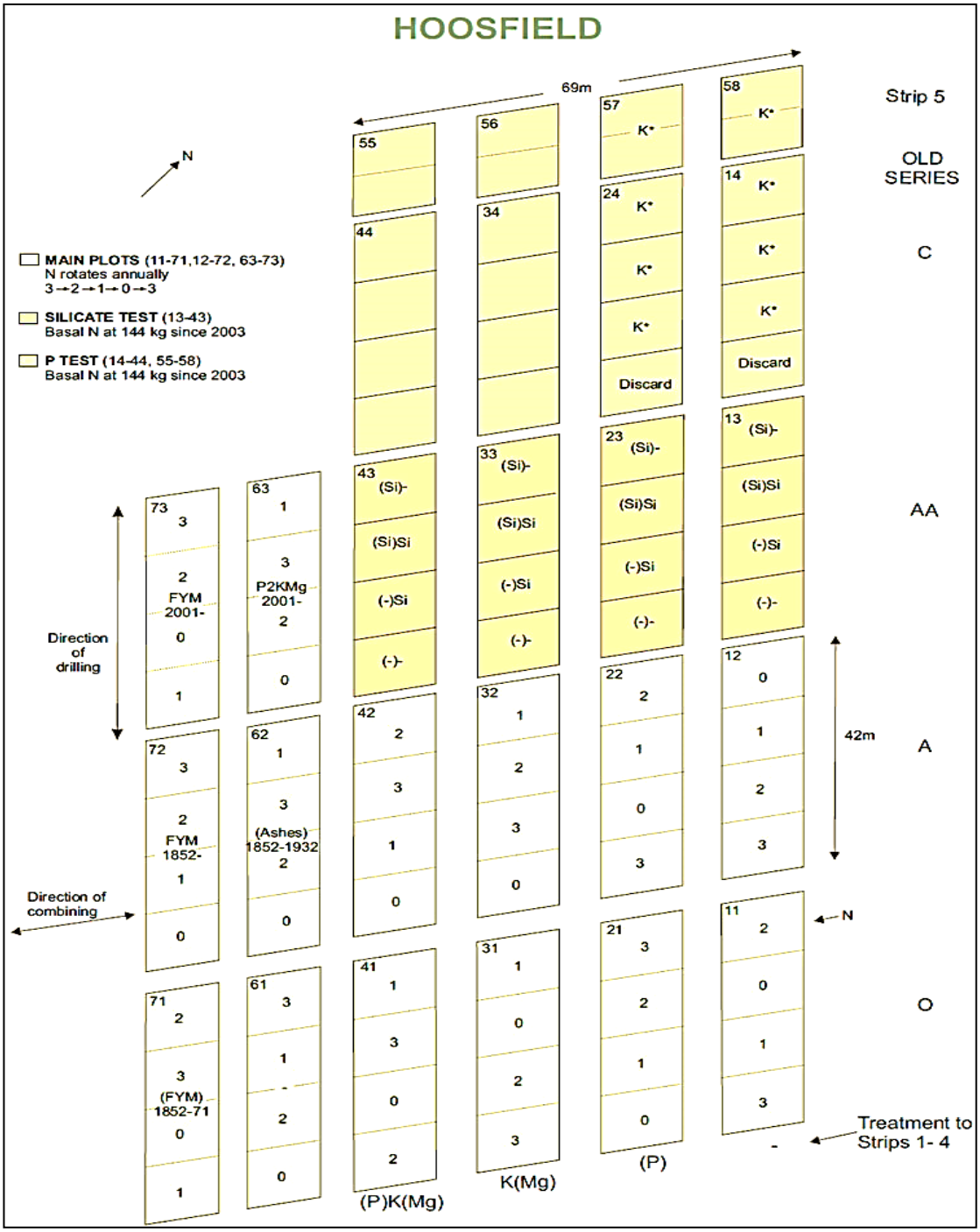

Figure 3.3 *Layout of Hoosfield Barley experiment [164].*

Figure 3.4 *Aerial view of Hoosfield barley experiment in present day. The plots used for sampling are highlighted by the red rectangles.*

3.3 Soil sampling plots

Nine plots on section 9 (continuous wheat section adjacent to the drainage ditch) of Broadbalk site were selected for collection of soil samples to give a range of SOM contents including: Nil (Plot 3); PKMg (Plot 5); FYM-farm yard manure (Plot 2.2); N1(PKMg) (Plot 6); N2(PKMg) (plot 7); N3(PKMg) (plot 8); N4(PKMg) (plot 9); N5(PKMg) (plot 15) and N6(PKMg) (plot 16). Among the nitrogen plots, nitrogen has been applied with P, K, Mg in N1, N2 N3 and N4 plots where Na was applied until 1967 and P has been withheld since 2001. In N5 plot 96 kg N ha^{-1} was applied along with PKNaMg until 1967, then 144 kg N ha^{-1} was applied with PKMg until 1985 and P has been withheld since 2000. On N6 plot 96 kg N ha^{-1} was applied since 1985; Na was applied until 1967 and P has been withheld since 2001 [97, 99]. According to Schjonning *et al.* [19], management effects on soil physical properties can be isolated, while interferences from textural differences could safely be ignored. So, in this study, the strips (section 9) at the base of the slope were used for sampling to minimize the effect of clay content [33].

In addition, soil samples were collected from plot 42 (inorganic fertilisers), plot 72 (FYM+N applied from 1852-present), plot 73 (FYM+N applied from 2001-present) and plot 71 (FYM applied from 1852-1871) on the Hoosfield Barley Experiment. The properties and generic features of the soil from the selected plots of both experimental fields are summarised in Table 3.1.

Table 3.1 *Properties of soils that have been studied [164].*

Properties	**Broadbalk Wheat Experiment**									**Hoosfield Experiment**			
	Nil	PKMg	FYM	N1	N2	N3	N4	N5	N6	FYM 1852-71	FYM since 1852	FYM since 2001	NPKMg Since 1852
Location	Rothamsted Res., Hertfordshire									Rothamsted Res., Hertfordshire			
Latitude	51°48’36’’ N									51° 48' 39.6" N			
Longitude	0°22’30’’ W									0° 22' 33.6" W			
Treatments		PKMg; no N*	FYM; 35 t ha $^{-1}$	48 kg N ha^{-1}	96 kg N ha^{-1}	144 kg N ha^{-1}	192 kg N ha^{-1}	240 kg N ha^{-1}	288 kg N ha^{-1}	NPK Mg	FYM + N	FYM + N	FYM
Soil type													
SSWE Soil classification	Batcombe Series									Batcombe Series			
FAO Classification	Chromic Luvisol									Chromic Luvisol (or Alisol)			
US Taxonomy	Paleudalf									Aquic (or Typic) Paleudalf			
Land use**	A; C	A; C; IF	A; C; FYM	A; C; IF	A; C; IF	A; C; IF	A; C; IF	A; C; IF	A; C; IF	A; C	A; C; FYM	A; C; FYM	A; C; IF
Texture	Clay loam									Flinty silty clay loam			
Water content at which soils are packing, g/g	0.11	0.15	0.24	0.14	0.16	0.18	0.17	0.18	0.19	0.14	0.24	0.19	0.17
SOC, t/ha	8.4	8.95	31.75	10.75	11.49	12.35	12.88	11.48	12.82	14.02	37.38	20	9.67
C: N	9.5	9.6	10.7	10	10	10.5	10	10.2	9.9	10.6	11	11.1	9.8
pH	8.18	7.80	7.68	7.29	7.44	7.05	7.32	6.92	7.24	7.24	7.22	7.50	7.27

* Na was applied until 1967 and P has been withheld since 2001; **Land use A= arable; C= cereal; IF= fertilised; FYM= farmyard manure.

3.4 Soil sampling and preparation

Top-soils (0-23 cm) were collected as composite samples (about 25 cores) from different portions of the Broadbalk experimental plots and from 4 sub plots of each selected plots from Hoosfield by hand using 3 cm diameter gouge augers. The samples were collected about 1 m from the edge on either side of each plot to avoid crop damage except on plot 2.2 of Broadbalk where soil was collected from the south edge only (adjacent to the path). The soil samples collected within each plot were combined and mixed thoroughly. Then the soil was passed manually through a 4 mm mesh sieve to make a homogeneous bulked sample to be more representative of the treatment plot. Since the soils at both fields contained many stones and pebbles, it was necessary to sieve the samples before use. Finally, the soil samples were stored in a cold room at 4^{o} C.

3.5 Statistics used in soil sampling

The plots were chosen based on the objectives of the study and to find the answers for the research questions mentioned in chapter 1. Soil samples were collected from each plot by collecting subsamples following a systematic 'W' pattern for sampling shown in Figure 3.5. This is a recommended approach for estimating the overall effect of fertilizer application on soil properties in a field [225]. But this method of sampling has a limitation that it may not capture spatial variability.

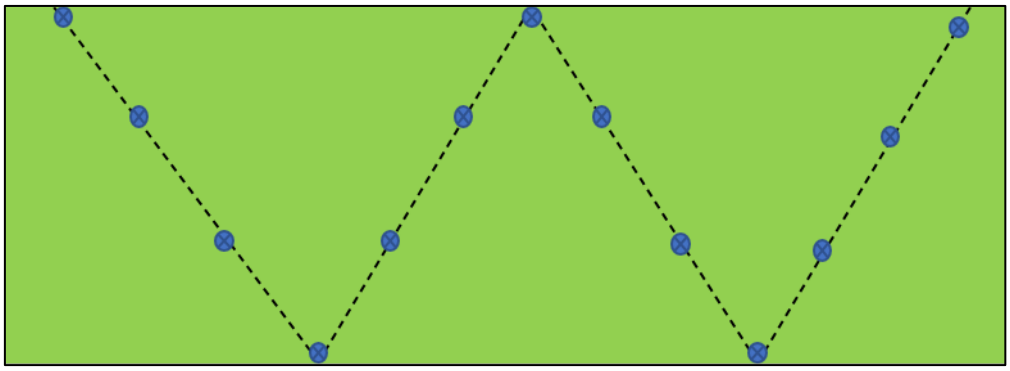

Figure 3.5 *Sampling pattern used for soil sample collection.*

Chapter 4. Characterisation and measurements of soil properties

4.1 Introduction

Soils can be described by their physical, chemical, biological, and mechanical properties. Soil management has a large impact on a range of soil properties including particle density, plastic and liquid limits, soil carbon content. The particle density of soils can vary due to the presence of heavier minerals (such as iron oxides) or organic matter (which has a low density and reduces the overall particle density value) [165]. So, the soil samples collected from the long-term experimental plots with different SOM content should have different particle densities. The interrelationships of porosity, bulk density, and air space, and rates of sedimentation of particles in fluids depend on particle density [167]. So, data for particle density will help to interpret the measurements in described in this chapter and other chapters. However, many studies assume a constant value, typically 2.65 g cm^{-3} for arable, mineral soils [168].

On the other hand, consistency of soil, also known as Atterberg limits, can be described as the states of soil at different water contents, from dry to viscous. The plastic limit is the minimum water content at which the soil exhibits plasticity [169]. The range of moisture content over which a soil shows plastic properties is given by the plasticity index (PI) [170]. Since plastic and liquid limits are important and useful parameters to describe soil mechanical behaviour and to predict some soil properties *i.e.*, soil compressibility [170, 171], the Atterberg limit measurements for soils with different SOC reported in Chapter 6 are valuable in indicating the extent to which they are influenced by SOC.

Although several studies have shown that consistency limits of soil rely on the amount of clay and organic matter content [172, 173, 174, 175], there are few data on the influence of long-term fertilisation on these limits. So, this study focuses on how SOM in samples from the long-term experiments influences soil physical behaviour. To understand the effect of

SOM on soil properties, it is important to study the composition and distribution of SOM in soil. Thermogravimetric (TG) analysis of soil samples has been used to investigate the composition of SOM and the effects of soil managements on it. TG analysis can give a detailed information about the type and quantity of SOM of soils from the selected fields which can help to interpret the impact of SOC on soil properties.

Moreover, a study on some fundamental soil physical properties observed for different treatments of Broadbalk and Hoosfield experiments are presented in this chapter. The objective of this chapter is to find out how different long-term agricultural treatments change soil properties. Furthermore, the measurements of soil particle density, consistency limits (plastic and liquid limits of soil), total and organic carbon content, SOM, and its composition discussed in this chapter will be used to interpret and compare with data about the other soil properties described in subsequent chapters.

4.2 Methods and materials

4.2.1 Pycnometer method to measure soil particle density

Soil particle density is one of the basic physical properties of soils and represents an essential element of diverse pedotransfer functions [165, 166]. Soil particle density can be described as the ratio of dry soil mass including solid particles to volume of soil, excluding pore spaces between particles [167]. The particle density of soil samples was measured by the pycnometer method. A pycnometer is a glass flask of precise volume fitted with a glass stopper which is pierced length wise by a capillary opening. The empty pycnometer with the stopper was weighed before a sample was introduced. 10 g of 2 mm sieved air-dried soil was placed in a 50 ml volumetric flask. Then the pycnometer with soil was weighed again including the stopper. Distilled water was then added to the pycnometer and the flask with the contents boiled with gentle agitation avoiding the spilling of contents due to foaming. The boiled suspension was then cooled down to room temperature and the flask filled with cold boiled distilled water up to the mark and weighed with stopper. The outside of the flask

was cleaned and dried prior to weighing and the stopper was inserted carefully to avoid loss of suspension by the capillary. The temperature of the suspension was recorded. Initially, a blank measurement was carried out with boiled distilled water at same temperature [176]. Using these measurements, the particle density can be calculated from equation (4.1).

$$\rho_s = \rho_w(w_s - w_a)/\{(w_s - w_a) - (w_{sw} - w_w)\} \quad (4.1)$$

where,

ρ_s=particle density of soil sample (g/cc)

ρ_w=density of water at temperature observed (g/cc)

w_s= weight of pycnometer and soil corrected with oven dried moisture content (g)

w_a= weight of empty pycnometer (g)

w_{sw}= weight of pycnometer filled with soil and boiled distilled water suspension (g)

w_w= weight of pycnometer filled with boiled distilled water at observed temperature (g).

4.2.2 Consistency limits measurement

The water content at which the soil changes from the plastic state to the liquid state is its liquid limit and the water content at which the soil changes from the semi-solid state to the plastic state is known as its plastic limit. When the water content of a given soil is more than its liquid limit, the soil will be in liquid state and has negligible shear strength. As the water content continues to reduce due to drying, there is a range of water content (between the liquid and plastic limits) at which the soil can be moulded into any desired shape without rupture. The soil at this state is said to exhibit 'plastic' behaviour *i.e.*, the ability to deform continuously without rupture [169].

In this study, plastic and liquid limits of both soils (Broadbalk and Hoosfield) were measured following the British standard [177]. For both measurements soil samples were air-dried and ground finely to pass through a 425-micron sieve. About 400 g of finely ground soil was used for the measurements. It was thoroughly mixed with distilled water on a glass plate and placed in the airtight plastic bag over night.

4.2.2.1 Plastic limit measurement

The hand rolling method was followed to measure plastic limits of soil samples. About 20 g from the soil paste prepared was taken and spread on the glass mixing plate, allowing the soil to dry partially until it became plastic enough to mould into a ball. The ball of soil was then pressed between fingers and rolled between palms and remoulded. Over time, the heat of hands helped the soil to dry sufficiently. The soil ball was divided into two equal subsamples weighing about 10 g each. Then each of the sub samples was rolled into a thick thread and cut into four equal pieces. Each sub sample of soil was moulded between first finger and thumb of each hand to make an 8 mm thread. Then the thread was rolled again with the fingers in five to ten complete forward and reverse strokes of the hand on the surface of the glass plate, putting sufficient pressure to reduce the thread to about 3 mm diameter. The pressure should be uniform throughout the rolling process. The moulding and rolling process were repeated until the soil thread crumbled. The first crumbling point was taken to be the plastic limit. The crumbled portions of soil thread were gathered and placed in pre-weighed tin. The same process was followed for the other three portions of soil thread, and they were placed in the same tin. Finally, the moisture content of the crumbled soil threads was determined by oven drying.

4.2.2.2 Liquid limit measurement

The liquid limit of soil is the absolute moisture content at which soil passes from plastic state to liquid state. It was measured on the soil samples by the cone penetrometer method. This method is very easy to conduct and results in reproducible data. In this method, a cone of stainless steel is used which is approximately 35 mm long with a polished surface and a cone opening angle of about 30^{o}.

About 300 g of soil paste was placed on the glass plate prepared as described above for the first step of plastic limit test. Then the wet soil paste was transferred to the cylindrical metal cup of cone penetrometer apparatus, ensuring that no air was trapped. Finally, the soil paste

was levelled to the top of the cup and placed on the base of the cone penetrometer apparatus. The cone penetrometer was adjusted so that the cone point just touched the levelled surface of the soil paste in the cup. The vertical clamp was then released allowing the cone to penetrate the soil paste under its own weight for 5 seconds. After 5 seconds, the penetration depth of the cone was recorded to the nearest millimetre. The test for each sample was repeated to have at least four sets of values of penetration in the range of 14 to 28 mm. The exact moisture content of each trial was determined by oven drying the soil paste from the cup after the cone penetration depth recorded. A graph representing water content on the Y – axis and the cone penetration depth on the X – axis was plotted. A best fitting straight line was drawn. The moisture content corresponding to cone penetration depth of 20 mm was taken as the liquid limit of the soil. The liquid limit should be reported to the nearest first decimal place.

Soil used for liquid limit determination should not be oven dried prior to testing. Wet soil was weighed immediately after each trail to avoid any loss of moisture due to evaporation. Both plastic and liquid limit test mentioned above were carried out following the British Standard [177].

4.2.3 Determination of soil carbon (C)

Soil carbon (C) was determined by dry combustion using a LECO TruMac analyser (LECO, Michigan, USA). This method requires a pulverised homogeneous soil sample. So, soil samples were air-dried and finely milled to make a homogenous sample. About 0.4 g finely milled soils was weighed in ceramic boats before incineration to determine C content. Total carbon can be expressed as,

Total Carbon = Inorganic Carbon + Organic Carbon (4.2)

In this study, the soil organic carbon (SOC) was determined by subtracting the amount of inorganic C (which was negligible) from the total C. This measurement was done in the analytical unit at Rothamsted Research.

This dry combustion method can only measure the total carbon content as it works at high temperature *i.e.*, 900-1600 ºC, whereas in TG analysis, soil samples are burnt in the temperature of about 105-650 ºC and the different components of organic carbon can be measured.

4.2.4 Thermogravimetric (TG) measurement

Thermogravimetric (TG) analysis can be defined as a technique for evaluating thermal stability and composition of materials by interpreting the change in the weight of a material with varying temperature [178, 179]. A material consisting of various substances with different molecular structures will display several weight loss peaks at different temperatures. The weight loss obtained in a thermal reaction can be measured between the inflection points of the TG curve [179].

The exothermic degradation of the soil sample recorded as weight loss in the temperature range of 105-650 °C can be illustrated by three different phases such as evaporation of hygroscopic water (some inorganic and organic substance also be decomposed), soil organic carbon (SOM) breakdown, and carbonate decomposition [180, 181]. According to Siewert [180] and Wang *et al.* [182], hygroscopic water in the sample is completely removed when soil temperature reaches about 200 °C and SOM starts to fully breakdown. Gaal *et al.* [183] and Siewert [180] report that carbonate starts decomposition when soil temperature reached 550 °C. Gao *et al.* [42] and Lopez-Capel *et al.* [46] describe the weight loss associated with thermal decomposition (between 200 and 600 °C) as the total weight of SOM or total exotherm (Exotot). According to Lopez-Capel *et al.* [46] and Dorodnikov *et al.* [181], the total weight of SOM (Exotot) can be further divided into three fractions: a labile fraction (Exo1), an intermediate stable fraction (Exo2), and a recalcitrant fraction (Exo3). The proportions of SOM with different thermal stabilities can be evaluated as Exo1/Eoxtot, Exo2/Exotot, and Exo3/Exotot, where Exotot = Exo1 + Exo2 + Exo3. Another parameter, TG-T50 (the temperature where 50% of total SOM weight is lost) can be applicable to

demonstrate the thermal stability of SOM [184, 185]. Siewert [180] and Rovira *et al.* [186] illustrate that lower TG-T50 indicates more thermally unstable SOM. In TG analysis, a thermo-balance placed in the analyser measure the mass change of samples as a function of temperature or time under defined and controlled environment with respect to heating rate, gas atmosphere, flow rate and crucible type. The analyser is connected to an air supply of nitrogen (N_2) as a protective gas but in some experiments, air can be used [42].

In this study, the TG measurement was carried out with a TG 209F3 analyser (Netzsch-Gerätebau GmbH, Selb, Germany), as described by Gao *et al.* [42]. The analyser was calibrated before the measurement with empty Al_2O_3 crucible in two different heating conditions to set up two different baselines.

Baseline 1 calibration: The furnace temperature was raised gradually from room temperature to 650 ºC at a rate of 10 ºC per minute under 20 ml/min air atmosphere (20% O_2 and 80% N_2) with protective gas (20 ml N_2/min).

Baseline 2 calibration: The furnace with empty Al_2O_3 crucible was heated from room temperature to 105 ºC holding the temperature at 105 ºC for 10 minutes and then heated up to 650 ºC at a rate of 10 ºC per minute under air atmosphere (20% O_2 and 80% N_2) with protective gas (20 ml N_2/min).

In this experiment, baseline 1 calibration was used because no difference was found between the two calibrations while testing them both with a test sample.

In this analysis, finely ground (passed through 0.053 mm mesh sieve) air dried soil samples were used. The soil samples (about 30-40 mg) were placed in an alumina (Al_2O_3) crucible with an aluminium lid and placed on the sample holder of the TG apparatus. Then the sample was burnt in the furnace under the synthetic air environment (20% O_2 and 80% N_2, 20 ml min^{-1} with a protective gas (N_2, 20 ml min^{-1}) at temperatures from 30 ºC to 650 ºC. First, the sample was heated up to 105 °C under the artificial air atmosphere and the temperature was maintained at 105 °C for 5 min. Then the furnace temperature was increased from 105 °C to 650 °C at a rate of 10 °C min^{-1}. The weight of a sample was recorded during the heating

cycle. Three replicate samples from each treatment of Broadbalk and Hoosfield were analysed in the TG apparatus. This analysis was done at Prof. Tushen Ren's laboratory in China Agricultural University (CAU), in Beijing, China.

4.2.5 Data and statistical analysis

The statistical analysis of all data from this chapter were done by using GenStat V17. Data were analysed with ANOVA and regression analysis (simple linear regression). Three replication of soil samples were used in each measurement except for the liquid limit measurement. In the TG analysis, soil samples (39 samples) including three replications were run randomly in the apparatus.

The plasticity index (PI) for each soil sample was calculated from the plastic limit (PL) and the liquid limit (LL) data using the equation (4.2).

$$PI = LL - PL \tag{4.3}$$

4.3 Results from different analysis

4.3.1 Result from particle density measurement

The particle densities of Broadbalk and Hoosfield soils range from 2.5 to 2.75 g/cc (Figures 4.1 and 4.2). For both soils, not only do the soils with higher organic matter content show lowest particle densities but also the particle density decreased with increasing soil organic carbon content.

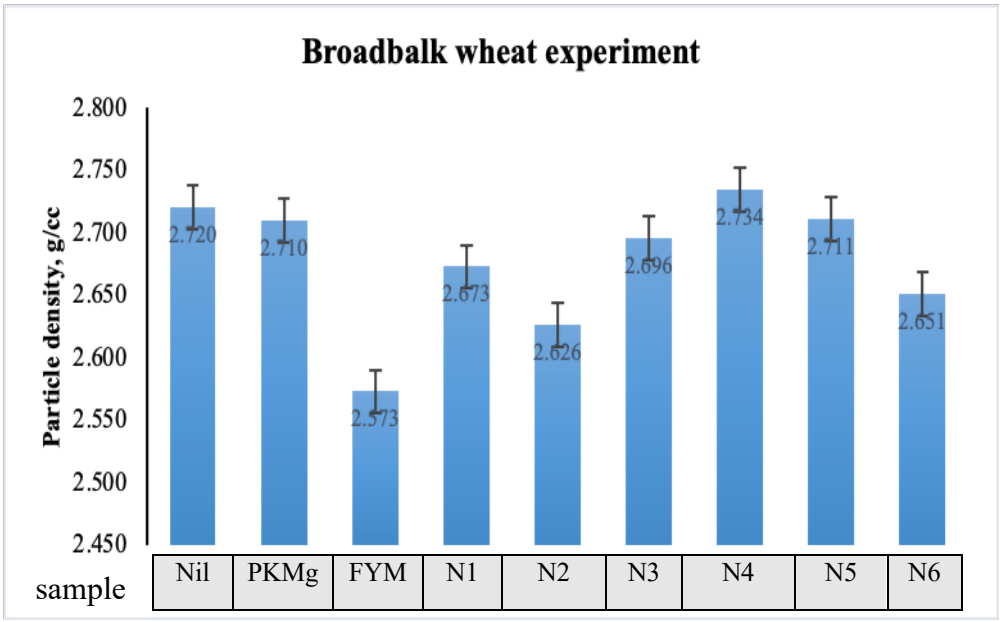

Figure 4.1 *Particle densities with standard error bar of Broadbalk soil samples (F= 2.73; P<0.05) showing lower values with increasing SOC content (P<0.05; s.e.d=0.035; Var.= 0.538) (see Tables 4.1 and 4.3 for the data associated with sample designations).*

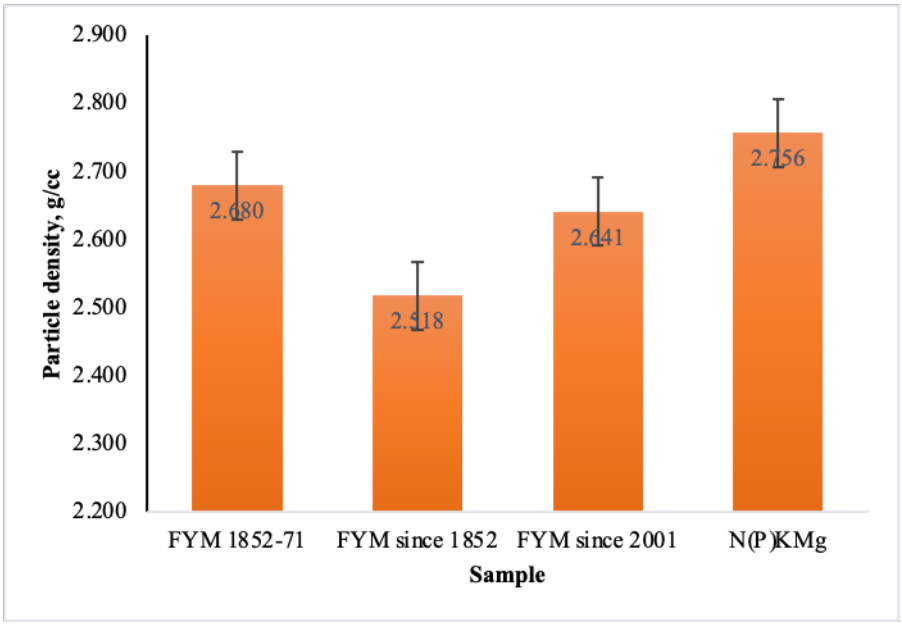

Figure 4.2 *Particle densities with standard error bar of Hoosfield soil samples (F= 7.29; P<0.05) showing that the soil sample with highest SOC content (FYM since 1852) has lowest density (P<0.05; s.e.d=0.019; Var.= 0.964).*

4.3.2 Results obtained from soil carbon determination

The data obtained from carbon analysis is shown on Table 4.1. The data shows that SOC content for all soil samples from Broadbalk and Hoosfield were very consistent with total carbon content.

Table 4.1 *Total soil carbon measured by dry combustion method and soil organic carbon (SOC) calculated from total soil carbon data by deducting carbonated carbon (inorganic carbon) content, for Broadbalk and Hoosfield soils.*

Source	Soil treatment	Total soil carbon, g/100g	SOC, g/100g
Broadbalk	FYM	2.978	2.959
	Nil	0.904	0.847
	PKMg	0.972	0.915
	N1(P)KMg	1.089	1.078
	N2(P)KMg	1.170	1.156
	N3(P)KMg	1.227	1.218
	N4(P)KMg	1.289	1.274
	N5(P)KMg	1.148	1.131
	N6(P)KMg	1.284	1.265
Hoosfield	FYM since 1852	3.650	3.650
	FYM since 2001	2.181	2.181
	FYM from 1852-71	1.454	1.454
	N(P)K(Mg)	0.991	0.991

4.3.3 Results from consistency limit measurement

The plastic and the liquid limits of Broadbalk and Hoosfield soil samples with their plasticity indices are shown in Table 4.2. The results showed that FYM plot of Broadbalk (contained highest SOC) had higher plastic and liquid limit value and same observation found on Hoosfield soils, *i.e*., the plot receiving FYM since 1852 has the high SOC content, showed higher value for the plastic and the liquid limit.

Table 4.2 *Consistency limits (plastic and liquid limit and plasticity index) of soils from Broadbalk and Hoosfield.*

Source	Soil treatment	Plastic limit, g/100g	Liquid limit, g/100g	Plasticity Index
Broadbalk	FYM	26	43	17
	Nil	20	36	16
	PKMg	20	37	17
	N1(P)KMg	21	40	19
	N2(P)KMg	21	41	20
	N3(P)KMg	21	40	19
	N4(P)KMg	20	42	22
	N5(P)KMg	21	35	14
	N6(P)KMg	21	35	14
Hoosfield	FYM since 1852	27	45	18
	FYM since 2001	23	37	14
	FYM from 1852-71	22	40	18
	N(P)K(Mg)	20	36	16

4.3.4 Results from TG analysis

In Figures 4.3 and 4.4, 3 peaks of % mass loss in 3 different temperature ranges can be explained as due to the different portions of SOM, including water bound with soil particles. The 1st peak which appears under 200 ºC, depends on hygroscopic water. The 2nd peak in the temperature range 200-400 ºC can be attributed to labile SOM or organic C. The 3rd peak which appears at high temperature range (> 400 ºC) must be associated with recalcitrant or more stable SOM or organic C. Figure 4.3 shows that the soil sample from FYM treated plot of Broadbalk has the highest value for labile portion of SOM whereas Figure 4.4 shows that the soil sample from Hoosfield which has received FYM for longest period, also has the highest peak value for labile SOM.

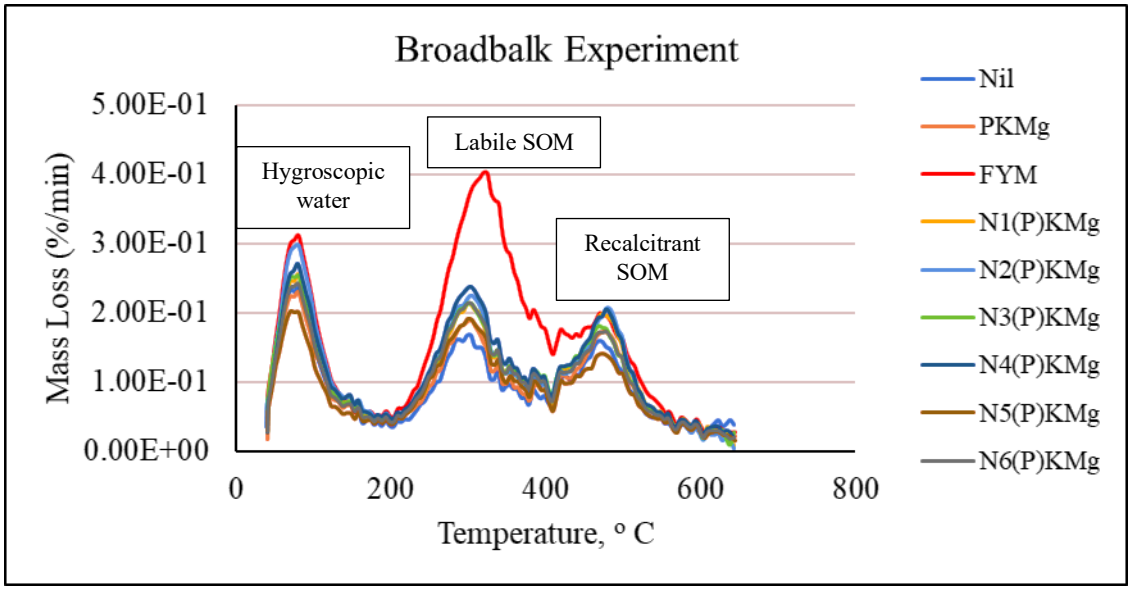

Figure 4.3 *Composition of SOM of Broadbalk soils (T=15.96, p<0.001) showing positive relation between SOC content and labile portion of SOM (P<0.05; s.e.d=0.041; Var.= 0.411).*

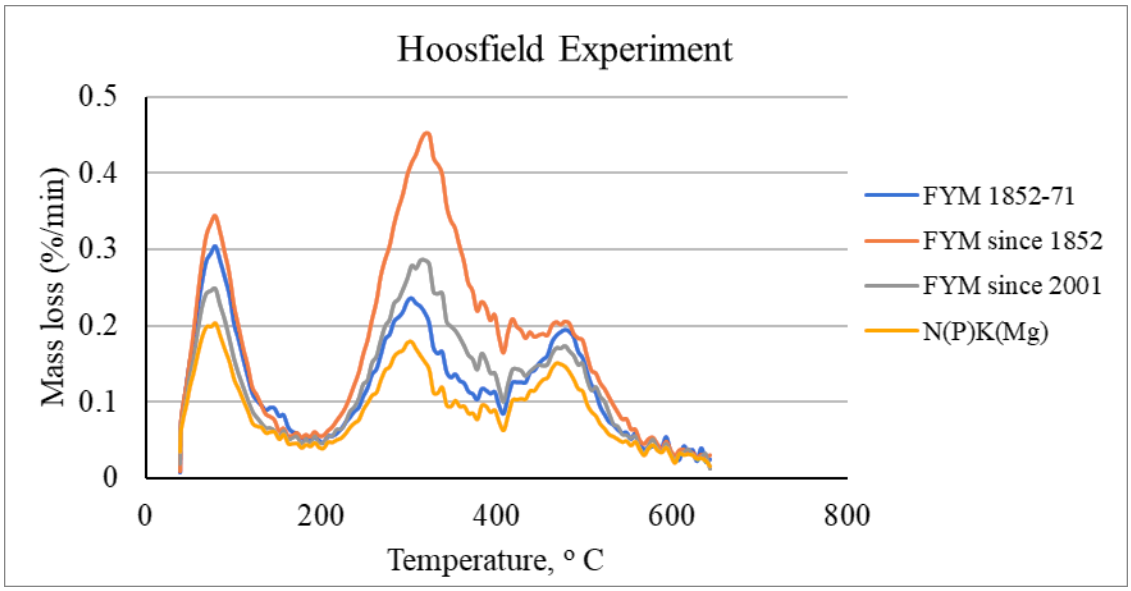

Figure 4.4 *Composition of SOM of Hoosfield soils (T= 9.94, P<0.001) showing good relation of labile portion of SOM with SOC content (P<0.05; s.e.d=0.069; Var.= 0.348).*

4.4 Discussion

The particle density of soil depends on the composition of both the mineral (soil texture) and the organic soil components. Soil samples with higher SOM content have lower particle densities than soil samples with similar textures but with low SOM [166]. London [187] reported that soil particle density increases with soil depth because of the concurrent

decrease in SOM. Regression analysis of the results of particle density analysis of both Broadbalk and Hoosfield soil shows a significant relationship with SOC content (Table 4.3). Other studies [168, 188] suggest that soil particle density ranges from 2.4–2.9 g cm^{-3}. Particle density data from this study are consistent with these previous studies. The data of particle density are used to estimate the void ratio in chapter 6.

Table 4.3 *Particle density of soils from Broadbalk and Hoosfield showing strong corelation with their respective SOC by regression analysis.*

Source	**Soil treatment**	**Particle density, g/cc**	**SOC, g/100g**	**Statistics**	
				F probability	**s.e.**
Broadbalk	FYM	2.573	2.959	<0.001	+/- 0.033
	Nil	2.720	0.847		
	PKMg	2.710	0.915		
	N1(P)KMg	2.673	1.078		
	N2(P)KMg	2.626	1.156		
	N3(P)KMg	2.696	1.218		
	N4(P)KMg	2.734	1.274		
	N5(P)KMg	2.711	1.131		
	N6(P)KMg	2.651	1.265		
Hoosfield	FYM since 1852	2.518	3.650		
	FYM since 2001	2.641	2.181		
	FYM from 1852-71	2.680	1.454		
	N(P)K(Mg)	2.756	0.991		

The results from consistency limit measurements show a positive relation with SOC content for both Broadbalk ($P<0.001$ with variance of 94 %) and Hoosfield ($P<0.05$ with variance of 98 %) soil samples (Figure 4.5). Soil organic carbon (SOC) content explains 98 percent of the variance in plastic limit, has been widely reported [170]. Stanchi *et al.* [172] observed that plastic limits (PL) are more controlled by the organic fraction, while liquid limit (LL) and plasticity index (PI) are more influenced by SOM and clay minerals and their interactions.

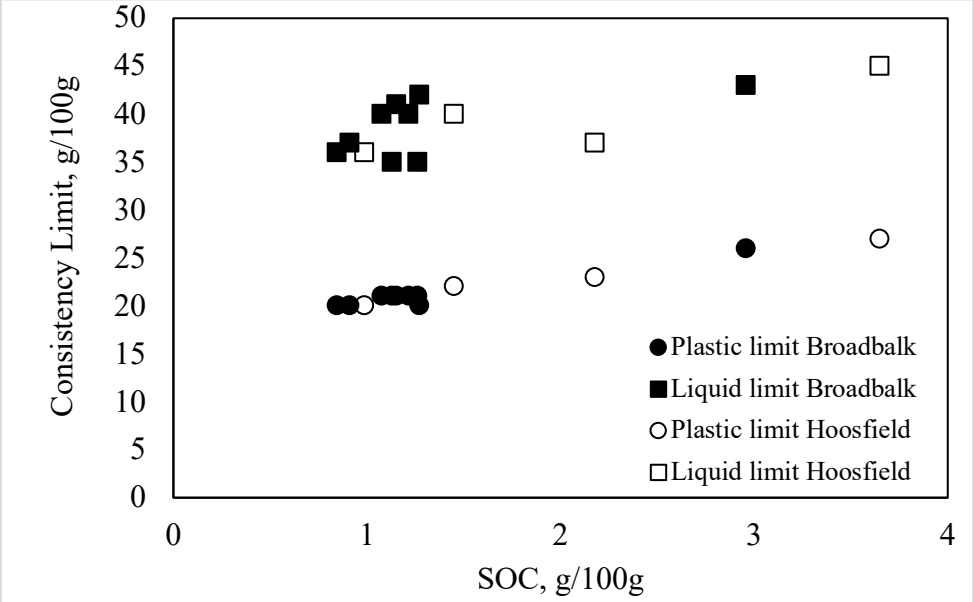

Figure 4.5 *Consistency limits plotted with soil organic carbon (SOC) showing positive relationship.*

The TG analysis shows that agricultural treatments have significant effects on the fractions of SOM, especially, on the labile portion of SOM for both experiments (Figures 4.3 and 4.4). According to Haynes [229], labile SOM are very sensitive to the changes in soil management practices and that influence the soil functions as well. Other studies have also reported that the labile SOM seems to be responsible for the changes in soil physical properties [44, 45]. In this study, regression analysis for the data obtained from TG analysis showed that the labile portion of SOM correlated positively with total organic carbon (SOC) content for both Broadbalk and Hoosfield soils (Figure 4.6). So, there is no scope for explanations beyond the total amount of carbon (SOC).

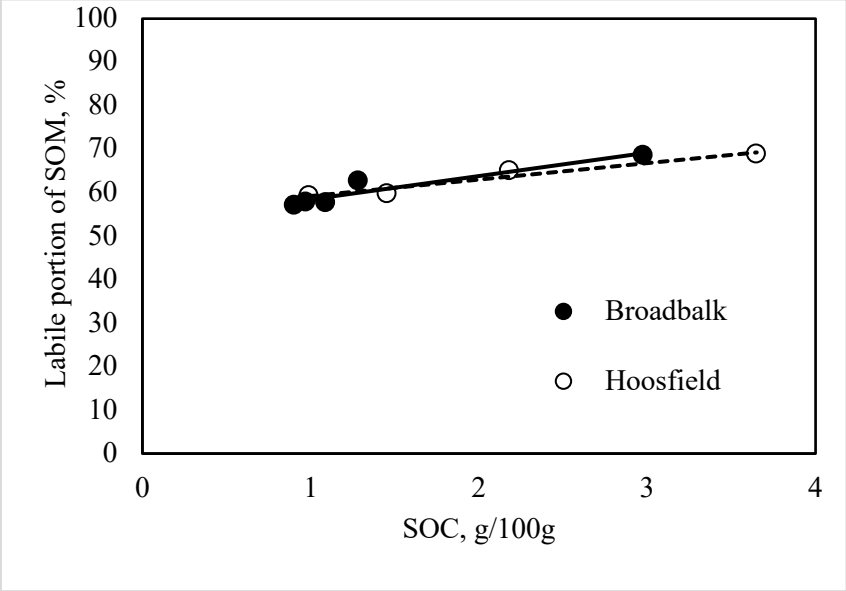

Figure 4.6 *Corelation between labile portion of SOM and SOC of Broadbalk (P <0.05 with 41% of variance in labile portion of SOM accounted for) and Hoosfield (P <0.05 with 35% of variance in labile portion of SOM accounted for) soils.*

4.5 Summary

This Chapter has reported measurements of soil particle density, consistency limits (plastic and liquid limits of soil), total and organic carbon content, SOM, and its composition on soil samples with differing organic matter content from long term experiments. The particle densities reported here are within the expected range for the arable soils and decreases with increasing SOM. The consistency limits showed positive relation with SOC content. The TG analysis indicates that the labile portion of SOM is consistent with the SOC results. Moreover, the result from the different analysis discussed in this chapter, shows that different agricultural treatments do have impacts on the soil properties including particle density and consistency limits.

Chapter 5. Water retention properties of soil

5.1 Introduction

Soil hydraulic properties reflect the structure of the soil pore network comprising different geometry and sizes of pores and pore connectivity [14, 189, 190]. Soil water release characteristics (SWRC) describing soil water content as a function of soil matric potential, are an important soil hydraulic property [191]. Soil water retention is a complex function of soil structure that regulates soil functioning in an ecosystem [192]. Most soil functions depend on soil water release characteristics directly or indirectly [117]. Variation in soil water retention characteristics can be used to compare different soils and soil states. The effects of soil water retention depend on soil textural variation and most importantly on soil organic carbon content [192]. Soil organic matter can alter and improve the soil structure and the pore system which ultimately influences on the soil water retention characteristics (SWRC). So, the objectives of this chapter are to find out whether the SOC content in the selected experimental plots has any impact on SWRC and how the data obtained from this experiment relates to and helps to interpret the other soil functions. This chapter also describes the methods used to obtain the soil water release characteristics of the target soils and their results.

5.2 Materials and methods

5.2.1 Sample preparation

When extracted, the soil samples collected from Broadbalk and Hoosfield (see chapter 3) contained stones, pebbles and large aggregates. So, to make them more homogeneous, the samples at field condition moisture were passed through 4 mm mesh and then repacked in metallic cores of 39 mm ID (inner diameter) and 18 mm height using 10 kPa axial pressure in a hydraulic chamber.

5.2.2 Measurement method

Soil water release characteristics have been measured by the suction plate method since, this is the most used method for soil water release. The plates were soaked in deionized water overnight before being loaded with soil samples. The soil cores with 3 replicates of each sample were saturated for 24 hours before placing on the pre-saturated ceramic plates randomly. The samples on the ceramic plate were covered loosely with the lid and dark polythene sheet to avoid evaporation during wetting. Subsequently, the soil core samples were subjected to different matric suctions for different time periods. In this experiment, soil cores were equilibrated at 8 different matric potentials such as –0.01, –0.03, –0.1, –0.3, –1, –3, –5 and –15 Bar. Equilibration of samples at higher matric potentials (–0.01 to –0.3 Bar) were carried out on a plate suction table (ceramic suction plate) for 2-10 days while samples at lower matric potentials (–1 to –15 Bar) were equilibrated in pressure chambers (pressure plate apparatus) for 12-36 days [108, 193]. The water content at the 8 different water potentials was derived from the mass of packed soil mix after equilibrium [194]. The gravimetric water content at the 8 matric potentials was measured by oven-drying the soil at 105^{o} C for 48 h. The volumetric water content was calculated from the product of gravimetric water content and bulk density.

Three replications of each sample were taken for each matric potential. Plates were cleaned after each use by soaking in distilled water, gently brushing and rinsing, and then allowing them to air dry.

5.2.3 Data and statistical analysis

The van Genuchten model (1980) was used to fit the water retention data,

$$\theta = (\theta_s - \theta_r)[1 + (\alpha h)^n]^{-m} + \theta_r \quad (5.1)$$

The pore volume distribution function, $S_v(\psi)$ was used to explore the changes of pore size distribution in the different manure treatments. $S_v(\psi)$ can be explained as the slope of the volumetric water release curve plotted against equivalent pore diameter, d_e, on a $\log_{10}$ scale [195, 196].

$S_v(\psi)$ is given by

$$S_v(\psi) = \frac{d(\theta_v)}{d\,(\log_{10}[\psi])} = -mn(\theta_s - \theta_r)\alpha^n\psi^n[1 + (\alpha\psi)^n]^{-(m+1)} \quad (5.2)$$

where θ_s is the saturated volumetric water content, θ_r is the residual volumetric water content, ψ is the matric potential and α, m, and n are the parameters of van Genuchten model. The equivalent pore diameter, d_e (mm), is given by Jury *et al.* [197]

$$d_e = \frac{4\gamma\cos\omega}{\rho_\omega g h} \approx \frac{300}{h} \quad (5.3)$$

where γ is pore water surface tension (7.36 g s^{-2}), ρ_ω is water density (1.0 g cm^{-3}), g is the gravitational acceleration (980 cm s^{-2}), ω is the water-pore contact angle, h is the water suction (value of ψ) (cm). $d_{(mode)}$ and $d_{(median)}$ are the two main indicators of pore size. $d_{(mode)}$ is the pore size where the inflection point of soil water release curve occurs [98]. $d_{(median)}$is the pore size at which 50% of the soil water has drained during drying. They are given respectively by,

$$d_{mode} = \frac{300\alpha}{m^{-\frac{1}{n}}} \quad (5.4)$$

and

$$d_{median} = \frac{300\alpha}{(0.50^{-1/m}-1)^{-\frac{1}{n}}} \quad (5.5)$$

where, α, m, and n are the van Genuchten parameters introduced earlier. Matthews [228] explained that because of percolation effects the simple approach to estimating pore size distribution does not always work well, because some of the larger pores are shielded by smaller pores, and prevented form draining, however, it is still a very useful comparative guide.

The data were also analysed in Genstat using ANOVA. The block structure used was Plot/Replicate with a treatment structure of N rate*matric potential.

For values of *pF* between 1 and 4.176 (inclusive) the model is a quadratic linear model with different intercepts slopes and quadratic parameters for each soil type:

$$\ln(Vol_i) = \alpha_{\text{soil}} + \beta_{1\text{soil}}.pF_i + \beta_{2\text{soil}}.pF_i^2 + e_i \quad (5.6)$$

This was used to test for differences between soil treatments and matric potentials.

5.4 Results and discussion

Water release curves for the soil samples of both experiments have been drawn by plotting gravimetric moisture content (θ) versus soil matric potentials (Figures 5.1 and 5.2). The volumetric water contents were deduced from the gravimetric water content and bulk densities. The VG model curves represent predictions of the van Genuchten model (see Chapter 2). Both graphs show that amount of water dropped as matric suction is increased. Sharp decrease of water content can be observed from -1 kPa to -10 kPa. According to the retention curve, soils from FYM plot at Broadbalk and the longest FYM application since 1852 plot of Hoosfield show highest water retention even at the dry end (at -1500 kPa). The water retention data of Hoosfield soil samples seems more complicated as because of the temporal pattern of SOM additions (Figure 5.2).

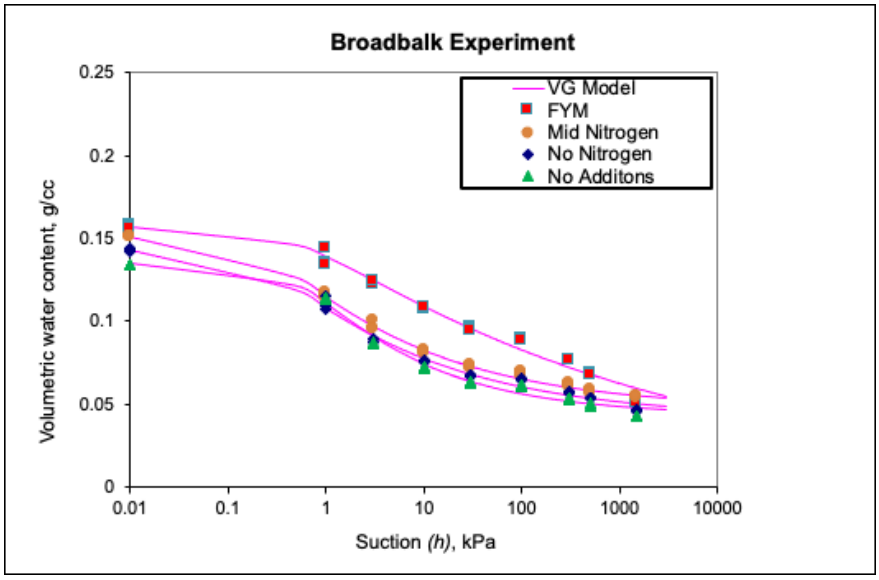

Figure 5.1 *Water release curve (WRC) for Broadbalk soils (P<0.001; s.e.d=0.079; Var. = 0.994).*

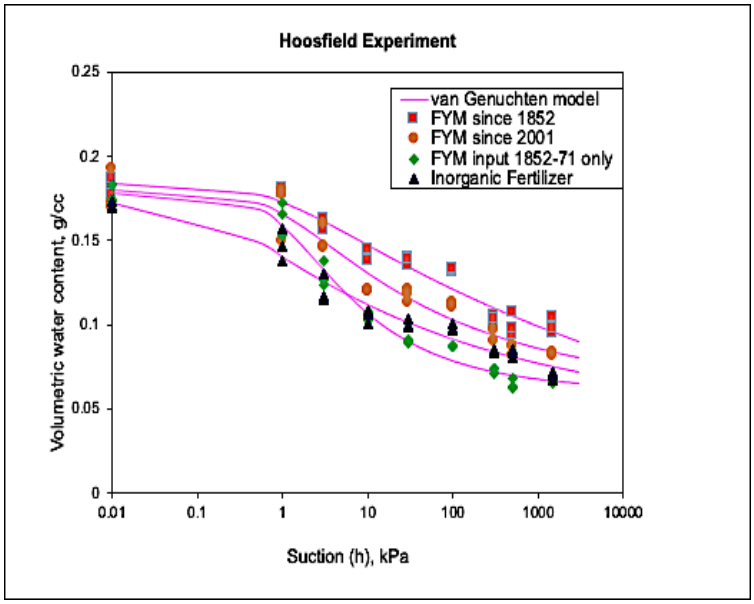

Figure 5.2 *Water release curve (WRC) for Hoosfield soils (P<0.001; s.e.d=0.099; Var.= 0.846).*

Note that the least significant difference (LSD) for $P<0.05$ is shown in Figure 5.6. The accompanying statistical analysis is given in the supplemental data (see appendix 1). The effect of soil organic matter observed here is consistent with reported accounts [36, 192, 198] that soil density decreases with increasing soil organic matter content. The FYM plot retains a greater amount of water at all matric potentials.

Gao *et al.* [199] have reported that different tillage and depths of soil are significantly responsible for the variations in van Genuchten parameters. Fitting the water release data in Figures 5.1 and 5.2 by the VG model also shows that different values of the fitted van Genuchten parameters correspond to different inputs of manure and fertiliser (Table 5.1).

Table 5.1 *Parameters of the van Genuchten function of volumetric water content as a function of matric potential.*

Site	Soil treatment	van Genuchten function parameters			
		θ_s (cm^3/cm^3)	θ_r (cm^3/cm^3)	α	n
Broadbalk (BK)	FYM	0.444	0.088	0.823	1.205
	Nil	0.390	0.117	2.237	1.139
	PKMg	0.423	0.112	6.593	1.280
	N1(P)KMg	0.486	0.127	1.224	1.426
	N2(P)KMg	0.488	0.144	0.914	1.513
	N6(P)KMg	0.388	0.032	4.409	1.256
Hoosfield (HB)	FYM since 1852 (72)	0.452	0.167	1.223	1.260
	FYM since 2001 (73)	0.416	0.134	2.024	1.287
	FYM from 1852-71 (71)	0.447	0.136	2.004	1.435
	N(P)K(Mg) (42)	0.357	0.104	5.854	1.231

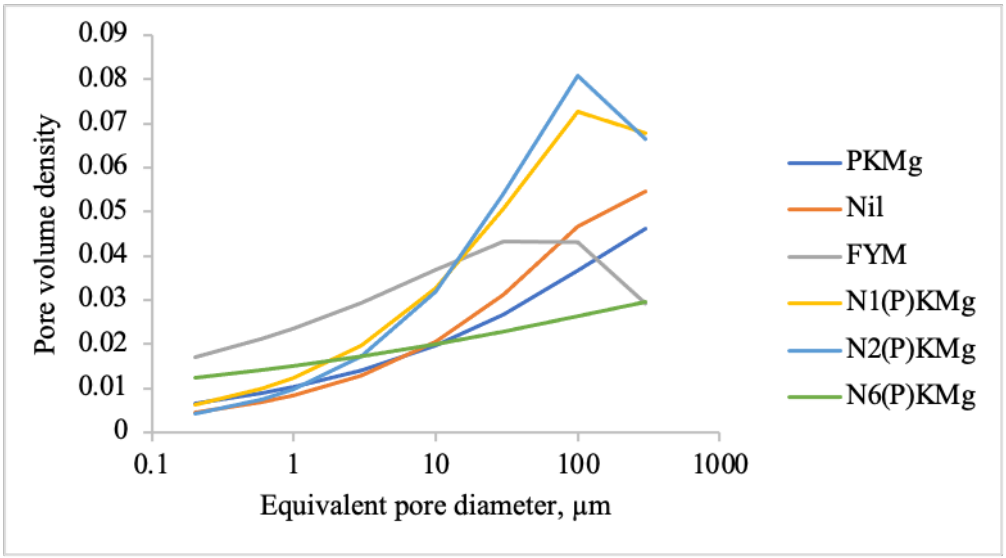

Figure 5.3 *Effect of different management practices on the pore volume distribution function* $S_v(\psi)$ *(see equations 5.2 and 5.3) for Broadbalk soils.*

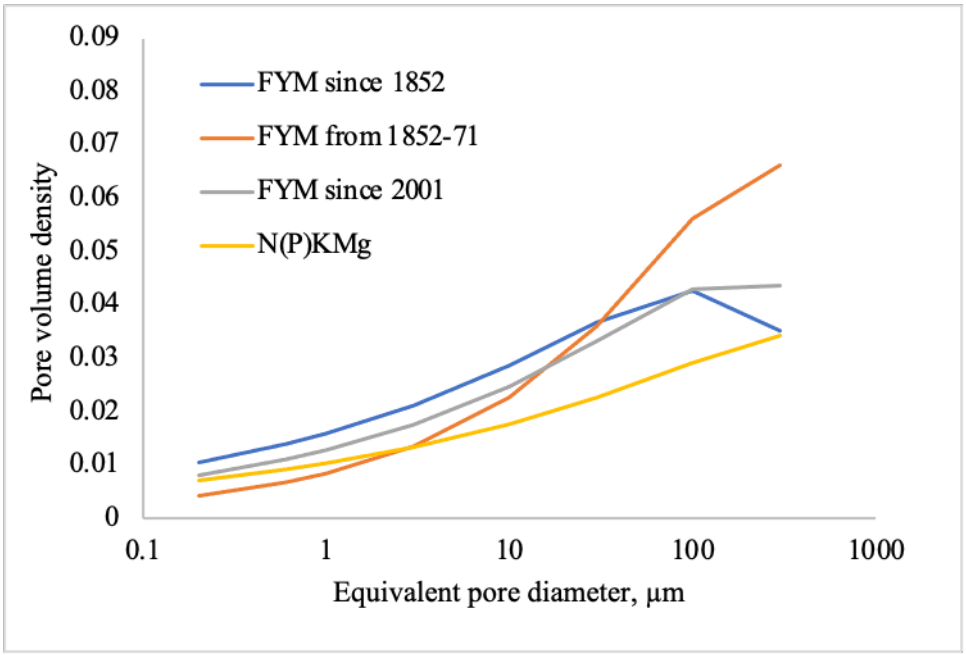

Figure 5.4 *Effect of different management practices on the pore volume distribution function* $S_v(\psi)$ *for Hoosfield soils.*

It has been reported that the numbers of capillary pores are higher in the clay soil compared to the sandy loam soil [200], whereas the proportions of non-capillary (rapidly drainable) pores which release water at low suctions, are higher in sandy soil than in clay soil [108]. Table 5.2 and Figures 5.3 and 5.4 show the changes in pore volume distribution due to the soil managements, *i.e.*, application of different fertiliser and manure in the long-term experiments. A common result is an increase in the proportion of larger pores with the SOC content which would mean an **increase** in median pore size if no other aspect of the pore size distribution changes. However, Figure 5.5 and Table 5.2 show that the median pore size **decreases** with soil organic carbon content.

The data in Figures 5.3 and 5.4 show that FYM and nitrogen treatments have increased the numbers of smaller pores and have also increased the bulk porosity. The increase in bulk porosity with SOM observed from water retention is demonstrated further using different methods of soil compression and acoustic reflection in chapters 6 and 7.

Table 5.2 *Parameters of pore volume distribution of Broadbalk and Hoosfield repacked soil samples derived from water release curve. Statistical analyses are in appendix 1.*

Site	Soil treatment	SOC, g/100g	Soil pore diameter	
			d_{mode} (µm)	d_{median} (µm)
Broadbalk (BK)	FYM	2.959	56	9
	Nil	0.847	106	5
	PKMg	0.915	603	172
	N1(P)KMg	1.078	157	78
	N2(P)KMg	1.156	134	78
	N6(P)KMg	1.265	372	91
Hoosfield (HB)	FYM since 1852	3.650	104	26
	FYM since 2001	2.181	189	56
	FYM from 1852-71	1.454	261	131
	N(P)K(Mg)	0.991	451	89

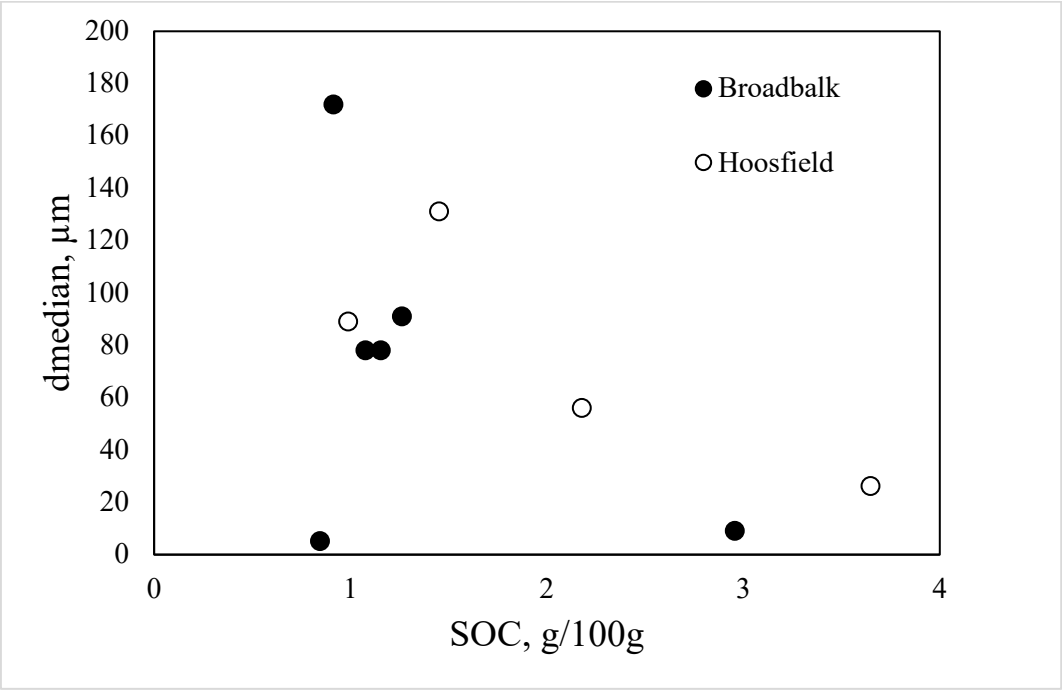

Figure 5.5 *Median pore size (d_{median}) with different Soil Organic Carbon (SOC).*

The water release data for the N treatments, are plotted in Figure 5.6. These soils have SOM contents which are not significantly different from each other. These data show that increased N levels lead to increased drainage at high matric potentials and hence a greater number of larger pores.

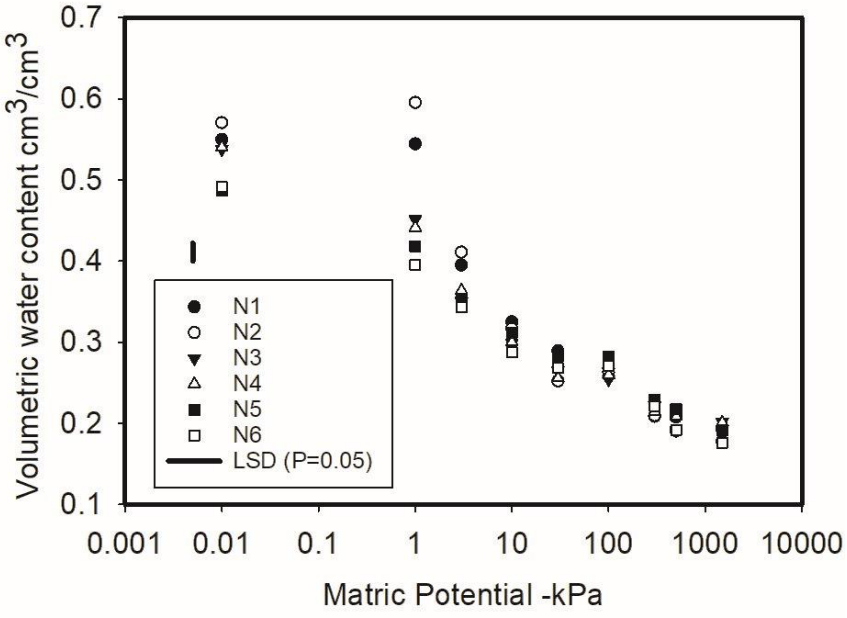

Figure 5.6 *Water retention data for the N treatments of Broadbalk including N1(48 Kg N per ha), N2 (96 Kg N ha^{-1}), N3 (144 Kg N ha^{-1}), N4(192 Kg N ha^{-1}), N5 (240 Kg N ha^{-1}) and N6 (288 Kg N ha^{-1}).*

Particularly interesting is that the N1 and N2 treatments show no drainage between saturation (–0.01 kPa) and -1kPa, whereas all of the treatments with higher N rates demonstrate drainage of pores. It can be concluded that in the N1 and N2 treatments, based on the Laplace-Young equation, there are few pores with a radius greater than approximately 135µm. In the treatments with higher N rates there is significant drainage of water from pores with a radius greater than 135µm. When the soils were prepared, a pressure of 10 kPa was applied to the surface. This is a relatively low applied pressure equivalent to that which might be applied by an all-terrain vehicle. However, even this low pressure resulted in the loss of pores with a radius greater than 135µm in the N1 and N2 treatments (Figure 5.3). The protective effect of higher N rates on larger pores is likely to be related to increased root activity and associated higher rates of root exudation. Exudates are known to strengthen soil because of their stimulating effect on microbial activity [203]. As the soil was sieved and repacked before the water release measurements, the preservation of larger pores in the

higher N treatments is not likely to related to the alteration of soil structure in the immediate vicinity of the roots [204].

5.5 Conclusion

Long-term agricultural treatment with soil organic matter can cause significant changes in soil water release characteristics (SWRC). It has also significant impact on pore size distribution. This study has shown that although soil organic matter increases bulk porosity, it decreases median pore diameter since the increased proportion of smaller pores due to SOM more than compensates for the associated increase in larger pores. Also, the water retention data indicate that nitrogen fertiliser application has more or less the same effects on pore size distribution since the SWRC for all nitrogen applications are quite similar.

Chapter 6. Soil mechanics

6.1 Introduction

Soil mechanics is the part of soil physics that studies mechanical behaviour of soil including soil strengths, stresses. An agricultural soil can be modified due to farming activities. For instance, different agricultural activities influence soil strength, the stresses acting on the soil matrix, soil compaction and consolidation. So, it is very important to explore consolidation behaviour and mechanical strength of soil, especially, for agricultural soil. Several studies have described the mechanical behaviour and critical state of agricultural soils [129, 230, 231, 232]. Moreover, understanding and predicting soil mechanical behaviour is quite complicated as the soil is a heterogeneous mixture of solid particles, liquid and gas and a stress-dependent particulate material. There are too few data that allow an understanding of how soil organic matter, and hence management, affect the critical state parameters.

As it has been hypothesised whether the agricultural managements have impacts on soil mechanical characteristics, this thesis focuses on the relationship between compaction and mechanical behaviour of soils in long-term agricultural managements and the impact of SOM on this relationship. So, this chapter presents some research on soil compaction due to farm activities including the mechanical and compression characteristics of soil and how SOM influences its stress-strain functions using samples from the Rothamsted long-term experiments. After discussing some of the mechanical parameters of soil mechanics such as consolidation behaviour, compression index and soil strength, the measured effects of soil organic matter on these parameters are presented.

6.2 Measurement methods and materials

Some classical methods have been used to derive the mechanical properties of the soil samples of interest. To observe consolidation behaviour of soil, both uniaxial and triaxial compression tests were conducted and to measure mechanical strength of soil,

an indirect tension test method was used. All the measurements were done in the soil physics lab at Rothamsted Research, Harpenden.

6.2.1 Consolidation behaviour of soil

6.2.1.1 Uniaxial compression test

Uniaxial compression tests were done using an Instron 5944 Load frame (UK) running with Instron Bluehill Universal v4.03 software, as described by Gregory *et al.* [205]. The soils were packed into plastic rings (inner diameter 46 mm, height 20 mm) with mesh underneath using pneumatic pressure chamber at a very low compression (10 kPa). The soil samples were saturated overnight and equilibrated at -10 kPa matric potential on a tension table for 7 days. Then the soils were placed on the loading frame (Instron Compression Instrument). The soil samples were compressed with a uniaxial load at a rate of 100 kPa per minute up to 2 kN (maximum load = 1.95 kN). The software recorded time (s), vertical displacement (mm), force (kN), compressive stress (MPa) and compressive displacement (mm). After the compression tests the soil samples were dried at 105 ºC for 48 hours. Soil samples from N1(P)KMg treatment plot of Broadbalk were not compressed due to the shortage of samples.

6.2.1.2 Triaxial compression test

The consolidated-drained (CD) test was used on saturated soils. Triaxial deformation quantifies the normal consolidation curve (NCL)

$$e = N + \lambda \log(\sigma) \tag{6.1}$$

and the critical state line (CSL)

$$e = N' + \lambda' \log(\sigma) \tag{6.2}$$

where σ is the mean effective for triaxial compression and total stress for uniaxial compression which is described earlier in section 6.2.1.1, N and N' are constants, λ and λ' are slopes of NCL and CSL, respectively, on log-linear plot and λ is also described as compression index. The void ratio, e, can be defined by,

$$e = \frac{V_f}{V_S} \tag{6.3}$$

where V_f is volume of pore space or void (cm^3), and V_s is volume of soil solid (cm^3) [8].

The normal consolidation characteristics and the critical state behaviour of the repacked soil sample were determined by Bishop and Wesley triaxial cell (GDS Instruments, Hook, UK) as described by Chakraborty *et al.* [11]. The soils were repacked into a split-part mould with dimension of 50 mm inner diameter (ID) and height of 100 mm, in approximately six layers with an axial pressure of 10 kPa with a pneumatic pressure press. A membrane suction stretcher was used to place the rubber membrane around the soil. The soil sample surrounded by rubber membrane was placed in position on the pedestal of the triaxial apparatus. The triaxial cell and other components were assembled following placement of soil sample. The cell was fitted with deionized water while pressure/volume controllers were connected. First, the docked sample was saturated with effective mean stress 10 kPa for 24 hours. This process was done by increasing both cell and back pressure with a difference of 10 kPa up to 600 kPa. The saturation process was conducted to ensure all voids within the test sample were filled with water. Then the sample was consolidated to an effective mean stress. Four different effective mean stresses were applied to the samples *i.e.*, 50 kPa, 150 kPa, 300 kPa and 600 kPa. The sample was consolidated to bring the specimen to the effective stress state required for shearing. The shear deformation was conducted by decreasing the cell pressure whilst maintaining a constant back pressure. The final volume of the soil specimen after shear test was measured by oven-drying the sample at 105°C for 48 hours to determine the mass of water and solid, converted to volumes. The volume of water of the consolidated soil specimen corresponded to the volume of pores in the soil. The volume of soil, V_s was calculated from particle density (ρ_s) as soil particle density is an important soil property for calculating soil porosity (void ratio) parameters [167].

$$\rho_s = \frac{M_s}{V_s} \tag{6.4}$$

where, M_s *is* mass (weight) of soil solid after oven dry [8].

The NCL (normal consolidation line) and critical state line (CSL) for each soil sample was determined with four different compression pressures (50, 150, 300 and 600 kPa) by independent tests.

6.2.2 Mechanical strength of soil (Indirect tensile strength measurement)

The tensile strength of soil is generally considered to be a sensitive measure of soil structure [215]. In this study, the Brazilian splitting method (Indirect tension test) was used to investigate soil tensile strength. Small cylindrical plastic cores with dimension of 29 mm in diameter (ID) and 15 mm in height, were packed with soil samples under 15 kPa pressure in a hydraulic chamber. Three replicates of each sample were prepared. The soil core samples were then saturated and equilibrated at -15 Bar for 36 days. After equilibration, the dimension of soil discs was measured, and they were stored in zipped-locked poly bags to avoid evaporation.

The tensile strength of soils was measured by compressing the soil discs throughout the diameter using Davenport DN Nene compression testing systems with the load speed of 1 mm/min. The compression load until failure of the soil samples was recorded by the computer connected balance software 'Sarah'. The tensile strength can be described as the stress applied per unit area at failure of soil disc under tension. The stress (σ) can be determined as

$$\sigma = 100 \times \left(\frac{2F_{max}}{\pi DL}\right) \quad (6.5)$$

here F_{max}=the applied load at failure (Kg), D=the diameter of soil disc (mm) and L= length of soil disc (mm) [81].

6.2.3 Data and statistical analysis

All statistical analyses of collected data were carried out using GenStat V17. Data were analysed with ANOVA and grouped regression analysis. Deformation testing in the triaxial cell was randomised according to both the soil treatment and the final pressure during normal

consolidation. The testing procedures of all soil samples were then conducted according to a prearranged test sequence of 40 independent tests.

6.3 Results obtained from different methods

6.3.1 Result from uniaxial compression test

The compression index values of soils from uniaxial tests are shown on Table 6.1. From this result, some evidence of relationship between compression index and soil organic carbon (SOC) was found.

Table 6.1 *Compression indices of sampled soils with statistical analysis (regression with their respective SOC content) derived from uniaxial compression test.*

Source	Soil treatment	Compression index	Statistics	
			F probability	s.e.
Broadbalk	FYM	0.391	0.03	+/- 0.047
	Nil	0.288		
	PKMg	0.288		
	N2(P)KMg	0.248		
	N3(P)KMg	0.301		
	N4(P)KMg	0.179		
	N5(P)KMg	0.280		
	N6(P)KMg	0.351		
Hoosfield	FYM since 1852	0.343		
	FYM since 2001	0.327		
	FYM from 1852-71	0.248		
	N(P)K(Mg)	0.259		

6.3.2 Results from triaxial test

The initial density, prior to triaxial testing depended on SOC and ranged from approximately 1.0–1.2 g cm^{-3} for samples with the highest to the lowest SOC, respectively. Following triaxial testing, the void ratio of different soils is plotted against logarithm of effective mean stress for deformation observed before and after shear to obtain NCL and CSL (see Figures 6.1 of Broadbalk and 6.2 of Hoosfield). According to these Figures, soil samples from the FYM plot of Broadbalk show the high void ratios through the compression and deformation process. However, the lowest values were observed from soil samples from the Nil plot.

Figures 6.1 and 6.2 show that all soils reacted differently at the normal compression and shear stresses.

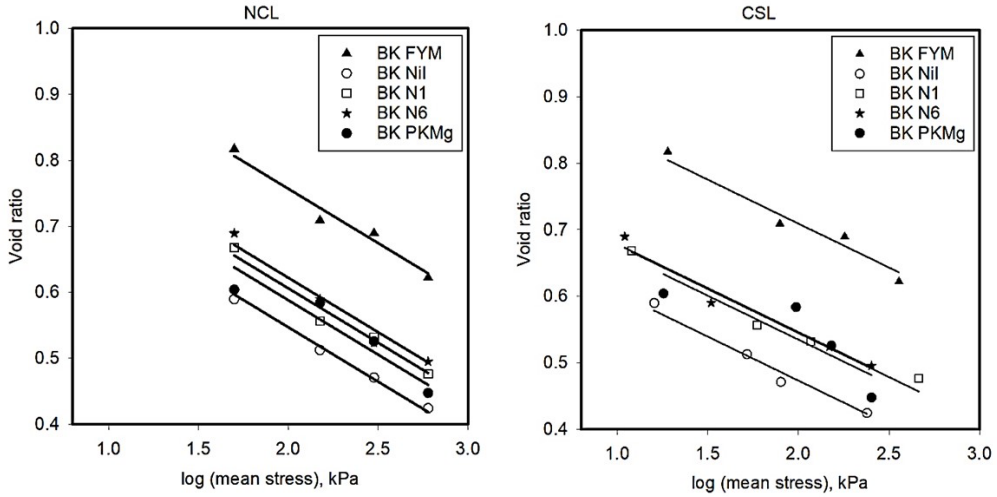

Figure 6.1 *Normal consolidation (P<0.001; s.e.d=0.01; Var. = 0.968) and Critical state lines (P<0.001; s.e.d=0.02; Var. = 0.952) for Broadbalk soils shows the similar slopes with different intercepts (void rato).*

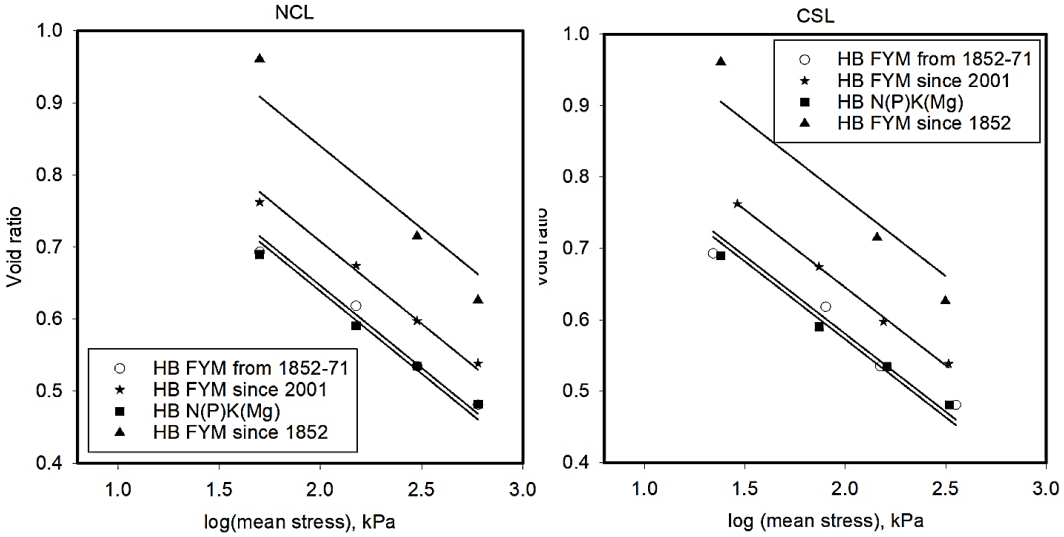

Figure 6.2 *Normal consolidation (P<0.001; s.e.d=0.008; Var.= 0.995) and Critical state lines (P<0.001; s.e.d=0.01; Var. = 0.992) for Hoosfield soils.*

Grouped regression showed that the data could be described by a set of parallel curves with different intercepts when analysed with Genstat® (Table 6.2). Different slopes were needed to explain the effects of soil type (*i.e.*, Broadbalk or Hoosfield) as well as for the NCL and

CSL conditions, although all the slopes (for both NCL and CSL) were similar in value (Table 6.2). O'Sullivan *et al.* [206] found that CSL lines showed greater slope than NCL.

Table 6.2 *Parameters of the NCL and CSL estimated from linear regression while group regression explained 90 percent of variance in void ratio.*

Source	**Soil treatment**	**Normal consolidation line (NCL)**		**Critical state line (CSL)**	
		Slope, λ (+/-SE)	Intercept, N (+/-SE)	Slope, λ' (+/-SE)	Intercept, N' (+/-SE)
Broadbalk (BK)	FYM	-0.165 (+/-0.010)	1.087 (+/-0.024)	-0.132 (+/-0.010)	0.973 (+/-0.023)
	Nil		0.877 (+/-0.024)		0.737 (+/-0.021)
	PKMg		0.918 (+/-0.024)		0.799 (+/-0.023)
	N1(P)KMg		0.936 (+/-0.024)		0.809 (+/-0.022)
	N6(P)KMg		0.952 (+/-0.024)		0.810 (+/-0.021)
Hoosfield (HB)	FYM since 1852 (72)	-0.228 (+/-0.016)	1.297 (+/-0.039)	-0.217 (+/-0.016)	1.206 (+/-0.037)
	FYM since 2001 (73)		1.165 (+/-0.038)		1.081 (+/-0.036)
	FYM from 1852-71 (71)		1.103 (+/-0.038)		1.016 (+/-0.036)
	N(P)K(Mg) (42)		1.096 (+/-0.038)		1.008 (+/-0.036)

Among the samples from Broadbalk, the FYM sample has the highest void ratio (0.97 at critical state) whereas the smallest void ratio (0.73 at critical state) was observed from soil samples from the Nil (control) plot. Similarly, on Hoosfield, soil samples from the plot given FYM since 1852 (highest SOM content) show the highest void ratio (1.2 at critical state) (Figure 6.3, Table 6.3).

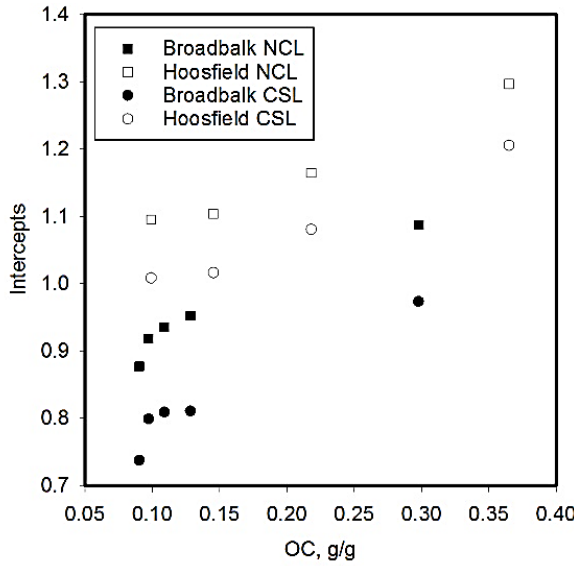

Figure 6.3 *Intercepts of NCL (P<0.001; s.e.d=0.088; Var.= 0.784) and CSL (P<0.001; s.e.d=0.095; Var.= 0.768) with Soil Organic C.*

Table 6.3 *Intercepts vs OC shown in Figure 6.3*

Source	Soil	Slope (+/-SE)	Intercept (+/-SE)	F probability (Grouped regression)
NCL	Broadbalk	1.074 (+/-0.03)	0.7984 (+/-0.05)	<0.001
	Hoosfield	1.837 (+/-0.04)	0.7869 (+/-0.08)	
CSL	Broadbalk	1.139 (+/-0.1)	0.6622 (+/-0.03)	<0.001
	Hoosfield	1.737 (+/-0.2)	0.7233 (+/-0.04)	

The straight lines fitted to plots of mean effective stress against the deviator stress (p-q) diagram are shown in Figure 6.4. While the projection of critical state lines for both soils do not pass-through the origin, the slopes ranging from 0.3 to 0.6 are similar to those reported by O'Sullivan and Robertson [130] for wet soil (0.1 to 0.6). In the stress plane, Hoosfield soil is stiffer than Broadbalk soil.

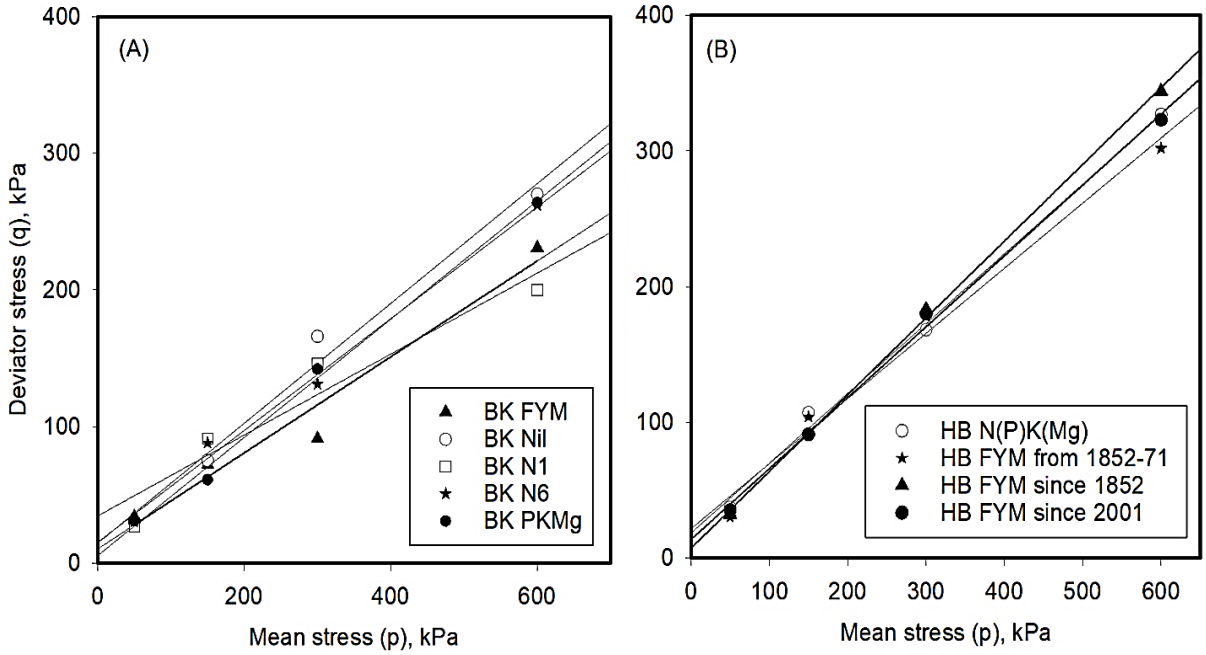

Figure 6.4 *The projection of consolidation behaviour of soils from (A) Broadbalk (P<0.001; s.e.d=0.291; Var.= 0.88)and (B) Hoosfield (P<0.001; s.e.d=0.117; Var.= 0.99) on stress (p-q) plane.*

6.3.3 Results from indirect tensile measurements

Figures 6.5 and 6.6 show the variation in tensile strength of soils from different management practices (Broadbalk and Hoosfield experiment). Samples from Broadbalk Nil and N1(P)KMg plots show the lowest tensile strength. Figure 6.5 shows that tensile strength increases gradually from nitrogen plot N1(P)KMg (lowest N input) to N6(P)KMg (highest N input) from Broadbalk. Soil from the FYM plot in Broadbalk shows a quite similar pattern in tensile strength at as concentration level 4 of nitrogen application (N4(P)KMg). But among the soil samples from Hoosfield, samples from the inorganic fertiliser plot rather than the FYM plots shows higher tensile strength.

The tensile strength of soil depends on how strongly the soil particles bound together. A dense arrangement of soil particles leads to higher tensile strength [207]. According to Zhang *et al.* [208], bonding between soil particles correlate to the mechanical resistance to rupture.

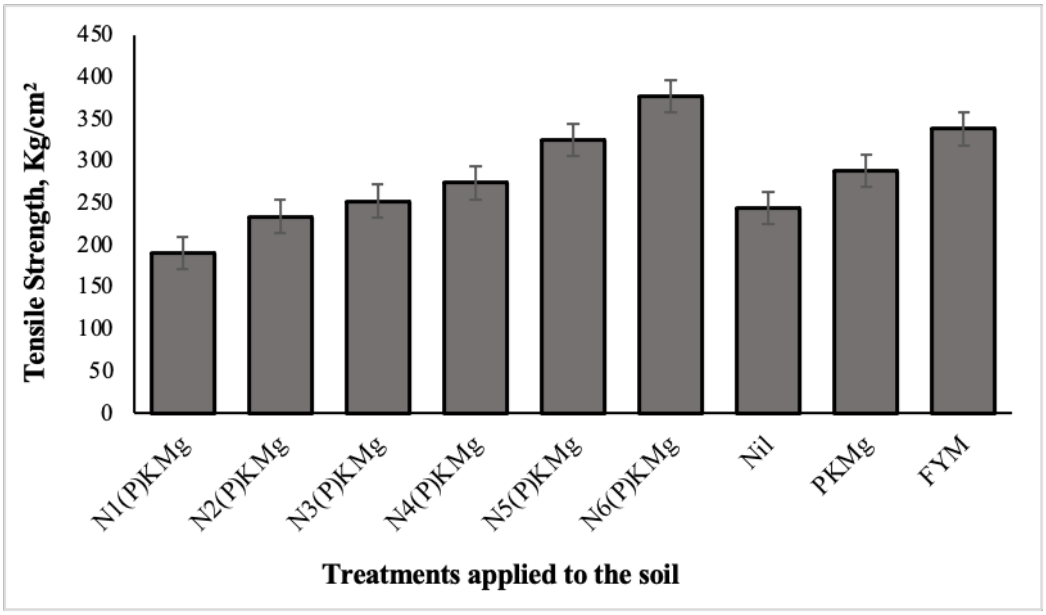

Figure 6.5 *Tensile strength with standard error bar (s.e) of soil samples from the Broadbalk Wheat experiment (F= 10.04; P<0.001) showing a positive correlation between tensile strength and the rate of nitrogen applied (P<0.001; s.e.d=0.039; Var. = 0.706).*

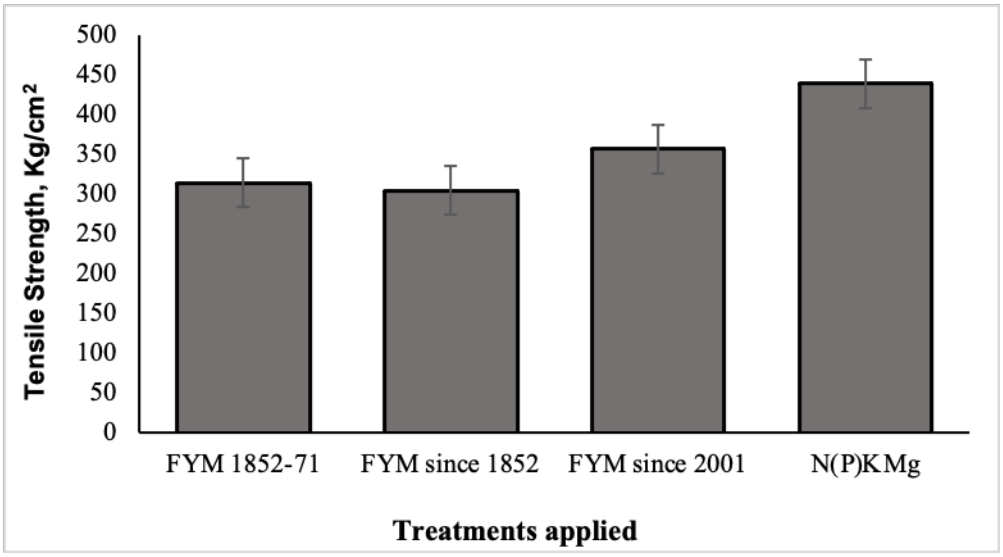

Figure 6.6 *Variation of tensile strength with treatments showing the standard error bar across soil samples from the Hoosfield experiment (F= 4.44; P<0.05).*

6.4 Discussion

Zhang and Hartge [16] reported inconsistent accounts of the effects of soil organic carbon on soil compression index. Some previous data from uniaxial compression tests of repacked soil samples with different clay content ranging from 14 to 75%, equilibrated at -5 kPa matric potential, reported by Gregory *et al.* [205], shows that compression index increases with clay

content and organic matter content. Although, it should be noted that soil organic carbon and clay content are correlated. These data are summarised in Table 6.4.

Table 6.4 *Compression index (in Figure 6.7) of different soils from Bedfordshire, UK by axial compression with other selected properties [205].*

Soil	**Location**	**Sand** (0.06-2 mm)**, g/100g**	**Silt** (0.002-0.06 mm)**, g/100g**	**Clay (<0.002 mm), g/100g**	**SOC, g/100g**	**Compression index** (estimated by Gompertz model)	
						0-100 kPa	**0-200 kPa**
Calcareous pelosol	Boot Field I	9.8	14.3	75.8	4.4	1.411	1.210
	SRC	39.4	19.5	41.2	3.6	1.191	1.001
	Clover Hill	9.8	19.2	71.0	5.1	1.328	0.999
	Long Shot	31.9	15.7	52.4	3.8	1.221	0.809
Brown sand	Cashmore II	48.9	14.6	36.5	3.2	0.837	0.697
	East Drive	69.7	13.9	16.4	1.4	0.629	0.528
	Burton's Gate	68.0	17.9	14.2	1.7	0.606	0.547

These data are compared with those from the present study in Figure 6.7. Although the slopes are significantly different, both sets of data show positive correlations between compression indices and soil organic carbon (SOC) content.

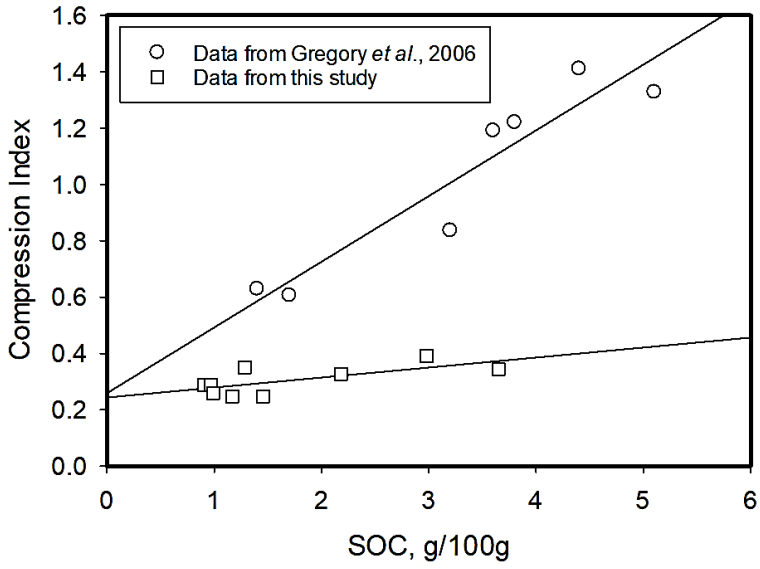

Figure 6.7 *Comparison of the data obtained from uniaxial compression of repacked clay loam (Broadbalk) and silty clay loam (Hoosfield) soils equilibrated to -10 kPa matric potential ($P<0.05$; s.e.d=0.047; Var. = 0.303) with data from Gregory et al. [205].*

Uniaxial compression tests reported by Keller *et al.* [209] have found that the compression index was independent of organic matter, but it was dependent on the initial void ratio. However, they used a uniaxial test where drainage of initially wet soils (at ψ=-100hPa) was needed for consolidation to occur. It was found also that the compression index depended on initial void ratio [205], for the same soils as tested in the research presented in this study. It is possible that soils with higher void ratio were more compactable because drainage is closely correlated with void ratio [100]. Another study using similar compression tests by Arthur *et al.* [210] has found a positive relationship between the initial void ratio and compression index. Interestingly, in a comparison of three agronomic treatments (mixed forage cropping, mixed cash cropping and cereal cash cropping) which had different soil organic carbon content (*i.e.*, organic matter contents of 2.1, 1.4 and 1.0 g/100g respectively), but similar textures, it was found that the treatment with higher organic matter had the smaller compression index and concluded that soils with higher soil organic matter content were better able to resist changes in bulk density [210].

The uniaxial compression experiment conducted on Rothamsted soils *i.e.*, FYM and PKMg of Broadbalk, which is rapid compared to the triaxial compression, so includes the effects of pore pressure due to insufficient time for drainage. Consequently, in these uniaxial compression tests, compressibility might depend on SOM, by its effects on Ksat. So, the data reported here from the more rapid uniaxial compression tests of initially wet soil, may reflect differences in hydraulic conductivity rather than in intrinsic mechanical property.

In this study, no effect of soil carbon content on the compression index was found, when obtained from a slow drained triaxial test. For triaxial compression, the compression equation is

$$e = \lambda \, Log_{10} \, P + N \tag{6.6}$$

Compressibility for the Broadbalk and Hoosfield soils depends only on the applied pressure, and it is not affected by organic matter content.

$$\frac{de}{dP} = \frac{\lambda}{P \ln (10)} \tag{6.7}$$

where e is void ratio and P is the applied pressure. According to grouped regression, λ is the same for all soils. However, the actual porosity and initial pressure do depend on SOM. Note that here P is effective stress, and it does not include pore pressure.

This study compared the compression characteristics, obtained from drained tests, of soils with a similar particle size distribution, but with a range of SOCs. Following compression soil samples were sheared at a constant volume. And it was found that for Broadbalk and Hoosfield soils, the slope of the compression characteristic, or the compression index, depended on the source of the soil (*i.e.*, Broadbalk or Hoosfield), but not on the amount of organic carbon in the soil (Table 6.2). The compression indices for the NCL and CSL for Hoosfield and Broadbalk were similar, although O'Sullivan *et al.* [206] reported higher compression index for CSL lines than NCL. The change in void ratio due to an increment in effective stress can be written as

$$de = \Lambda \frac{d\sigma}{\sigma} \tag{6.8}$$

where Λ is a lumped parameter (plastic compression index) that takes account of total and elastic strain during compression [211]. Results from this study show that for a given soil texture, Λ is constant and does not depend on organic matter content. According to the analysis of McDowell *et al.* [211], for soils with particles a low variability in particle strength, a similar slope in the compression characteristic implies a similar fractal dimension. The question arises, what is a particle? In an agricultural context, the compression pressures of no more than 1 MPa are small compared with up to 10 MPa or greater which are frequently used in civil engineering studies [212, 213]. For 0.5 mm quartz grains to fracture approximately 50 MPa will be needed. In this study, 4 compression pressures ranging from 0.05 MPa (50 kPa) to 6 MPa (600 kPa) were used. Thus, in this study, a particle can be conceptualised as transient collection primary particles (or aggregates) held together by organic matter, which break into smaller units with increasing pressure. McDowell *et al.* [211] further explain that

$$\Lambda \, \alpha \, \Gamma^{1-m(D-1)/4} \tag{6.9}$$

Where Γ is the surface free energy, m is the Weibull modulus and D is the fractal dimension. Our data imply that all these parameters are independent of soil organic matter. However, the void ratio of soil does depend on organic matter content. Figure 6.8 shows that the void ratio of soil in normal consolidation at an effective stress of 200 kPa (i. e., 200 kPa can be equivalent pressure applied by farm vehicles on arable soil) is closely correlated with the soil organic carbon content. Although the void ratio depends closely on organic matter, at a given effective stress, an additional increment in effective stress will give the same reduction in void ratio in all the soils that have been tested according to equations 6.8 and 6.9, albeit that Λ will depend on the soil type (Broadbalk or Hoosfield).

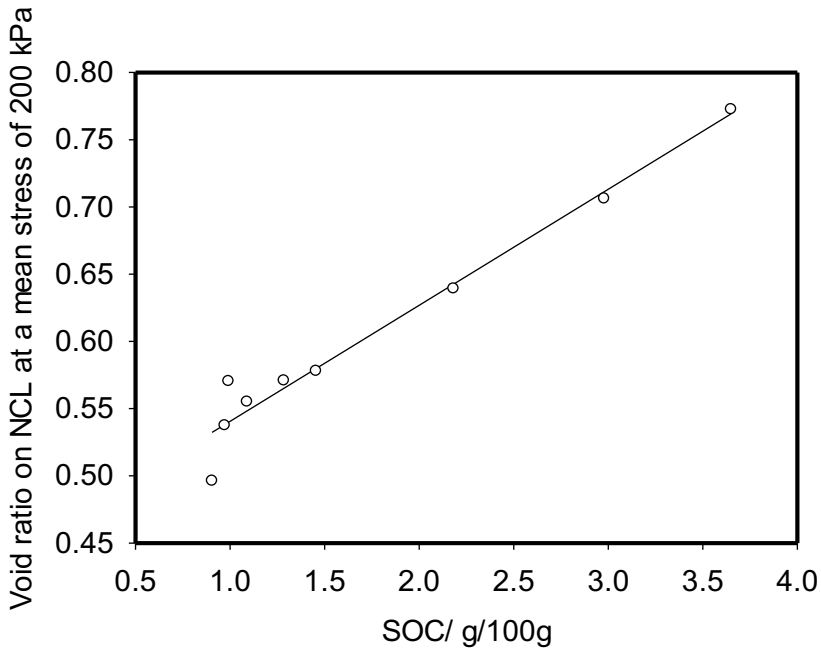

Figure 6.8 *The void ratio of soil in normal consolidation an effective stress of 200 kPa plotted against soil organic carbon (P<0.001; s.e.d=0.037; Var. = 0.861).*

McDowell [214] showed the fractal compression was consistent with a compression characteristic written in the form

$$\ln(e) = \ln(e_y) - \frac{1}{2b}\ln\left(\frac{\sigma}{\sigma_y}\right) \tag{6.10}$$

where e is the void ratio. The parameter *b* defines the rate at which average particle strength increases with decreasing size and given the slope of the compression characteristic is independent of organic matter, the same is true for *b* (Table 6.5) which was not correlated with soil organic matter. It is implicit that irrespective of the void ratio similar patterns of aggregate failure occur. This suggests that the structures that confer strength to aggregates are similar at all size scales.

Table 6.5 *Parameters from ln(e) vs ln(σ) relationship.*

Source	Soil treatment	Slope, 1/2b	Estimated $\ln e_y$	Calculated $\ln e_y$
Broadbalk (BK)	FYM	0.105	-0.048	-0.184
	Nil	0.131	-0.176	-0.346
	PKMg	0.132	-0.155	-0.308
	N1(P)KMg	0.137	-0.127	-0.298
	N6(P)KMg	0.118	-0.109	-0.289
Hoosfield (HB)	FYM since 1852	0.171	0.021	-0.231
	FYM since 2001	0.141	-0.082	-0.290
	FYM from 1852-71	0.150	-0.107	-0.316
	N(P)K(Mg)	0.144	-0.103	-0.291

Rahimi *et al.* [216] reported that the soils with a higher content of organic matter show increased tensile strength. In another study, Causarano [122] investigated the relationship between tensile strength and organic matter in the case of clay soils with 1.3%–10.4% soil organic matter and reported that SOM increases the tensile strength of moist soil aggregates and decreases the tensile strength of dry soil aggregates. This study found no relation between SOM and soil strength, but application of nitrogen fertilizer showed positive relation with tensile strength of soil (F value for simple linear regression is <0.001 with 95.9% of variance), when analysed by Genstat®. According to Hallet *et al.*, [217] tensile failure occurs due to the propagation of cracks in the stressed sample. For a moist soil, stress concentration takes place in the air-filled cracks and pores. The water-filled pores have no stress concentration because the load is uniformly borne by the pore water [218].

6.5 Summary

Data presented in this chapter show that the results from more rapid uniaxial compression tests of initially wet soil, may reflect differences in hydraulic conductivity rather than in intrinsic mechanical property. On the other hand, in case of triaxial compression, the void ratio of the soils depends on soil organic carbon but not on the compressibility. This has not been reported previously. Moreover, it seems that the effects of soil organic carbon on strength do not depend on scale, but N application rates are positively corelated to the soil tensile strength. Overall, it seems application of SOM (FYM) to be beneficial treatment in

respect of porosity and soil compaction for both experiments.

Chapter 7. Using acoustics to investigate soil pore networks

7.1 Introduction

So far acoustical methods are not used widely to study soils. In principle they offer an opportunity to make non-contact *in situ* measurements and thereby, observe the characteristics of undisturbed soils. But, given the inhomogeneity of the soils in the long-term experiments at Rothamsted it has been preferable to make laboratory measurements on sieved repacked soils from extracted cores. In principle also acoustical measurements can be used to give information about the elastic moduli of the soil frame [226] and thereby, relate more closely to the measurements reported in Chapter 6. However, this Chapter reports non-contact laboratory measurements of the normalised acoustic surface impedance or admittance (inverse of impedance) of a soil using an impedance tube. Essentially such measurements investigate the acoustical influence of the soil pore network rather than of the granular frame which is assumed to be acoustically rigid. The acoustic surface admittance (β_s) of a rigid-framed porous solid is sensitive to the structure of its pore network. For soils it depends also on the degree of compaction and the moisture content [141]. This chapter describes measurements of acoustic impedance of soil samples and how they have been used to deduce the influence of SOM on the soil pore network.

7.2 Materials and methods

7.2.1 Sample preparation

The soil samples intended for the impedance tube measurements were partially saturated by adding water by weight based on their water retention curves (discussed in chapter 4). The soil samples were air-dried and passed through 2 mm mesh sieve. The initial water contents in these air-dry soils are very low and quite similar. The water content for Nil, FYM, N3(P)KMg (144 Kg N/ha) and N6(P)KMg (288 Kg N/ha) air-dry samples are 1.8%, 2.6%, 1.9% and 1.9% respectively. All partially saturated soils were allowed to equilibrate for at least 24 hours in air-tight plastic bags at a

constant temperature to prevent evaporation before impedance tube measurements. By using a pneumatic pressure chamber immediately before the measurements, the dry and moist samples were packed to different densities into a sample holder with a hard base specially designed to fit in the impedance tube. The thickness of the soil samples was about 4 cm.

7.2.2 Impedance tube measurement

In this study, a three microphone Bruel & Kjaer 100 mm impedance tube (Type B&K 4206) was used**,** operated in the wide-spacing mode (100 mm microphone spacing) in the frequency range between 50 and 1600 Hz, connected to a National Instruments data acquisition system. Measurements were made to investigate the influence of organic content at different moistures and compactions on absorption coefficient spectra in a similar way to that described by Horoshenkov and Mohamed [140]. The impedance tube was set up vertically by screwing on to a laboratory wall shown in Figure 7.1. The 100 mm inner diameter sample holder including the soil sample to be tested was clamped to the impedance tube.

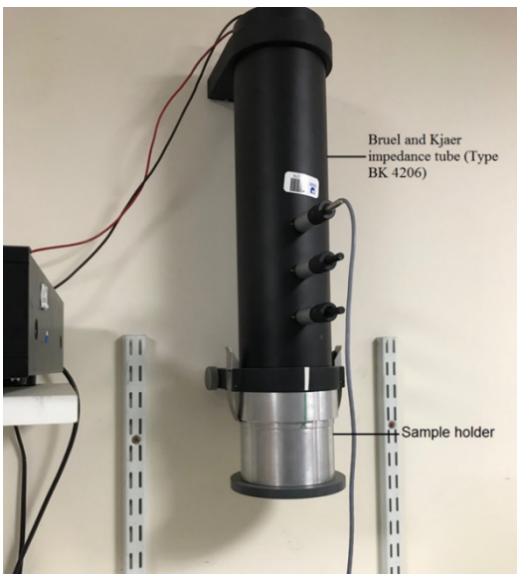

Figure 7.1 *Vertical impedance tube set up.*

A single microphone method (see Chapter 2) was used with a white noise signal to measure the transfer function of the acoustic pressure between two different positions in the measurement tube with the same microphone. The reflection coefficient at the reference plane is estimated from the transfer function. Finally, the impedance and normal incidence absorption coefficient are calculated from the reflection coefficient. The use of the same microphone for measuring the pressure at the two different positions does not require a relative calibration between two microphones. This study was conducted in a laboratory at Rothamsted Research, UK.

Some measurements were also made using 5 cm thick fine sand samples with different moisture content to compare with the published results [140].

7.2.3 Data analysis

The data acquisition, processing and analysis were carried out with MatLab® codes. And the statistical analysis of the collected data was done by Genstat® V20. T test (one sample T test) was done for both sand and soil data.

7.3 Results and discussion

7.3.1 Results with sand samples

Initially, measurements were made on 50 mm thick fine sand samples with different moisture content. The results (Figure 7.2) show that as the percentage of water in sand increases, the absorption gradually decreases, in agreement with Horoshenkov and Mohamed [140].

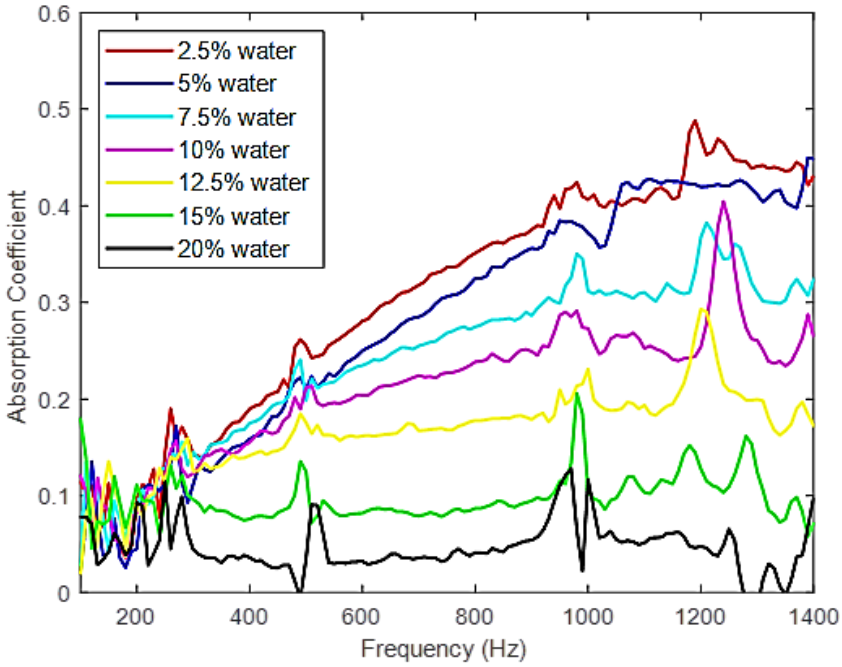

Figure 7.2 *Absorption coefficient spectra of fine sand samples with different water content (t=5.17; P<0.05).*

7.3.2 Results from impedance tube measurement

7.3.2.1 Repeatability

First, the repeatability of the measurements was checked. The example absorption spectra in Figure 7.3 show good repeatability between 200 Hz and 1400 Hz.

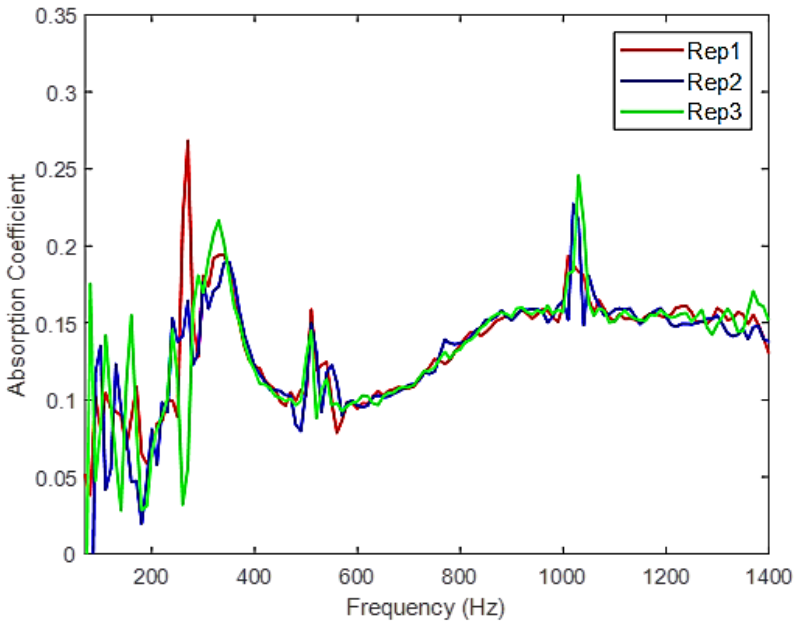

Figure 7.3 *Three absorption coefficient spectra deduced from three measurements (by rotating the sample clockwise) on a soil sample from FYM plot of Broadbalk (SD=±0.002; P>0.05).*

7.3.2.2 Air-dry soils

Results of impedance tube measurements show that air-dried soils (when soils are in stress dependent condition) packed to same density (1.3 g/cm^3), but with different organic matter content give rise to different absorption spectra. For the air-dry soil samples all the nitrogen treatments (even the control sample with no nitrogen) result in higher absorption than obtained for the FYM sample (Figure 7.4).

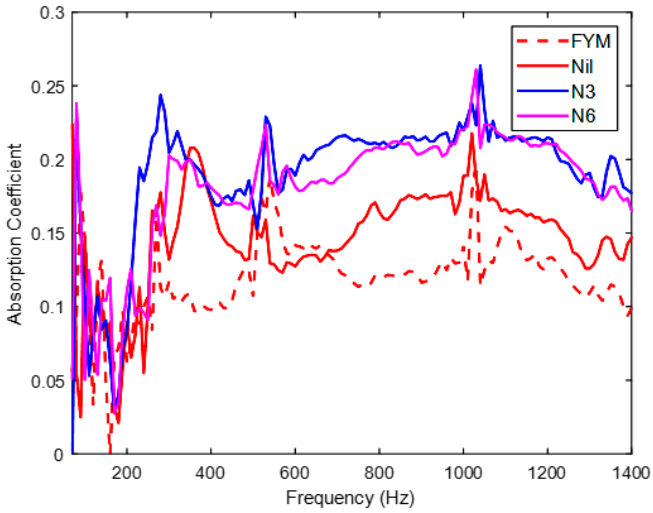

Figure 7.4 *Absorption coefficient spectra of 4 cm thick Air-dry soils with same packing density of 1.3 g/cc (t=8.84; P<0.05). The spikes shown at about 500 Hz and 1100 Hz are resonance peaks associated with impedance tube and not maxima in the absorption.*

On the other hand, when the dry soil samples were packed at 10 kPa pneumatic pressure, which implies lower densities, soil samples with high organic matter (FYM) along with higher nitrogen (N6) show higher absorption (Figure 7.5).

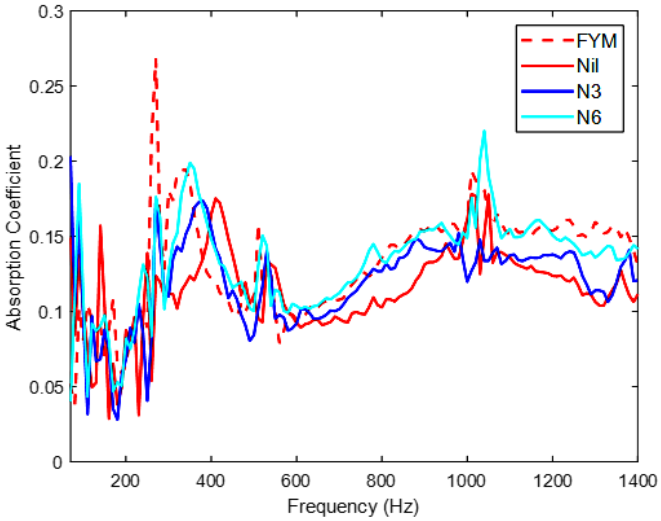

Figure 7.5 *Absorption coefficient spectra for air-dry soil samples packed at 10 kPa pressure (t= 13.43; P<0.001). The peaks at about 500 Hz and 1100 Hz are resonance peaks associated with impedance tube and not maxima in the absorption.*

7.3.2.3 Effects of partial saturation

The absorption of partially saturated (so stress and strain dependent) soil samples from FYM has a strong dependence on water content. The FYM sample has higher absorption than the N6 sample (received high rate of nitrogen) when water content is high and at same matric potential (Figure 7.6). But the same samples with reduced moisture content, *i.e.*, in drier conditions, give higher absorption (Figure 7.7).

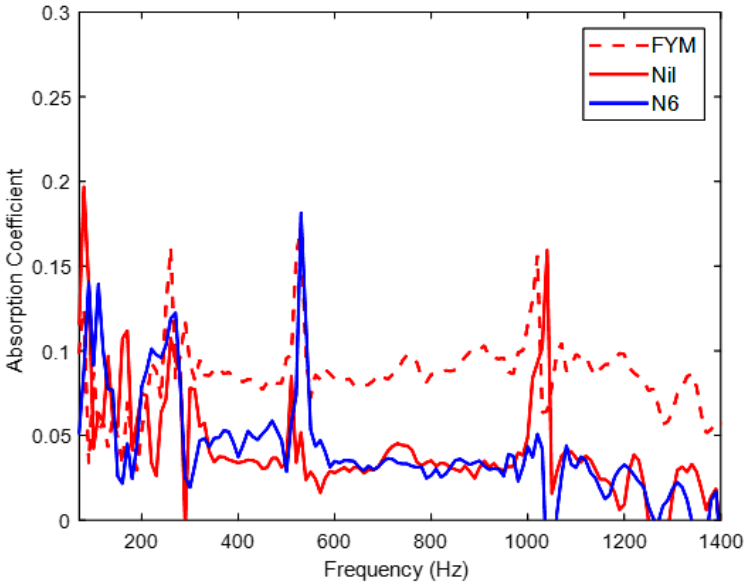

Figure 7.6 *Absorption coefficient spectra of soil samples with moisture content at -300 kPa matric potential and packed to 1.3 g/cc (t=4.58; P<0.05).*

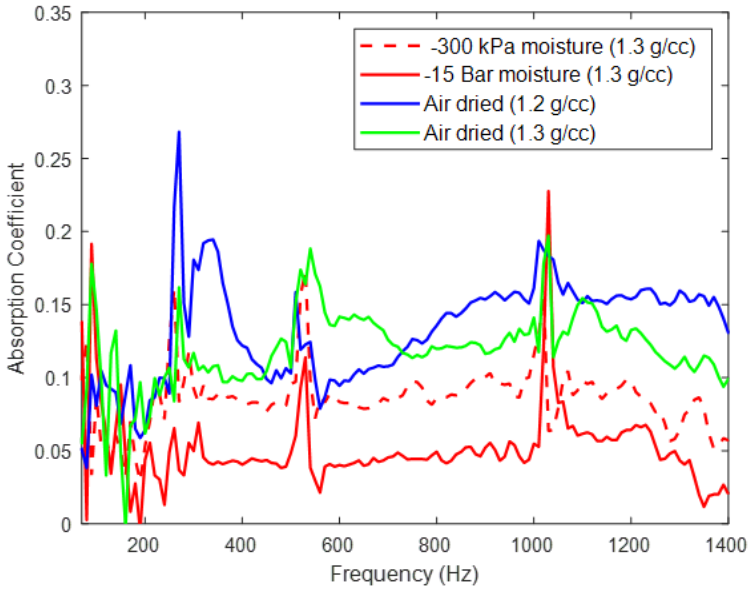

***Figure** 7.7 Absorption coefficient spectra of FYM soil samples with different packing and moisture conditions (t=5.77; P<0.05).*

7.3.3 Discussion

Horoshenkov and Mohamed [140] found that changes in the acoustic surface admittance result from a relatively small change (from 0 to 15%) of the water content in sand as supported by the data in Figure 7.2. It has been observed that organic matter particles fill in the coarse pore fraction to produce a greater number of fine pores and increase total porosity [12].

The increase in measured absorption with organic matter is consistent with the predicted effects of increasing the bulk porosity and permeability on the acoustical properties of a 4 cm thick rigid-porous hard-backed layer because it is compatible with the sample tested. Figures 7.8 and 7.9 show some representative predictions of the effects of changes in porosity and permeability using the Johnson-Champoux-Allard (JCA) model [149, 220] outlined in literature review, section 2.3.2.

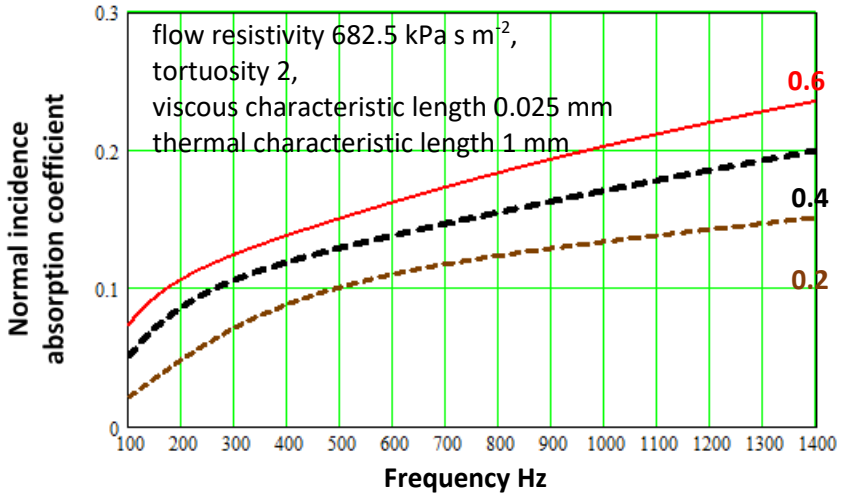

Figure 7.8 *Predicted effect of changes in porosity (assuming constant permeability) on the normal incidence absorption coefficient of a 4 cm thick rigid-porous hard-backed layer to be compatible with sample.*

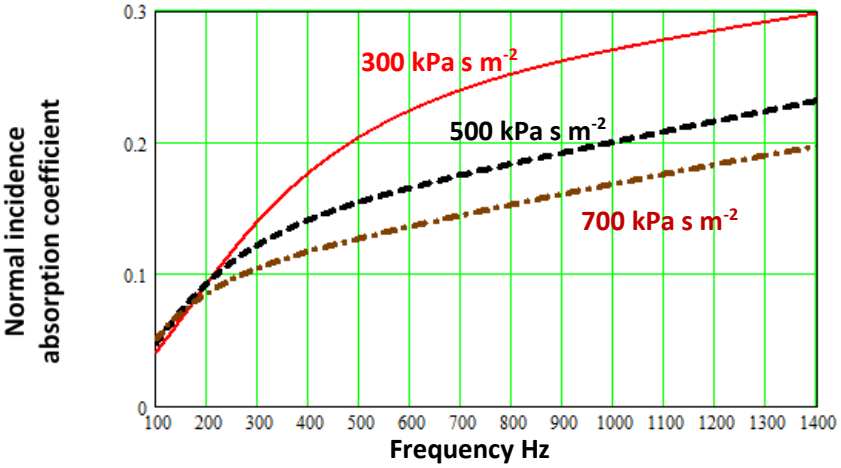

Figure 7.9 *Predicted effect of changes in flow resistivity (viscosity coefficient/permeability) assuming constant porosity 0.4, on the normal incidence absorption coefficient of a 4 cm thick hard-backed layer.*

In making these predictions, no attempt has been made to find best fit parameters for the measured absorption spectra other than to ensure that the predicted absorption coefficients have similar magnitudes to those measured. Furthermore, in the predictions, the characteristic lengths have been kept constant whereas, strictly, they should have been changed also. Nevertheless, these predictions suggest that the

changes in absorption coefficient spectra observed in Figures 7.6 to 7.7 are consistent with the predicted effects of changes in porosity and permeability in a rigid-porous air-filled hard-backed layer.

7.4 Conclusion

Measurements of soil absorption coefficient spectra have been made using a vertical impedance tube. Confirming a previous publication [140], it has been found that the acoustical impedance of soils increases (absorption coefficient decreases) with moisture content. The new result is that absorption coefficient spectra of soils with similar moisture content and packing density also show a strong dependence on SOM. The influence of increasing SOM on absorption coefficient spectra for the soil samples are consistent with predicted effects of increasing porosity and air permeability (according to the JCA model).

Chapter 8. General discussion and conclusion

8.1 Comparison of results obtained from different methods

This study has shown that both long-term organic treatment (FYM) and long-term nitrogen fertiliser treatments can cause important changes in soil properties. The changes have been investigated using classical methods including compression characteristics and critical state, water release and TG analysis together with relatively novel methods including neutron diffraction and acoustic reflection.

According to the TG analysis, the labile portion of SOM and total organic carbon are highly correlated so there is no scope for explanations beyond the total amount of carbon. So, all the results from different measurements have been interpreted in respect of total SOC.

In general, the water release characteristics are consistent with the widely reported effects of organic matter on water retention [36, 192] as water retention increased with increased soil organic matter. According to this study, increasing SOC decreases median pore size while increasing the number of fine pores. However, there were subtle effects of N rate on water retention at high matric potentials which have not been previously reported. It seems that the higher N rates lead to an increase in the number of pores that drain between saturation and a matric potential of -1 kPa. This corresponds to an increase in the number of pores of approximately 30 μm or greater. An increase in the size of these pores will be of value to root growth, due to improved aeration and presumably a lower denitrification rate, and overall improve soil structure. It is important to note that in these soils there was little difference in the soil organic matter content.

The water content at the plastic limit is found to be correlated with the water content at the inflection point of the water release curve (Figure 8.1). While the tested soils had very different structures, it is interesting that such a correlation is found. At the plastic limit the soil is the critical state and during the test cracks occur because air enters the thread of soil that has been rolled. In contrast, in the water release experiment soil has

some structure (repacked in this case) and air enters soil at, or close to, the inflection point. The differences in structure are reflected by differences in water content; the soil samples in the water release experiments have a higher water content.

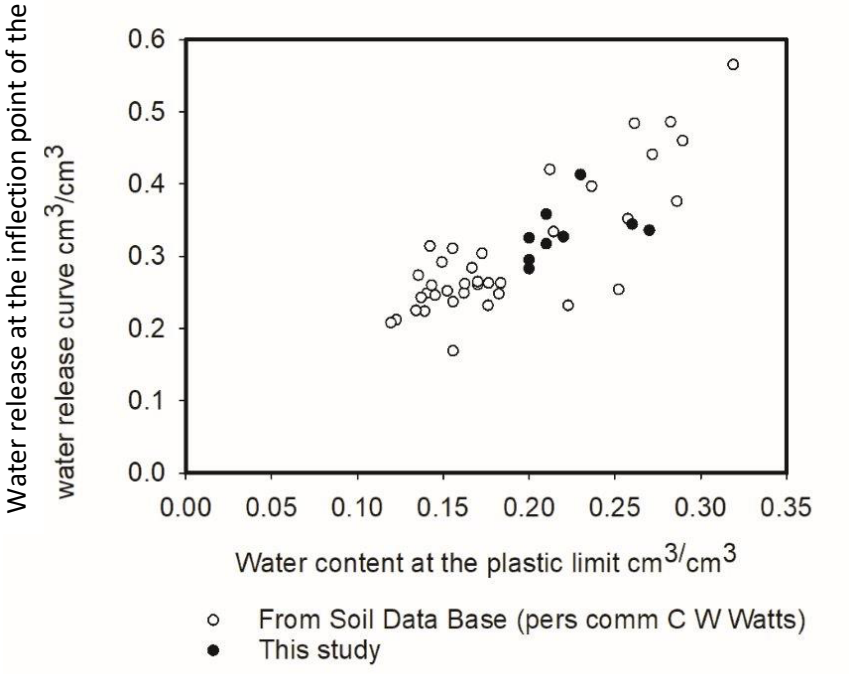

Figure 8.1 *The water content at the inflection point of the water release curve plotted against the water content at the plastic limit. The open circles (○) are data from a Defra funded project led by Dexter and Watts and the closed circles (●) are from this study (P<0.001; s.e.d=0.007; Var. = 0.767)*

Also, it has been observed that soils from different agricultural managements behave differently with respect to their mechanical properties. Differences in the tensile strength in soils from different long-term treatments have been noticed. Soil strengths of nitrogen fertilised soil in Broadbalk showed a positive relation with the amount of nitrogen fertiliser applied, as higher N rates lead to an increase in the number of large pores. According to Munkholm *et al*. [221], soil pore characteristics affect the soil mechanical behaviour, especially when tensile failure occurs. In another study, Guerif [222] found a strong negative correlation between macro-porosity and tensile strength of dry soil.

This study reports evidence to show that the compression index is independent of soil organic matter when the effective stress is used to plot the compression characteristic. By comparison with uniaxial compression data, from the literature, the apparent influence of soil organic carbon on the compression index is more likely to be due to its effect on soil hydraulic properties rather than any intrinsic effects on strength. In this study, no effects of soil carbon (SOC) content on the compression index were found, although void ratio at any particular effective stress was strongly correlated with soil carbon content.

The plastic limit test, based on hand rolling threads of soil, reduces soil structure to the critical state, where structure is only textural. Although the exact effective stress within the rolled thread is not known, the void ratio at the plastic limit is highly correlated with the void ratio at a mean effective stress of 100 kPa and close to a 1:1 relationship (Figure 8.2). The choice of an effective stress of 100 kPa is purely arbitrary but also closely relevant to compression pressure by hand, however, it has little effect in the strength of the correlation which accounts for 90 percent of the variation in the critical-state void ratio. Data from this study (Figure 8.2), suggests the plastic limit test might be a useful approach for comparing the density between different soils or treatments that overcomes the effect of any temporal patterns and is a simple test to allow direct comparison of soil physical behaviour. It seems to have been overlooked by those interested in “soil health”. A more detailed study to establish its predictive capabilities would be of value.

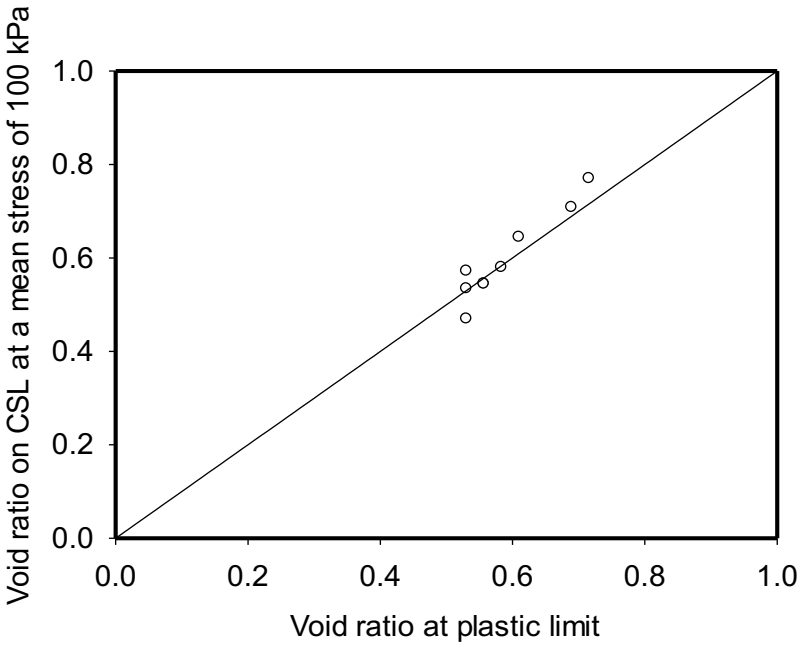

Figure 8.2 *The void ratio for the soil in the critical state at an effective stress of 100 kPa plotted (1:1) against the void ratio of soil at the plastic limit (P<0.05; s.e.d=0.045; Var. = 0.795) in the thread rolling experiment.*

From the impedance tube measurements, it has been observed that soil samples with similar packing density and moisture content, but higher organic matter content show relatively high absorption of sound. Furthermore, it has been confirmed that different levels of moisture content cause variations in the acoustical characteristics of both sand and soil. This study confirms previous work on sand [140], which stated that increasing moisture decreased the sound absorption. Moreover, the acoustical results of increasing organic matter content in soil are consistent with predictions of the effects of increasing porosity and permeability. That organic matter increases bulk porosity is suggested also by the water release data. The impedance tube study reported that measurements of acoustic reflection either in the laboratory or *in situ* could be used more extensively to describe soil health.

However, the common parameters discussed in almost all the experimental chapters is the increasing porosity with increasing SOC due to application of SOM. The SWRC data shows the porosity increases by increasing number of small pores because of SOM content, while the triaxial data explains that addition of SOM increases porosity by

approximately 52 % in FYM plot of Broadbalk and 56% in FYM since 1852 plot of Hoosfield. And the acoustic impedance analysis reports that the porosity increases by about 40% because of FYM addition in Broadbalk soil.

While neutron imaging of soil core samples has been investigated, it did not lend itself to studying the distribution of SOM as had been hoped. The darker areas in the images from neutron tomography (see Figure A3.4 in Appendix 3) could correspond to the high-water content but, alternatively, as the soil samples were air-dried, it could be because of the high SOM content. To find SOM distribution spatially, it would be necessary to check the 'ground truth' destructively.

8.2 Recommendations for future work

The effect of increasing SOM on soil acoustical properties observed in this study could provide the basis future *in situ* use of non-invasive sound reflection for monitoring soil condition. Further work will involve deducing physical parameters from the acoustical data for various soil states and comparing the acoustically deduced values with those obtained by other means.

Subsequently, it might be possible to deduce parameters for a log-normal pore size distribution from the acoustically deduced JCA parameters using the work by Horoshenkov *et al.* [223, 224]. The usefulness of acoustical monitoring might be improved by obtaining an empirical relationship between sound absorption and organic matter content at one or two frequencies, thereby only requiring measurements at these frequencies.

Velea *et al.* [219] investigated the effect of different saturation levels on the speed of compressional and shear waves in soils. A similar study could be carried out to study the influence of SOM on these soil frame wave speeds, possibly, by extending the work of Shin *et al.* [226].

The mechanisms by which application of N fertiliser improves soil structure needs to

be explored further.

The neutron transmission data did not offer sufficient statistical variation to find the mean SOM content. But given that the study has shown that neutron tomography of soil samples is possible, the issues need more study to find a better way to interpret the imaging data and manage the samples, perhaps after an independent (destructive) investigation of ‘ground truth’.

References

[1] D. Tilman, K.G. Cassman, P. A. Matson, R. Naylor, S. Polasky, (2002), 'Agricultural sustainability and intensive production practices', *Nature*, **418** (6898), 671-677

[2] D.C. Reicosky, W.D. Kemper, G.W. Langdale, C.L. Douglas, P.E. Rasmussen (1995), 'Soil organic matter changes resulting tillage and biomass production' *J. Soil Water Conserv*., **50** (3) 253-261

[3] M. L. Jat, C. M. Stirling, H. S. Jat, J. P. Tetarwal, R. K. Jat, R. Singh, S. Lopez-Ridaura, P. B. Shirsath (2018), 'Soil processes and wheat cropping under emerging climate change scenarios in South Asia', *Adv. Agron.*, **148**, 111-171

[4] K. G. Nierop, M. M. Pulleman, J. C. Marinissen (2001), 'Management induced organic matter differentiation in grassland and arable soil: a study using pyrolysis techniques', *Soil Biol. Biochem*, **33** (6), 755-764

[5] Z. B. Guo, G. Yan, R. H. Zhang, F. M. Li, Z. X. Zeng, H. Liu (2010), 'Improvement of soil physical properties and aggregate-associated C, N, and P after cropland was converted to grassland in semiarid Loess Plateau', *Soil Sci.*, **175**(2), 99-104

[6] L. D. Norton, A. Mamedov, C. Huang, G. J. Levy (2006), 'Soil aggregate stability as affected by long-term tillage and clay type', *Proceedings of the Soil Tillage Research Organization International Conference. 17th Triennial Conference, Sustainability-its Impact on Soil Management and Environment, August 28-September 3, 2006*, Kiel, Germany. 1521-1526.

[7] C. J. Bronick, R. Lal (2005), 'Soil structure and management: a review', *Geoderma,* **124**, 3–22

[8] D. Hillel (1998), '*Environmental Soil Physics'*, Academic press, London, WG1X 8RR, UK

[9] W.R. Whalley, E. Dumitru, A.R. Dexter (1995), 'Biological effects of soil compaction', *Soil Till. Res.,* **35** (1-2), 53-68

[10] N. Blair, R. D. Faulkner, A. R. Till, P. R. Poulton (2006), 'Long-term management impacts on soil C, N and physical fertility: Part I: Broadbalk experiment', *Soil Till. Res,* **91** (1), 30-38

[11] D. Chakraborty, C. W. Watts, D. S. Powlson, A. J. Macdonald, R. W. Ashton, R. P. White, W. R. Whalley (2014), 'Triaxial testing to determine the effect of soil type and organic carbon content on soil consolidation and shear deformation characteristics', *Soil Sci. Soc. Am. J,* **78** (4), 1192-1200

[12] B. Zhang, R. Horn, P.D. Hallett (2005), 'Mechanical resilience of degraded soil amended with organic matter' *Soil Sci. Soc. Am. J*, **69** (3), 864-871

[13] B.S. Griffiths, P.D. Hallett, H.L. Kuan, Y. Pitkin, M.N. Aitken (2005), 'Biological and physical resilience of soil amended with heavy metal-contaminated sewage sludge', *Eur. J. Soil Sci.*, **56**, 197-205

[14] A.R. Dexter (1988), 'Advances in characterization of soil structure'**,** *Soil Till. Res.,* **11** (3-4), 199-238

[15] S.H. Anderson, C.J. Gantzer, J.R. Brown (1990), 'Soil physical properties after 100 years of continuous cultivation', *J. Soil Water Conserv*., **45** (1), 117-121

[16] H. Q. Zhang, K.H. Hartge (1995), 'Mechanical properties of soils as influenced by the incorporation of organic matter. *Advances in soil science: Soil structure, its development and function', (Eds K. H. Hartge, B. A. Stewart),* 93-108

[17] H. M. Moore, K. Attenborough (1992), 'Acoustic determination of air-filled porosity and relative air permeability of Soils, *J. Soil Sci*, **43**, 211-228

[18] D. W. Hopkins, I. S. Waite, A. G. O'Donnell (2011), 'Microbial biomass, organic matter mineralization and nitrogen in soils from long-term experimental grassland plots (Palace Leas meadow hay plots, UK)', *Eur. J. Soil Sci*, **62** (1), 95-104

[19] P. Schjonning, B. T. Christensen, B. Carstensen (1994), 'Physical and chemical properties of a sandy loam receiving animal manure, mineral fertiliser or no fertiliser for 90 years', *Eur. J. Soil Sci.*, **45** (3) 257-268

[20] N. Brady, R. Weil (2002), '*The Nature and Properties of Soils'*, 13th Edition, Prentice Hall, New Jersey.

[21] U. Stockmann, M. A. Adams, J. W. Crawford, D.J. Field, N. Henakaarchchi, M. Jenkins, B. Minasny, A. B. McBratney, V. D. de Courcelles, K. Singh, I. Wheeler, L. Abbott, D. A. Angers, J. Baldock, M. Bird, P. C. Brookes, C. Chenu, J. D. Jastrowh, R. Lal, J. Lehmann, A. G. O'Donnell, W. J. Parton, D. Whitehead, M. Zimmermann (2013), 'The knowns, known unknowns and unknowns of sequestration of soil organic carbon', *Agric. Ecosyst. Environ.,* **164**, 80-99

[22] R. S. Antil, M. H. Gerzabek, G. Haberhauer, G. Eder (2005), 'Long-term effects of cropped vs. fallow and fertilizer amendments on soil organic matter I. Organic carbon', *J. Plant Nutr. Soil Sci.*, **168**, 108–116

[23] S. H. Villarino, G. A. Studdert, P. Laterra (2019), 'How does soil organic carbon mediate trade-offs between ecosystem services and agricultural production?', *Ecol. Indic.*,**103**, 280-288

[24] J. L. Hatfield, B. A. Stewart (1998), '*Animal waste utilization: Effective use of manure as a soil resource'*, Lewis publishers, Washington DC.

[25] G. Esser, J. Kattge, A. Sakalli, (2011), 'Feedback of carbon and nitrogen cycles enhances carbon sequestration in the terrestrial biosphere' *Glob. Chang. Biol*, **17** (2), 819-842

[26] R. H. Cong, X. J. Wang, M. G. Xu, W. J. Zhang, L. J. Xie, X. Y. Yang, S. M. Huang, B. R. Wang (2012), 'Dynamics of soil carbon to nitrogen ratio changes under long-term fertiliser addition in wheat-corn double cropping systems of China' *Eur. J. Soil Sci*, **63** (3), 341-350

[27] E. Xu, H. Zhang, Y. Xu, Y (2020), 'Exploring land reclamation history: Soil organic carbon sequestration due to dramatic oasis agriculture expansion in arid region of Northwest China', *Ecol. Indic.*, **108**, 105746

[28] R. Lal (2014), 'Societal value of soil carbon', *J. Soil Water Conserv.*, **69**, 186A–192A

[29] D. W. Reeves (1997), 'The role of soil organic matter in maintaining soil quality in continuous cropping systems', *Soil Till. Res.*, **43**, 131-167

[30] J. Six, H. Bossuyt, S. Degryze, K. Denef, (2004), 'A history of research on the link between (micro) aggregates, soil biota, and soil organic matter dynamics', *Soil Till. Res*, **79** (1), 7-31

[31] J. L. Morel, L. Habib, S. Plantureux, A. Guckert (1991), 'Influence of maize root mucilage on soil aggregate stability', *Plant. Soil*, **136**, 111-119

[32] A. M. Ahmed, E. Kroener, M. Holz, M. Zarebanadkouki, A. Carminati (2014), 'Mucilage exudation facilitates root water uptake in dry soils', *Funct. Plant Biol*, **41,** 1129-1137

[33] C. W. Watts, L. J. Clark, P.R. Poulton, D. S. Powlson, A.P. Whitmore (2006), 'The role of clay, organic carbon and long-term management on mouldboard plough draught measured on the Broadbalk wheat experiment at Rothamsted', *Soil Use Manage*, **22**, 334–341

[34] J. M. Tisdall, J. M. Oades (1982), 'Organic matter and water-stable aggregates in soils', *J. Soil Sci*, **33**, 141–163

[35] C. W. Watts, A. R. Dexter, (1997), 'The influence of organic matter in reducing the destabilization of soil by simulated tillage', *Soil Till. Res*, **42** (4), 253-275

[36] W. R. Whalley, J. To, B.D. Kay, A. P. Whitmore (2007), 'Prediction of the penetrometer resistance of agricultural soils with models with few parameters', *Geoderma*, **137**, 370–377

[37] J. Xu, H. Han, T. Ning, Z. Li, R. Lal (2019), 'Long-term effects of tillage and straw management on soil organic carbon, crop yield, and yield stability in a wheat-maize system', *Field Crops Res.*, **233**, 33-40

[38] B. Majumder, B. Mandal, P. K. Bandyopadhyay, A. Gangopadhyay, P. K. Mani, A. L. Kundu, D. Mazumdar (2008), 'Organic Amendments Influence Soil Organic Carbon Pools and Rice–Wheat Productivity', *Soil Sci. Soc. Am. J.*, **72**, 775-785

[39] J. M. Duxbury, M. S. Smith, J. W. Doran (1989), 'Soil organic matter as a source and sink of plant nutrients', In: D.C. Coleman, J.M. Oades, G. Uehara (eds.) *Dynamics of soil organic*

matter in tropical ecosystem, University of Hawaii Press, USA, 33–67.

[40] E. Lichtfouse, C. Chenu, F. Baudin, C. Leblond, M. Da Silva, F. Béhar, S. Derenne, C. Largeau, P. Wehrung, P. Albrecht (1998), 'A novel pathway of soil organic matter formation by selective preservation of resistant straight-chain biopolymers: chemical and isotope evidence', *Org. Geochem.*, **28**(6), 411-415

[41] M. Schnitzer (1991), 'Soil organic matter, the next 75 years', *Soil Science,* **151**, 41-58

[42] W. Gao, T. Zhou, T. Ren (2015), 'Conversion from conventional to no tillage alters thermal stability of organic matter in soil aggregates', *Soil Sci. Soc. Am. J*, **79** (2), 585-594

[43] R. Lal (2004), 'Soil carbon sequestration impacts on global climate change and food security', *Science,* **304**, 1623–1627

[44] A. Golchin, J.M. Oades, J. O. Skjemstad, P. Clarke (1994), 'Soil structure and carbon cycling', *Aust. J. Soil Res.,* **32**,1043-1068

[45] P. Puget, C. Chenu, J. Balesdent (1995), 'Total and young organic matter distributions in aggregates of silty cultivated soils', *Eur. J. Soil Sci*., **46**, 449-459

[46] E. Lopez-Capel, S. P. Sohi, J. L. Gaunt, D. A. Manning (2005), 'Use of thermogravimetry–differential scanning calorimetry to characterize modelable soil organic matter fractions', *Soil Sci. Soc. Am. J*, **69** (1), 136-140

[47] M. Strobl, I. Manke, N. Kardjilov, A. Hilger, M. Dawson, J. Banhart (2009), 'Advances in neutron radiography and tomography', *J. Phys. D. Appl. Phys*, **42** (24), 243001

[48] Banhart, J. (Ed.). (2008). *Advanced tomographic methods in materials research and engineering* (Vol. 66). Oxford University Press.

[49] S. M. Rabbi, M. K. Tighe, R. J. Flavel, B. N. Kaiser, C. N. Guppy, X. Zhang, I. M. Young (2018), 'Plant roots redesign the rhizosphere to alter the three-dimensional physical architecture and water dynamics', *New Phytol*, **219** (2), 542-550

[50] J. A. Atkinson, M. J. Hawkesford, W. R. Whalley, H. Zhou, S. J. Mooney (2020), 'Soil strength influences wheat root interactions with soil macropores', *Plant. Cell. Environ*, **43** (1), 235-245

[51] J. Banhart, A. Borbély, K. Dzieciol, F. Garcia-Moreno, I. Manke, N. Kardjilov, A. R. Kaysser-Pyzalla, M. Strobl, W. Treimer (2010), 'X-ray and neutron imaging–Complementary techniques for materials science and engineering', *Int. J. Mat. Res*., **101**(9), 1069

[52] D. Schwarz, P. Vontobel, E.H. Lehmann, C. A. Meyer, G. Bongartz (2005), 'Neutron tomography of internal structures of vertebrate remains: a comparison with X-ray computed tomography, *Palaeontol. Electron.,* **8**, 1-11

[53] E. Deschler-Erb, E. H. Lehmann, L. Pernet, P. Vontobel, S. Hartmann (2004), 'The complementary use of neutrons and X-rays for the non-destructive investigation of archaeological objects from Swiss collections', *Archaeometry*, **46**(4), 647-661

[54] I. S. Anderson, R. L. McGreevy, H. Z. Bilheux (2009), '*Neutron imaging and applications: A Reference for the Imaging Community'*, Springer Science+ Business Media, LLC

[55] H. Borner, J. Brown, C. J. Carlile, R. Cubitt, R. Currat, A. J. Dianoux, B. Farago, A. W. Hewat, J. Kulda, E. Lelièvre-Berna, G. J. McIntyre (2003), '*Neutron Data Booklet*', OCP Science.

[56] A. Tengattini, N. Lenoir, E. Andò, G. Viggiani (2021), 'Neutron imaging for geomechanics: a review', *Geomech. Energy Environ.*, **27,** 100206

[57] N. Watanabe (2003), 'Neutronics of pulsed spallation neutron sources', *Rep. Prog. Phys*, **66** (3), 339

[58] T. Minniti, K. Watanabe, G. Burca, D. E. Pooley, W. Kockelmann (2018), 'Characterization of the new neutron imaging and materials science facility IMAT', *Nuclear Instruments and Methods in Physics Research Section A: Accelerators, Spectrometers, Detectors and Associated Equipment*, **888,** 184-195

[59] D. Micieli, T. Minniti, V. Formoso, W. Kockelmann, G. Gorini (2018), 'A comparative study of reconstruction methods applied to Neutron Tomography', *J. Instrum*, **13** (6), C06006

[60] G. Burca, S. Nagella, T. Clark, D. Tasev, I. A. Rahman, R. J. Garwood, A. R. Spencer, M. J. Turner, J. F. Kelleher (2018), 'Exploring the potential of neutron imaging for life sciences on IMAT', *J. Microsc.*, **272**(3), 242-247

[61] M. Young, E. Blanchart, C. Chenu, M. Dangerfield, C. Fragoso, M. Grimaldi, J. Ingram, L. J. Monrozier (1998), 'The interaction of soil biota and soil structure under global change', *Glob. Chang. Biol.*, **4**(7), 703–712

[62] D. M. Wendell, K. Luginbuhl, J. Guerrero, A. E. Hosoi (2012), 'Experimental Investigation of Plant Root Growth Through Granular Substrates', *Exp. Mech.*, **52**(7), 945–949

[63] C. Totzke, N. Kardjilov, I. Manke, S. E. Oswald (2017), 'Capturing 3D Water Flow in Rooted Soil by Ultra-fast Neutron Tomography', *Sci. Rep*., **7** (1), 1-9

[64] M. Zarebanadkouki, Y. X. Kim, A. Carminati (2013), 'Where do roots take up water? Neutron radiography of water flow into the roots of transpiring plants growing in soil', *New Phytol*., **199**, 1034–1044

[65] M. Menon, B. Robinson, S. E. Oswald, A. Kaestner, K. C. Abbaspour, E. Lehmann, R. Schulin (2007), 'Visualization of root growth in heterogeneously contaminated soil using neutron radiography', *Eur. J. Soil Sci*, **58**, 802–810

[66] C. L. Cheng, M. Kang, E. Perfect, S. Voisin, J. Horita, H. Z. Bilheux, J. M. Warren, D. L. Jacobson, D. S. Hussey (2012), 'Average soil water retention curves measured by neutron radiography', *Soil Sci. Soc. Am. J.*, **76**, 1184–1191

[67] A. Carminati, A. Kaestner, R. Hassanein, O. Ippisch, P. Vontobel, H. Flühler (2007), 'Infiltration through series of soil aggregates: Neutron radiography and modelling', *Adv. Water Resour*. **30**, 1168–1178

[68] M. A. Arshad, G. M. Coen (1992), 'Characterization of soil quality: physical and chemical criteria', *Am. J. Alternative Agr*, ***7*** (1-2), 25-31

[69] M. Mohanty, D. K. Painuli, A. K. Misra, P. K. Ghosh (2007), 'Soil quality effects of tillage and residue under rice–wheat cropping on a Vertisol in India', *Soil Till. Res.*, **92**(1-2), 243-250

[70] E. J. B. N. Cardoso, R. L. F. Vasconcellos, D. Bini, M. Y. H. Miyauchi, C. A. D. Santos, P. R. L. Alves, A. M. D. Paula, A. S. Nakatani, J. D. M. Pereira, M. A. Nogueira (2013), 'Soil health: looking for suitable indicators. What should be considered to assess the effects of use and management on soil health?', *Sci. Agric.*, **70**, 274-289.

[71] R. K. Maikhuri, K. S. Rao (2012), 'Soil quality and soil health: A review', *Int. J. Ecol. Environ. Sci.*, *38*(1), 19-37

[72] D. L Karlen, M. J. Mausbach, J. W. Doran, R. G. Cline, R. F. Harris, G. E. Schuman (1997), 'Soil quality: A concept, definition and framework for evaluation', *Soil Sci. Soc. Am. J.*, **61**, 4-10

[73] S. H. Schoenholtz H. V. Miegroet J. A. Burger (2000), 'A review of chemical and physical properties as indicators of forest soil quality: challenges and opportunities', *For. Ecol. Manage*., **138**, 335–356

[74] E. Amezketa (1999), 'Soil aggregate stability: A review', *J. Sustain. Agr,* **14** (2-3), 83-151

[75] P. Hinsinger, A. G. Bengough, D. Vetterlein, I. M. Young (2009), 'Rhizosphere: biophysics, biogeochemistry and ecological relevance', *Plant. soil*, **321**(1), 117-152

[76] M. Watt, M. E. McCully, C. E. Jeffree (1993), 'Plant and bacterial mucilages of the maize rhizosphere: comparison of their soil binding properties and histochemistry in a model system', *Plant. Soil*, **151**, 151-165

[77] N.G. Juma (1998), '*The pedosphere and its dynamics: a systems approach to soil science',* Volume 1. Quality Colour Press Inc, Edmonton, Canada. 315

[78] B. Koo, D. Adriano, N. Bolan, C. Barton (2005), 'Root exudates and microorganisms', *Encyclopedia of Soils in the Environment*, Academic Press, New York, USA. 421-428

[79] S. Czarnes, A. R. Dexter, F. Bartoli (2000), 'Wetting and drying cycles in the maize rhizosphere under controlled conditions. Mechanics of the root-adhering soil', *Plant. Soil*, **221**, 253–271

[80] A. A. Albalasmeh, T.A. Ghezzehei (2014), 'Interplay between soil drying and root exudation in rhizosheath development', *Plant. Soil,* **374**, 739–751

[81] S. Czarnes, P. D. Hallett, A. G. Bengough, I. M. Young (2000), 'Root-and microbial-derived mucilages affect soil structure and water transport' *Eur. J. Soil Sci*, **51**, 435-443

[82] J. M. Oades (1984), 'Soil organic matter and structural stability: mechanisms and implications for management', *Plant. Soil*, **76** (1-3), 319-337

[83] B. D. Kay, D. A. Angers, P. H. Groenevelt, D.C. Baldock (1988), 'Quantifying the influence of cropping history on soil structure', *Can. J. Soil Sci,* **68**, 359-368

[84] Y. L. Le Bissonnais (1996), 'Aggregate stability and assessment of soil crustability and erodibility: I. Theory and methodology', *Eur. J. Soil Sci*, **47** (4), 425-437

[85] J. M. Oades, A.G. Waters (1991), 'Aggregate hierarchy in soils', *Soil Res*, **29** (6), 815-828

[86] W. Markgraf, R. Horn (2007), 'Scanning electron microscopy–energy dispersive scan analyses and rheological investigations of South-Brazilian soils', *Soil Sci. Soc. Am. J*, **71** (3), 851-859

[87] M. Bonsu (1993), 'Field determination of sorptivity as a function of water content using a tension infiltrometer', *J. Soil Sci*, **44** (3), 411-415

[88] J. R. Philip (1957), 'The theory of infiltration: 4. Sorptivity and algebraic infiltration equations', *Soil Sci,* **84**, 257–264

[89] P. D. Hallett (2008), 'A brief overview of the causes, impacts and amelioration of soil water repellency–a review', *Soil Water Res.*, **3**(1), 521-528

[90] P. D. Hallett (2007), 'An introduction to soil water repellency', *Proceedings of the 8th International Symposium on Adjuvants for Agrochemicals, (ISAA2007)*, **6**, 9

[91] S. K. Woche, M. O. Goebel, M. B. Kirkham, R. Horton, R. R. Van der Ploeg, J. Bachmann (2005), 'Contact angle of soils as affected by depth, texture, and land management', *Eur. J. Soil Sci*, **56**(2), 239-251

[92] I. McKissock, R. J. Gilkes, E. L.Walker (2002), 'The reduction of water repellency by added clay is influenced by clay and soil properties', *Appl. Clay Sci*., **20**, 225–241

[93] R. W. Tillman, D. R. Scotter, M. G. Wallis, B. E. Clothier (1989), 'Water-repellency and its measurement by using intrinsic sorptivity', *Aust. J. Soil Res.*, **27**, 637–644

[94] L. W. Dekker, S. H. Doerr, K. Oostindie, A. K. Ziogas, C. J. Ritsema (2001), 'Water repellency and critical soil water content in a dune sand', *Soil Sci. Soc. Am. J*, **65**, 1667–1674

[95] B. E. Clothier, I. Vogeler, G. N. Magesan (2000), 'The breakdown of water repellency and solute transport through a hydrophobic soil', *J. Hydrol*., **231**, 255–264

[96] M. M. Roper (2006), 'Potential for remediation of water repellent soils by inoculation with wax-degrading bacteria in south-western Australia', *Biologia*, **61**(19), S358–S362

[97] U. Buczko, O. Bens, R. E. Huttl (2006), 'Tillage effects on hydraulic properties and macroporosity in silty and sandy soils', *Soil Sci. Soc. Am. J*, **70**, 1998–2007

[98] A. R. Dexter (2004), 'Soil physical quality: Part I. Theory, effects of soil texture, density, and organic matter, and effects on root growth', *Geoderma*, **120**(3-4), 201-214

[99] W. T. Hong, Y. S. Jung, S. Kang, J. S. Lee (2016), 'Estimation of soil-water characteristic curves in multiple-cycles using membrane and TDR system', *Mater. Sci. Eng*, **9** (12), 1019

[100] W. R. Whalley, G. P. Matthews, S. Ferraris (2012), 'The effect of compaction and shear deformation of saturated soil on hydraulic conductivity', *Soil Till. Res*, **125**, 23-29

[101] W. R. Whalley, E. S. Ober, M. Jenkins (2013), 'Measurement of the matric potential of soil water in the rhizosphere', *J. Exp. Bot,* **64** (13), 3951-3963

[102] A. S. Gregory, N. R. Bird, W. R. Whalley, G. P. Matthews, I. M. Young (2010), 'Deformation and shrinkage effects on the soil water release characteristic', *Soil Sci. Soc. Am. J*, **74** (4), 1104-1112

[103] M. Kutílek, L. Jendele (2008), 'The structural porosity in soil hydraulic functions-a review', *Soil Water Res.*, **3**(Special Issue 1), S7-S20

[104] S. Abiven, S. Menasseri, C. Chenu (2009), 'The effects of organic inputs over time on soil aggregate stability–A literature analysis', *Soil Biol. Biochem*, **41** (1), 1-12

[105] A. Bhogal, F. A. Nicholson, B. J. Chambers (2009), 'Organic carbon additions: effects on soil bio-physical and physico-chemical properties', *Eur. J. Soil Sci*, **60** (2), 276-286

[106] A. E. Johnston, P. R. Poulton, K. Coleman (2009), 'Soil organic matter: its importance in sustainable agriculture and carbon dioxide fluxes', *Adv. Agron*, **101**, 1-57

[107] D. S. Powlson, A. Bhogal, B. J. Chambers, K. Coleman, A. J. Macdonald, K. W. T. Goulding, A. P. Whitmore, (2012). 'The potential to increase soil carbon stocks through reduced tillage or organic material additions in England and Wales: a case study', *Agric. Ecosyst. Environ*, **146** (1), 23-33

[108] J. Townend, M. J. Reeve, A. Carter (2000), 'Water release characteristic', *Soil Environmental Analysis: Physical Methods,* 2nd ed. Marcel Dekker, New York, 95-140

[109] A. R. Dexter, G. Richard, D. Arrouays, E. A. Czyż, C. Jolivet, O. Duval (2008), 'Complexed organic matter controls soil physical properties', *Geoderma*, **144** (3), 620-627

[110] A. S. Gregory, C. W. Watts, B. S. Griffiths P. D. Hallett, H. L. Kuan, A. P. Whitmore (2009), 'The effect of long-term soil management on the physical and biological resilience of a range of arable and grassland soils in England', *Geoderma*, **153**, 172–185

[111] X. Li, L.M. Zhang (2009), 'Characterization of dual-structure pore-size distribution of soil' *Can. Geotech. J,* **46**, 129–141

[112] G. P. Matthews, G. M. Laudone, A. S. Gregory, N. R. A. Bird, A. G. Matthews, W. R. Whalley (2010), 'Measurement and simulation of the effect of compaction on the pore

structure and saturated hydraulic conductivity of grassland and arable soil', *Water Resour. Res*, **46** (5)

[113] M. T. Van Genuchten (1980), 'A closed-form equation for predicting the hydraulic conductivity of unsaturated soils', *Soil Sci. Soc. Am. J*, **44** (5), 892-898

[114] J. Lipiec, R. Walczak, B. Witkowska-Walczak, A. Nosalewicz, A. Słowinska-Jurkiewicz, C. Sławinski (2007), 'The effect of aggregate size on water retention and pore structure of two silt loam soils of different genesis', *Soil Till. Res*. **97**(2), 239–246

[115] D. Porebska, C. Slawinski, K. Lamorski, R. T. Walczak (2006), 'Relationship between van Genuchten's parameters of the retention curve equation and physical properties of soil solid phase', *Int. Agrophys.* **20**(2), 153–159

[116] A. R. Dexter, E.A. Czyż, G. Richard, A. Reszkowska (2008), 'A user-friendly water retention function that takes account of the textural and structural pore spaces in soil', *Geoderma*, **143**, 243–253

[117] S. Rousseva, M. Kercheva, T. Shishkov, G. J. Lair, N. P. Nikolaidis, D. Moraetis, P. Krám, S. M. Bernasconi, W. E. H. Blum, M. Menon, S. A. Banwart (2017), 'Soil water characteristics of European SoilTrEC critical zone observatories', *Adv. Agron.*, **142**, 29-72

[118] W. Durner (1994), 'Hydraulic conductivity estimation for soils with heterogeneous pore structure', *Water Resour. Res*, **30** (2), 211-223

[119] S. I. Hwang, E. Y. Yun, H. M. Ro (2011), 'Estimation of soil water retention function based on asymmetry between particle-and pore-size distributions', *Eur. J. Soil Sci*, **62** (2), 195-205

[120] Q. Zhai, H. Rahardjo, A. Satyanaga, G. Dai (2020), 'Estimation of tensile strength of sandy soil from soil–water characteristic curve', *Acta Geotech.*, **15**(12), 3371-3381

[121] S. K. Vanapalli, D.G. Fredlund, D. E. Pufahl, A.W. Clifton (1996), 'Model for the prediction of shear strength with respect to soil suction', *Can. Geotech. J*, **33** (3), 379-392

[122] H. Causarano (1993), 'Factors affecting the tensile strength of soil aggregates', *Soil Till. Res*., **28**, 15-25

[123] A. R. Dexter, C. W. Watts (2000), 'Tensile strength and friability. *Soil and environmental analysis: Physical methods*', **2**, 405-433

[124] A. R. Dexter, B. Kroesbergen (1985), 'Methodology for determination of tensile strength of soil aggregates', *J. Agric. Eng. Res.*, **31**(2), 139-147

[125] L. J. Munkholm, P. Schjønning, B. D. Kay (2002), 'Tensile strength of soil cores in relation to aggregate strength, soil fragmentation and pore characteristics', *Soil Till. Res.*, **64**(1-2), 125-135

[126] S. Czarnes, S. Hiller, A. R. Dexter, P. D. Hallett, F. Bartoli (1999), 'Root: soil adhesion in the maize rhizosphere: the rheological approach)' *Plant. Soil*, **211** (1), 69-86

[127] C. McPhee, J. Reed, I. Zubizarreta (2015), 'Geomechanics Tests', In: *Developments in Petroleum Science,* **64**, 671-779

[128] W. R. Whalley, E. Dumitru, A. R. Dexter (1995), 'Biological effects of soil compaction', *Soil Till. Res*, **35** (1), 53-68

[129] C. T. Petersen (1993), 'The variation of critical-state parameters with water content for two agricultural soils', *J. Soil Sci*, **44** (3), 397-410

[130] M. F. O'Sullivan, E. A. G. Robertson (1996), 'Critical state parameters from intact samples of two agricultural topsoils', *Soil Till. Res*, **39** (3-4), 161-173

[131] P. V. Lade (2016), '*Triaxial Testing of Soils*', John Wiley & Sons, Ltd

[132] K. N. Suravi, K. Attenborough, S. Taherzadeh, A. J. Macdonald, D. S. Powlson, R. W. Ashton, W. R. Whalley (2021), 'The effect of organic carbon content on soil compression characteristics', *Soil Till. Res*, *209*, 104975

[133] www.gdsinstruments.com accessed on 8 September 2016

[134] M. L. Oelze, W. D. O'Brien, R. G. Darmody (2002), 'Measurement of attenuation and speed of sound in soils', *Soil Sci. Soc. Am. J*, **66** (3), 788-796

[135] K. Attenborough (2002), 'A review of ground impedance models for propagation modelling' *Tech. Rep*, University of Hull, Hull, UK

[136] R. K. Sharma, A. K. Gupta, (2010), 'Continuous wave acoustic method for determination of moisture content in agricultural soil', *Comput. electron agric*,**73** (2), 105-111

[137] H.-C. Shin, S. Taherzadeh, K. Attenborough, W. R. Whalley, C. W. Watts (2013), 'Non-invasive soil parameter deduction using acoustic-seismic coupling and linear Biot-Stoll theory' *Eur. J. Soil Sci,* **64**, 308 – 323

[138] L. Zhiqu, J. M. Sabatier (2009), 'Effects of soil water potential and moisture content on sound speed', *Soil Sci. Soc. Am. J,* **73** (5), 1614-1625

[139] K. Attenborough, I. Bashir, S. Taherzadeh (2011), 'Outdoor ground impedance models,' *J. Acoust. Soc. Am*, **129** (5), 2806 – 2819

[140] K. V. Horoshenkov, M. H. Mohamed (2006), 'Experimental investigation of the effects of water saturation on the acoustic admittance of sandy soils', *J. Acoust. Soc. Am,* **120** (4), 1910-1921

[141] N. N. Voronina, K. V. Horoshenkov (2003), 'A new empirical model for the acoustic properties of loose granular media', *Appl. Acoust*, **64** (4), 415-432

[142] K. Attenborough, S. Taherzadeh (1995), 'Propagation from a point source over a rough finite impedance boundary', *J. Acoust. Soc. Am,* **98**, 1717–1722

[143] D. Leary, A. D. David, J. H. Craig (2009), 'Acoustic techniques for studying soil-surface seals and crusts', *Ecohydrol,* **2** (3), 257-262

[144] M. Connelly, M. Hodgson (2015), 'Experimental investigation of the sound absorption characteristics of vegetated roofs', *Build. Environ*, **92,** 335-346

[145] M. A. Biot (1956), 'Theory of propagation of elastic waves in a fluid-saturated porous solid I. Low frequency range', *J. Acoust. Soc. Am,* **28** (2), 168–178

[146] M. A. Biot (1956), 'Theory of propagation of elastic waves in a fluid-saturated porous solid II. Higher frequency range', *J. Acoust. Soc. Am,* **28** (2), 179-191

[147] K. Attenborough (1987), 'On the Acoustic Slow Wave in Air-filled Granular Materials', *J. Acoust. Soc. Am,* **81** (1), 95-102

[148] K. Attenborough (1982), 'Acoustical characteristics of porous materials', *Phys. Rep*, **82** (3), 179-227

[149] J-F. Allard, Y. Champoux (1992), 'New empirical equations for sound propagation in rigid frame fibrous materials', *J. Acoust. Soc. Am,* **91** (6), 3346–3353

[150] K. Attenborough (1993), 'Models for the acoustical properties of air-saturated granular media', *Acta. Acústica*, **1**, 213-226

[151] Y. Champoux, M. R. Stinson (1992), 'On acoustical models for sound propagation in rigid frame porous materials and the influence of shape factors', *J. Acoust. Soc. Am,* **92** (2), 1120-1131

[152] J. P. Dalmont (2001), 'Acoustic impedance measurement, Part I: A review'. *J. Sound Vib*, **243** (3), 427-439

[153] A. Lefebvre, G. P. Scavone, J. Abel, A. Buckiewicz-Smith (2007), 'A comparison of impedance measurements using one and two microphones', *Proceedings of ISMA*, **1** (1),1-8

[154] A. F. Seybert, D. F. Ross (1977), 'Experimental determination of acoustic properties using a two-microphone random-excitation technique', *J. Acoust. Soc. Am,* **61**, 1362–1370

[155] G. Krishnappa (1981), 'Cross-spectral method of measuring acoustic intensity by correcting phase and gain mismatch errors by microphone calibration', *J. Acoust. Soc. Am,* **69**, 307–310

[156] J. Y. Chung (1978), 'Cross-spectral method of measuring acoustic intensity without error caused by instrument phase mismatch', *J. Acoust. Soc. Am*, **64** (6), 1613-1616

[157] A. Mekrel (2002), *Final year project report*, The Open University, UK

[158] H. C. Shin, C. W. Watts, W. R. Whalley, K. Attenborough, S. Taherzadeh (2017), 'Non-invasive estimation of the depth profile of soil strength with acoustic-to-seismic coupling measurement in the presence of crops', *Eur. J. Soil Sci*, **68**(5), 758-768

[159] D. W. Franzen, L. J. Cihacek (1998), '*Soil sampling as a basis for fertilizer application. NDSU extension service*', North Dakota State University, Fargo, ND.

[160] www.dl.sciencesocieties.org accessed on 11 October 2016

[161] J. B. Lawes (1847), 'On agricultural chemistry', *J.R. Agric. Soc. Engl*, **8,** 226-260

[162] B. W. Avery, J. A. Catt (1995), '*The soil at Rothamsted'*, Lawes Agricultural Trust. IACR-Rothamsted, Harpenden, Hertfordshire, UK.

[163] A. J. Macdonald, P. R. Poulton, I. M. Clark, T. Scott, M. J. Glendining, S. A. M. Perryman, J. Storkey, J. R. Bell, I. F. Shield, V. E. Mcmillan, J. M. B. Hawkins (ed.) (2018), '*Rothamsted Long-term experiments: guide to the classical and other long-term experiments, datasets and sample archive*', Rothamsted Research, Harpenden

[164] www.era.rothamsted.ac.uk accessed on 18 September 2016

[165] J. Ruehlmann (2020), 'Soil particle density as affected by soil texture and soil organic matter: 1. Partitioning of SOM in conceptional fractions and derivation of a variable SOC to SOM conversion factor', *Geoderma*, **375**, 114542.

[166] J. Ruehlmann, M. Körschens (2020), 'Soil particle density as affected by soil texture and soil organic matter: 2. Predicting the effect of the mineral composition of particle size fractions', *Geoderma*, **375**, 114543

[167] G. R. Blake, K. H. Hartge (1986), 'Particle density', In: *Methods of soil analysis: Part 1 physical and mineralogical methods*, A. Klute (ed.), 5, 377-382

[168] P. Schjønning, R. A. McBride, T. Keller, P. B. Obour (2017), 'Predicting soil particle density from clay and soil organic matter contents', *Geoderma*, **286**, 83-87

[169] M. Budhu (2015), '*Soil mechanics fundamentals',* John Wiley & Sons.

[170] T. Keller, A. R. Dexter (2012), 'Plastic limits of agricultural soils as functions of soil texture and organic matter content', *Soil Res*, **50** (1), 7-17

[171] B. C. Ball, D. J. Campbell, E. A. Hunter (2000), 'Soil compactibility in relation to physical and organic properties at 156 sites in UK', *Soil Till. Res.*, **57**(1-2), 83-91

[172] S. Stanchi, M. Catoni, M. E. D'Amico, G. Falsone, E. Bonifacio (2017), 'Liquid and plastic limits of clayey, organic C-rich mountain soils: Role of organic matter and mineralogy', *Catena*, **151**, 238-246

[173] J. S. C. Mbagwu, O. G. Abeh, (1998), 'Prediction of engineering properties of tropical soils using intrinsic 413 pedological parameters', *Soil Sci*., **163**, 93–102

[174] R. M. Schmitz, C. Schroeder, R. Charlier (2004), 'Chemo-mechanical interactions in clay: a correlation between clay mineralogy and Atterberg limits', *Appl. Clay Sci*. **26**, 351-358

[175] E. De Jong, D. F. Acton, H. B. Stonehouse (1990), 'Estimating the Atterberg limits of Southern Saskatchewan soils from texture and Carbon contents', *Can. J. Soil Sci*., **70**, 543-554

[176] M.R. Carter, E.G. Gregorich (2008), '*Soil Sampling and Method Analysis*', 2nd ed. Taylor & Francis Group, LLC

[177] B. Standard (1990), '*Methods of test for soils for civil engineering purposes-Part 2: Classification tests*', London: UK: British Standard Institution, BS 1377-2: 1990

[178] M. Dell'Abate, A. Benedetti, P. Sequi (2000), 'Thermal methods of organic matter maturation monitoring during a composting process', ***J. Therm. Anal. Calorim***, **61** (2), 389-396

[179] A. F. Plante, J. M. Fernandez, J. Leifeld (2009), 'Application of thermal analysis techniques in soil science', *Geoderma*, **153**, 1–10

[180] C. Siewert (2004), 'Rapid screening of soil properties using thermogravimetry', *Soil Sci. Soc. Am. J*, **68** (5), 1656-1661

[181] M. Dorodnikov, A. Fangmeier, Y. Kuzyakov (2007), 'Effects of atmospheric CO2 enrichment on δ 13C, δ 15N values and turnover times of soil organic matter pools isolated by thermal techniques', *Plant. Soil*, **297** (1-2), 15-28

[182] Y. Wang, S. Lu, T. Ren, B. Li (2011), 'Bound water content of air-dry soils measured by thermal analysis' *Soil Sci. Soc. Am. J*, **75** (2), 481-487

[183] F. Gaal, I. Szollosy, M. Arnold, F. Paulik (1994), 'Determination of the organic matter, metal carbonate and mobile water in soils simultaneous TG, DTG, DTA and EGA techniques', *J. Therm. Anal. Calorim***, 42** (5), 1007-1016

[184] B. Duguy, P. Rovira (2010), 'Differential thermogravimetry and differential scanning calorimetry of soil organic matter in mineral horizons: effect of wildfires and land use', *Org. Geochem*, **41** (8), 742-752

[185] A. F. Plante, J. M. Fernandez, M. L. Haddix, J. M. Steinweg, R.T. Conant (2011), 'Biological, chemical and thermal indices of soil organic matter stability in four grassland soils', *Soil Biol. Biochem*, **43** (5), 1051-1058

[186] P. Rovira, C. Kurz-Besson, M. M. Couteaux, V. R. Vallejo (2008), 'Changes in litter properties during decomposition: a study by differential thermogravimetry and scanning calorimetry', *Soil Biol. Biochem*, **40** (1), 172-185

[187] J. R. London (1991), '*Booker Tropical soil manual: A handbook for soil survey and agricultural land evaluation in the tropics and subtropics',* Paperback edition, Longman Scientific and Technical, New York. 474

[188] J. Ruhlmann, M. Körschens, J. Graefe (2006), 'A new approach to calculate the particle density of soils considering properties of the soil organic matter and the mineral matrix', *Geoderma*, **130**(3-4), 272-283

[189] D. Hillel (1980), '*Fundamentals of Soil Physics'*, Academic Press, New York, 413

[190] M. Kutílek, L. Jendele (2008), 'The structural porosity in soil hydraulic functions—a review', *Soil Water Res*., **3** (special issue 1), S7-S20

[191] H. He, K. Aogu, M. Li, J. Xu, W. Sheng, S. B. Jones, J. D. González-Teruel, D. A. Robinson, R. Horton, K. Bristow, M. Dyck (2021), 'A review of time domain reflectometry (TDR) applications in porous media', *Adv. Agron*., **168**, 83-155

[192] W. J. Rawls, Y. A. Pachepsky, J. C. Ritchie, T. M. Sobecki, H. Bloodworth (2003), 'Effect of soil organic carbon on soil water retention', *Geoderma*, **116**(1-2), 61-76

[193] B. C. Ball, R. Hunter (1988), 'The determination of water release characteristics of soil cores at low suctions', *Geoderma*, **43** (2-3), 195-212

[194] P. Barre, P. D. Hallett (2009), 'Rheological stabilization of wet soils by model root and fungal exudates depends on clay mineralogy', *Eur. J. Soil Sci,* **60,** 525-538

[195] Jena, K. Gupta (2008), 'Determination of pore volume and pore distribution by liquid extrusion porosimetry without using mercury', *Proceedings* of *26th annual conference on composites, advanced ceramics, materials, and structures: B: ceramic engineering and science,* Volume **23**, 277-284

[196] W. D. Reynolds, C. F. Drury, C. S. Tan, C. A. Fox, X. M. Yang (2009), 'Use of indicators and pore volume-function characteristics to quantify soil physical quality', *Geoderma*, **152**(3-4), 252-263

[197] A.W. Jury, W.R. Gardner, W.H. Gardner (1991), '*Soil Physics'* John Wiley & Sons, New York

[198] J. To, B.D. Kay (2005), 'Variation in penetrometer resistance with soil properties: the contribution of effective stress and implications for pedotransfer functions', *Geoderma*, **126**, 161-276

[199] W. Gao, W. R. Whalley, Z. Tian, J. Liu, T. Ren (2016), 'A simple model to predict soil penetrometer resistance as a function of density, drying and depth in the field', *Soil Till. Res.*, **155**, 190-198

[200] A. M. Amer (2012), 'Water flow and conductivity into capillary and non-capillary pores of soils', *J. Soil Sci. Plant Nutr.*, **12**(1), 99-112

[201] J. L. Jensen, P. Schjonning, C. W. Watts, B. T. Christensen, L. J. Munkholm (2019), 'Soil Water Retention: Uni-Modal Models of Pore-Size Distribution Neglect Impacts of Soil Management', *Soil Sci. Soc. Am. J.*, **83**(1), 18-26

[202] M. Zaffar, L. U. Sheng-Gao (2015), 'Pore size distribution of clayey soils and its correlation with soil organic matter', *Pedosphere*, **25**(2), 240-249

[203] W. Gao, V. Muñoz-Romero, T. Ren, W. R. Ashton, M. Morin, I. M. Clark, D. S. Powlson, W. R. Whalley (2017), 'Effect of microbial activity on penetrometer resistance and elastic modulus of soil at different temperatures', *Eur. J. Soil Sci.,* **68**(4), 412-419

[204] J. R. Helliwell, C. J. Sturrock, A. J. Miller, W. R. Whalley, S. J. Mooney (2019), 'The role of plant species and soil condition in the structural development of the rhizosphere', *Plant, Cell Environ.*, **42**(6), 1974-1986

[205] A. S. Gregory, W. R. Whalley, C.W. Watts, N. R. A. Bird, P. D. Hallett, A. P. Whitmore (2006), 'Calculation of the compression index and precompression stress from soil compression test data', *Soil Till. Res*, **89** (1), 45-57

[206] M.F. O'Sullivan, D.J. Campbell, D.R.P. Hettiaratchi (1994), 'Critical state parameters derived from constant cell volume triaxial tests', *Eur. J. Soil Sci*, **45** (3), 249-256

[207] Ibarra, E. McKyes, R.S. Broughton (2005) Measurement of tensile strength of unsaturated sandy loam soil. *Soil Till. Res*, **81**, 15-23

[208] B. Zhang, P. D. Hallett, G. Zhang (2008), 'Increase in the fracture toughness and bond energy of clay by a root exudate', *Eur. J. Soil Sci*, **59**, 855-862

[209] T. Keller, M. Lamande, P. Schjonning, A. R. Dexter (2011), 'Analysis of soil compression curves from uniaxial confined compression tests', *Geoderma*, **163** (1), 13-23

[210] E. Arthur, P. Schjonning, P. Moldrup, L. W. de Jonge (2012), 'Soil resistance and resilience to mechanical stresses for three differently managed sandy loam soils', *Geoderma*, **173**, 50-60

[211] G.R. McDowell, M.D. Bolton, D. Robertson (1996), 'The fractal crushing of granular materials', *J. Mech. Phys. Solids*, **44** (12), 2079-2101

[212] Y. P. Cheng, D. J. White, E. T. Bowman, M. D. Bolton, K. Soga (2001), 'The observation of soil microstructure under load', *Proceedings of the 4th International Conference on Micromechanics of Granular Media, Powders and Grains* 2001, Sendai, 69–72

[213] J.P. de Bono, G. R. McDowell (2018), 'On the micro mechanics of yielding and hardening of crushable granular soils', *Comput. Geotech*, **97**,167-188

[214] G. R. McDowell (2005), 'A physical justification for log e–log σ based on fractal crushing and particle kinematics', *Géotechnique*, **55** (9), 697-698

[215] C. W. Watts, A. R. Dexter (1998), 'Soil friability: theory, measurement and the effects of management and organic carbon content', *Eur. J. Soil Sci*, **49** (1), 73-84

[216] H. Rahimi, E. Pazira, F. Tajik (2000), 'Effect of soil organic matter, electrical conductivity and sodium adsorption ratio on tensile strength of aggregates', *Soil Till. Res.*, **54**(3-4), 145-153

[217] P. D. Hallett, A. R. Dexter, J. P. K. Seville (1995), 'The application of fracture mechanics to crack propagation in dry soil', *Eur. J. Soil Sci.,* **46**, 591-599

[218] V. A. Snyder, R. D. Miller (1989), 'Soil deformation and fracture under tensile forces', *In: Larson, W.E., Blake, G.R., Allmaras, R.R., Voorhees, W.B., Gupta, S.C. (Eds.), Mechanics and Related Processes in Structured Agricultural Soils*. Vol. 172. Kluwer Academic Publishers, Dordrecht, Netherlands, 23–35

[219] D. Velea, F. D. Shields, J. M. Sabatier (2000), 'Elastic wave velocities in partially saturated Ottawa sand: Experimental results and modelling', *Soil Sci. Soc. Am. J,* **64**, 1226-1234

[220] J-F. Allard (1993), '*Propagation of sound in porous media: Modelling Sound Absorbing Materials*', Elsevier Applied Science, New York

[221] L. J. Munkholm, P. Schjonning, B. D. Kay (2002), 'Tensile strength of soil cores in relation to aggregate strength, soil fragmentation and pore characteristics', *Soil Till. Res*., **64**(1-2), 125-135

[222] J. Guerif (1990), 'Factors influencing compaction-induced increases in soil strength', *Soil Till. Res.*, **16**(1-2), 167-178

[223] K. V. Horoshenkov, J-P. Groby, O. Dazel (2016), 'Asymptotic limits of some models for sound propagation in porous media and the assignment of the pore characteristic lengths', *J. Acoust. Soc. Am,* **139** (5), 2463–2474

[224] K. V. Horoshenokov, A. Hurrell, J-P Groby (2019), 'A three-parameter analytical model for the acoustical properties of porous media', *J. Acoust. Soc. Am*, **145**, 2512-2517

[225] M. R. Carter, E. G. Gregorich (2007). *Soil sampling and methods of analysis*. CRC press.

[226] H. C. Shin, W. R. Whalley, K. Attenborough, S. Taherzadeh (2016), 'On the theory of Brutsaert about elastic wave speeds in unsaturated soils', *Soil Till. Res.*, **156**, 155-165.

[227] https://doi.org/10.23637/ROTHAMSTED-LONG-TERM-EXPERIMENTS-GUIDE-2018 accessed on 23 February 2022.

[228] G. P. Matthews, C. L. Levy, G. M. Laudone, K. L. Jones, C. J. Ridgway, I. L. Hallin, S. A. Gazze, L. Francis, W. R. Whalley, J. Schoelkopf, P. A. Gane (2018) 'Improved interpretation of mercury intrusion and soil water retention percolation characteristics by inverse modelling and void cluster analysis', *Transp. Porous Media*, **124** (2), 631-653.

[229] R. J. Haynes (2005) 'Labile organic matter fractions as central components of the quality of agricultural soils: an overview', *Adv. Agron.*, **5**, 221-268.

[230] J.M. Kirby (1998), 'Estimating critical state soil mechanics parameters from shear box tests', *Eur. J. Soil Sci.,* **49** (3), 503-512.

[231] D. Wulfsohn, B.A. Adams, D.G. Fredlund (1996) 'Application of unsaturated soil mechanics for agricultural conditions', *Can. Agric. Eng*., **38** (3), 171-181.

[232] B.A. Adams, D. Wulfsohn (1998) 'Critical-state behaviour of an agricultural soil', *J. Agric. Eng. Res*., **70** (4), 345-354.

Appendix 1 (statistical analysis)

Statistical analysis for the water release characteristics (WRC)

Three-part model was fitted using Linear regression. The response (Volumetric water) was $\log_e$ transformed to satisfy the assumptions of the analysis.

For values of pF between 1 and 4.176 (inclusive) the model is a quadratic linear model with different intercepts slopes and quadratic parameters for each soil type:

$$\text{Ln}(\text{Vol}_i) = \alpha_{\text{soil}} + \beta_{1\text{soil}}.pF_i + \beta_{2\text{soil}}.pF_i^2 + e_i$$

For pF=-1 an adjustment is added to this model as the observed values are all much lower than what would be expected from the model. The adjustment will be different for each soil. As this adjustment is only defined at a single value of pF we can just look at the predictions as a summary of the model at this value. (The adjustment is called 'lowerdummy' in the Genstat output)

$$\text{Ln}(\text{Vol}_i) = \mu_i + e_i$$

Similarly, the observed values were much lower than expected when pF≥5.17 so an adjustment was made to the model at this end as well. The model now takes the same form as the one defined for pF between 1 and 4.176 but the adjustments mean that the model now has different intercepts and slopes. The quadratic term remains the same as previously. (These adjustments are labelled 'upperdummy' in the Genstat output)

$$\text{Ln}(\text{Vol}_i) = \alpha'_{\text{soil}} + \beta'_{1\text{soil}}.pF_i + \beta_{2\text{soil}}.pF_i^2 + e_i$$

For values of *pF* in the ranges (-1,1) and (4.176,5.17) there was no data collected so we do not know what the shape of the relationship might be.

Predictions at *pF*=-1

	Prediction (μ_i)	s.e.
FYM	-1.71	0.04568
N1	-1.721	0.04568
N2	-1.683	0.04568
N3	-1.709	0.04568
N4	-1.73	0.04568
N5	-1.721	0.04568

N6	-1.763	0.04568
nil	-1.789	0.04568
PKMg	-1.76	0.04568

Model parameters for *pF* between 1 and 4.176 inclusive

	Intercept (α_{soil})	Linear slope (β_{1soil})	Quadratic term (β_{2soil})
FYM	-1.659	-0.0548	-0.0444
N1	-1.209	-0.5318	0.0397
N2	-1.014	-0.7408	0.0812
N3	-1.218	-0.6188	0.068
N4	-1.37	-0.5308	0.0541
N5	-1.544	-0.2848	0.0088
N6	-1.734	-0.1928	-0.0103
nil	-1.507	-0.4338	0.0316
PKMg	-1.618	-0.3368	0.0182

Model parameters for pF ≥ 5.17

	Intercept (α'_{soil})	Linear slope (β'_{1soil})	Quadratic term (β_{2soil})
FYM	-1.009	-0.3678	-0.0444
N1	2.081	-1.2318	0.0397
N2	3.496	-1.7158	0.0812
N3	3.662	-1.6958	0.068
N4	5.83	-1.9948	0.0541
N5	1.646	-1.0218	0.0088
N6	1.356	-0.8668	-0.0103
nil	1.513	-1.0948	0.0316
PKMg	0.402	-0.8188	0.0182

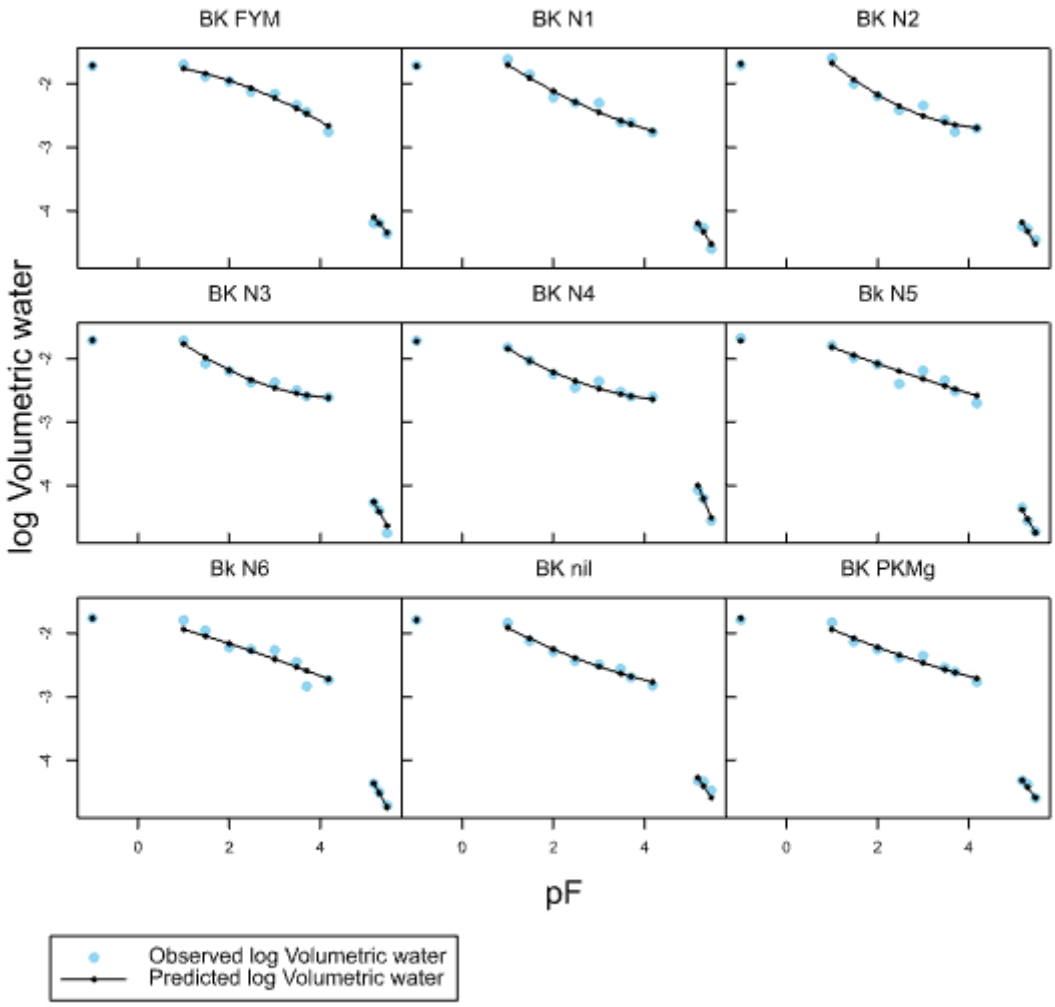

Figure A1.1: *Analysis of observed water content*

Regression analysis
Response variate: lVol
Fitted terms: Constant + pF + pF2 + lowdummy + highdummy + soil + pF.highdummy + pF.soil + pF2.soil + lowdummy.soil + highdummy.soil + pF.highdummy.soil
(FACTORIAL limit for expansion of formula = 3)

Summary of analysis

Source	**d.f.**	**s.s.**	**m.s.**	**v.r.**	**F pr.**
Regression	53	309.726	5.843893	933.59	<.001
Residual	270	1.690	0.006260		
Total	323	311.416	0.964138		

Percentage variance accounted for 99.4
Standard error of observations is estimated to be 0.0791.

Unit	Response	Residual
117	-2.1370	-3.04
204	-2.8297	-3.34
272	-2.6702	-3.16
310	-2.8336	-3.25

It can be noted that the residuals do not appear to be random; for example, fitted values in the range -2.1835 to -2.0671 are consistently larger than observed values and fitted values in the range -2.4649 to -2.4295 are consistently smaller than observed values.

Estimates of parameters

Parameter	**estimate**	**s.e.**	**t(270)**	**t pr.**
Constant	-1.659	0.107	-15.50	<.001
pF	-0.0548	0.0918	-0.60	0.551
pF^2	-0.0444	0.0175	-2.53	0.012
low dummy	-0.061	0.219	-0.28	0.780
high dummy	0.65	1.23	0.53	0.600
soil BK N1	0.450	0.151	2.97	0.003
soil BK N2	0.645	0.151	4.26	<.001
soil BK N3	0.441	0.151	2.91	0.004
soil BK N4	0.289	0.151	1.91	0.057
soil Bk N5	0.115	0.151	0.76	0.447
soil Bk N6	-0.075	0.151	-0.50	0.619
soil BK nil	0.152	0.151	1.01	0.315
soil BK PKMg	0.041	0.151	0.27	0.786
pF.highdummy	-0.313	0.240	-1.30	0.195
pF.soil BK N1	-0.477	0.130	-3.68	<.001
pF.soil BK N2	-0.686	0.130	-5.28	<.001
pF.soil BK N3	-0.564	0.130	-4.34	<.001
pF.soil BK N4	-0.476	0.130	-3.66	<.001
pF.soil Bk N5	-0.230	0.130	-1.77	0.077
pF.soil Bk N6	-0.138	0.130	-1.06	0.289
pF.soil BK nil	-0.379	0.130	-2.92	0.004
pF.soil BK PKMg	-0.282	0.130	-2.17	0.031
pF^2.soil BK N1	0.0841	0.0248	3.39	<.001
pF^2.soil BK N2	0.1256	0.0248	5.07	<.001
pF^2.soil BK N3	0.1124	0.0248	4.53	<.001
pF^2.soil BK N4	0.0985	0.0248	3.97	<.001
pF^2.soil Bk N5	0.0532	0.0248	2.15	0.033
pF^2.soil Bk N6	0.0341	0.0248	1.38	0.170
pF^2.soil BK nil	0.0760	0.0248	3.07	0.002
pF^2.soil BK PKMg	0.0626	0.0248	2.52	0.012
lowdummy.soil BK N1	-1.023	0.309	-3.31	0.001
lowdummy.soil BK N2	-1.430	0.309	-4.63	<.001
lowdummy.soil BK N3	-1.117	0.309	-3.61	<.001
lowdummy.soil BK N4	-0.884	0.309	-2.86	0.005
lowdummy.soil Bk N5	-0.410	0.309	-1.33	0.186
lowdummy.soil Bk N6	-0.150	0.309	-0.49	0.628
lowdummy.soil BK nil	-0.687	0.309	-2.22	0.027
lowdummy.soil BK PKMg	-0.436	0.309	-1.41	0.160
highdummy.soil BK N1	3.29	1.75	1.89	0.060
highdummy.soil BK N2	4.51	1.75	2.58	0.010
highdummy.soil BK N3	4.88	1.75	2.80	0.006
highdummy.soil BK N4	7.20	1.75	4.13	<.001
highdummy.soil Bk N5	3.19	1.75	1.82	0.069
highdummy.soil Bk N6	3.09	1.75	1.77	0.077

highdummy.soil BK nil	3.02	1.75	1.73	0.085
highdummy.soil BK PKMg	2.02	1.75	1.16	0.248
pF.highdummy.soil BK N1	-0.700	0.340	-2.06	0.040
pF.highdummy.soil BK N2	-0.975	0.340	-2.87	0.004
pF.highdummy.soil BK N3	-1.077	0.340	-3.17	0.002
pF.highdummy.soil BK N4	-1.464	0.340	-4.30	<.001
pF.highdummy.soil Bk N5	-0.737	0.340	-2.17	0.031
pF.highdummy.soil Bk N6	-0.674	0.340	-1.98	0.049
pF.highdummy.soil BK nil	-0.661	0.340	-1.94	0.053
pF.highdummy.soil BK PKMg	-0.482	0.340	-1.42	0.157

Parameters for factors are differences compared with the reference level:

Factor	Reference level
soil	BK FYM

Accumulated analysis of variance

Change	**d.f.**	**s.s.**	**m.s.**	**v.r.**	**F pr.**
+ pF	1	235.087	235.087	37556.4	<.001
+pF^2	1	57.4097	57.4097	9171.51	<.001
+ lowdummy	1	5.80256	5.80256	926.99	<.001
+ highdummy	1	7.79696	7.79696	1245.61	<.001
+ soil	8	1.14867	0.14358	22.94	<.001
+ pF.highdummy	1	1.10488	1.10488	176.51	<.001
+ pF.soil	8	0.28582	0.03573	5.71	<.001
+ pF^2.soil	8	0.43888	0.05486	8.76	<.001
+ lowdummy.soil	8	0.37253	0.04657	7.44	<.001
+ highdummy.soil	8	0.13688	0.01711	2.73	0.006
+ pF.highdummy.soil	8	0.14264	0.01783	2.85	0.005
Residual	270	1.690083	0.006260		
Total	323	311.416413	0.964138		

Statistical analysis for tensile Strength

For tensile strength data, one-way ANOVA was done for both Broadbalk and Hoosfield soils. And for nitrogen plots of Broadbalk, simple regression was done to look the relation between tensile strength and the rate of nitrogen applied.

Analysis of variance (one-way ANOVA)

Broadbalk soils

Variate: Tensile strength (kg cm^2)

Source of variation	**d.f.**	**s.s.**	**m.s.**	**v.r.**	**F pr.**
Sample name	8	108076.	13510.	10.04	<.001
Residual	27	36348.	1346.		
Total	35	144424.			

Tables of means

Variate: Tensile strength (kg cm^2)

Grand mean 280.6

Sample name	BB-FYM	BB-N1	BB-N2	BB-N3	BB-N4	BB-N5	BB-N6
	338.4	191.1	234.2	252.4	274.1	325.5	376.8

Sample name	BB-NIL	BB-PKMg
	244.0	289.0

Standard errors of differences of means

Table	**Sample name**
rep.	4
d.f.	27
s.e.d.	25.94

Hoosfield Soils

Variate: Tensile strength (kg cm^2)

Source of variation	**d.f.**	**s.s.**	**m.s.**	**v.r.**	**F pr.**
Sample name	3	45030.	15010.	4.44	0.026
Residual	12	40574.	3381.		
Total	15	85605.			

Tables of means

Grand mean 353.

Sample name	HB-42	HB-71	HB-72	HB-73
	439.	314.	305.	357.

Standard errors of differences of means

Table	**Sample name**
rep.	4
d.f.	12
s.e.d.	41.1

Broadbalk nitrogen plots

Regression analysis

Response variate: Tensile strength (kg cm^2)
Fitted terms: Constant, N Applied (kg/ha)

Summary of analysis

Source	**d.f.**	**s.s.**	**m.s.**	**v.r.**	**F pr.**
Regression	1	85613.	85613.	56.10	<.001
Residual	22	33574.	1526.		

Total	23	119187.	5182.

Percentage variance accounted for 95.9
Standard error of observations is estimated to be 13.4.

Estimates of parameters

Parameter	**estimate**	**s.e.**	**t(22)**	**t pr.**
Constant	153.3	18.2	8.43	<.001
N Applied (kg/ha)	0.7286	0.0973	7.49	<.001

Statistic for Compression characteristics

Regression analysis for Triaxial Compression

1. NCL for Broadbalk soils

Response variate: Void_ratio
Fitted terms: Constant + log_p_before_Shear

Summary of analysis

Source	**d.f.**	**s.s.**	**m.s.**	**v.r.**	**F pr.**
Regression	1	0.0869	0.086897	14.83	0.001
Residual	18	0.1055	0.005860		
Total	19	0.1924	0.010125		

Percentage variance accounted for 42.1
Standard error of observations is estimated to be 0.0766.

Estimates of parameters

Parameter	**estimate**	**s.e.**	**t(18)**	**t pr.**
Constant	0.9537	0.0995	9.58	<.001
log_p_before_Shear	-0.1654	0.0429	-3.85	0.001

Response variate: Void_ratio
Fitted terms: Constant + log_p_before_Shear + Sample

Summary of analysis

Source	**d.f.**	**s.s.**	**m.s.**	**v.r.**	**F pr.**
Regression	5	0.188174	0.0376349	125.38	<.001
Residual	14	0.004202	0.0003002		
Total	19	0.192376	0.0101251		
Change	-4	-0.101278	0.0253194	84.35	<.001

Percentage variance accounted for 97.0
Standard error of observations is estimated to be 0.0173.

Estimates of parameters

Parameter	estimate	s.e.	t(14)	t pr.
Constant	1.0869	0.0238	45.63	<.001
log_p_before_Shear	-0.16539	0.00972	-17.01	<.001
Sample BB-N1	-0.1514	0.0123	-12.36	<.001
Sample BB-N6	-0.1350	0.0123	-11.02	<.001
Sample BB-NIL	-0.2103	0.0123	-17.16	<.001
Sample BB-PKMg	-0.1693	0.0123	-13.82	<.001

Response variate: Void_ratio
Fitted terms: Constant + log_p_before_Shear + Sample + log_p_before_Shear.Sample

Summary of analysis

Source	d.f.	s.s.	m.s.	v.r.	F pr.
Regression	9	0.188941	0.0209934	61.10	<.001
Residual	10	0.003436	0.0003436		
Total	19	0.192376	0.0101251		
Change	-4	-0.000766	0.0001916	0.56	0.699

Percentage variance accounted for 96.6
Standard error of observations is estimated to be 0.0185.

Estimates of parameters

Parameter	estimate	s.e.	t(10)	t pr.
Constant	1.1050	0.0539	20.51	<.001
log_p_before_Shear	-0.1733	0.0233	-7.45	<.001
Sample BK-N1	-0.1526	0.0762	-2.00	0.073
Sample BK-N6	-0.1067	0.0762	-1.40	0.192
Sample BK-NIL	-0.2580	0.0762	-3.39	0.007
Sample BK-PKMg	-0.2389	0.0762	-3.14	0.011
log_p_before_Shear.Sample BK-N1	0.0006	0.0329	0.02	0.987
log_p_before_Shear.Sample BK-N6	-0.0124	0.0329	-0.38	0.715
log_p_before_Shear.Sample BK-NIL	0.0209	0.0329	0.64	0.539
log_p_before_Shear.Sample BK-PKMg	0.0305	0.0329	0.93	0.376

Parameters for factors are differences compared with the reference level:

Factor	Reference level
Sample	BK-FYM

2. CSL for Broadbalk soils

Response variate: Void_ratio
Fitted terms: Constant + log_p_After_Shear

Summary of analysis

Source	**d.f.**	**s.s.**	**m.s.**	**v.r.**	**F pr.**
Regression	1	0.0636	0.063576	8.88	0.008
Residual	18	0.1288	0.007156		
Total	19	0.1924	0.010125		

Percentage variance accounted for 29.3
Standard error of observations is estimated to be 0.0846.

Estimates of parameters

Parameter	estimate	s.e.	t(18)	t pr.
Constant	0.7900	0.0742	10.65	<.001
log_p_After_Shear	-0.1133	0.0380	-2.98	0.008

Response variate: Void_ratio
Fitted terms: Constant + log_p_After_Shear + Sample

Summary of analysis

Source	**d.f.**	**s.s.**	**m.s.**	**v.r.**	**F pr.**
Regression	5	0.185417	0.0370835	74.60	<.001
Residual	14	0.006959	0.0004971		
Total	19	0.192376	0.0101251		
Change	-4	-0.121842	0.0304605	61.28	<.001

Percentage variance accounted for 95.1
Standard error of observations is estimated to be 0.0223.

Estimates of parameters

Parameter	**estimate**	**s.e.**	**t(14)**	**t pr.**
Constant	0.9734	0.0232	42.04	<.001
log_p_After_Shear	-0.1322	0.0102	-13.01	<.001
Sample BK-N1	-0.1647	0.0158	-10.43	<.001
Sample BK-N6	-0.1632	0.0159	-10.26	<.001
Sample BK-NIL	-0.2362	0.0159	-14.86	<.001
Sample BK-PKMg	-0.1746	0.0158	-11.07	<.001

Response variate: Void_ratio

Fitted terms: Constant + log_p_After_Shear + Sample + log_p_After_Shear.Sample

Summary of analysis

Source	d.f.	s.s.	m.s.	v.r.	F pr.
Regression	9	0.185997	0.0206664	32.40	<.001
Residual	10	0.006379	0.0006379		
Total	19	0.192376	0.0101251		
Change	-4	-0.000580	0.0001450	0.23	0.917

Percentage variance accounted for 93.7
Standard error of observations is estimated to be 0.0253.

Estimates of parameters

Parameter	estimate	s.e.	t(10)	t pr.
Constant	0.9996	0.0545	18.33	<.001
log_p_After_Shear	-0.1453	0.0266	-5.47	<.001
Sample BK-N1	-0.2130	0.0699	-3.05	0.012
Sample BK-N6	-0.1806	0.0699	-2.58	0.027
Sample BK-NIL	-0.2427	0.0778	-3.12	0.011
Sample BK-PKMg	-0.2272	0.0801	-2.84	0.018
log_p_After_Shear.Sample BK-N1	0.0248	0.0346	0.72	0.490
log_p_After_Shear.Sample BK-N6	0.0082	0.0355	0.23	0.822
log_p_After_Shear.Sample BK-NIL	0.0022	0.0401	0.05	0.958
log_p_After_Shear.Sample BK-PKMg	0.0266	0.0396	0.67	0.517

Parameters for factors are differences compared with the reference level:

Factor	Reference level
Sample	BB-FYM

3. NCL for Hoosfield soils

Response variate: Void_ratio
Fitted terms: Constant + log_p_before_Shear

Summary of analysis

Source	d.f.	s.s.	m.s.	v.r.	F pr.
Regression	1	0.12541	0.125408	17.77	0.001
Residual	13	0.09173	0.007057		
Total	14	0.21714	0.015510		

Percentage variance accounted for 54.5
Standard error of observations is estimated to be 0.0840.

Estimates of parameters

Parameter	estimate	s.e.	t(13)	t pr.
Constant	1.143	0.123	9.30	<.001
log_p_before_Shear	-0.2227	0.0528	-4.22	0.001

Response variate: Void_ratio
Fitted terms: Constant + log_p_before_Shear + Sample

Summary of analysis

Source	d.f.	s.s.	m.s.	v.r.	F pr.
Regression	4	0.210946	0.0527365	85.11	<.001
Residual	10	0.006197	0.0006197		
Total	14	0.217142	0.0155102		
Change	-3	-0.085538	0.0285126	46.01	<.001

Percentage variance accounted for 96.0
Standard error of observations is estimated to be 0.0249.

Estimates of parameters

Parameter	estimate	s.e.	t(10)	t pr.
Constant	1.0956	0.0379	28.94	<.001
log_p_before_Shear	-0.2286	0.0157	-14.60	<.001
Sample HB71	0.0078	0.0176	0.44	0.667
Sample HB72	0.2014	0.0190	10.59	<.001
Sample HB73	0.0691	0.0176	3.93	0.003

Response variate: Void_ratio
Fitted terms: Constant + log_p_before_Shear + Sample + log_p_before_Shear.Sample

Summary of analysis

Source	d.f.	s.s.	m.s.	v.r.	F pr.
Regression	7	0.2166536	0.03095052	443.24	<.001
Residual	7	0.0004888	0.00006983		
Total	14	0.2171424	0.01551017		
Change	-3	-0.0057078	0.00190260	27.25	<.001

Percentage variance accounted for 99.5
Standard error of observations is estimated to be 0.00836.

Estimates of parameters

Parameter	estimate	s.e.	t(7)	t pr.
Constant	1.0152	0.0243	41.79	<.001

log_p_before_Shear	-0.1933	0.0105	-18.44	<.001
Sample HB71	0.0262	0.0344	0.76	0.470
Sample HB72	0.4735	0.0349	13.57	<.001
Sample HB73	0.1079	0.0344	3.14	0.016
log_p_before_Shear.Sample HB71	-0.0081	0.0148	-0.54	0.603
log_p_before_Shear.Sample HB72	-0.1179	0.0149	-7.90	<.001
log_p_before_Shear.Sample HB73	-0.0170	0.0148	-1.15	0.289

4. CSL for Hoosfield soils

Response variate: Void ratio
Fitted terms: Constant + log_p_After_Shear

Summary of analysis

Source	**d.f.**	**s.s.**	**m.s.**	**v.r.**	**F pr.**
Regression	1	0.12710	0.127096	18.35	<.001
Residual	13	0.09005	0.006927		
Total	14	0.21714	0.015510		

Percentage variance accounted for 55.3
Standard error of observations is estimated to be 0.0832.

Estimates of parameters

Parameter	**estimate**	**s.e.**	**t(13)**	**t pr.**
Constant	1.063	0.103	10.36	<.001
log_p_After_Shear	-0.2149	0.0502	-4.28	<.001

Response variate: Void ratio
Fitted terms: Constant + log_p_After_Shear + Sample

Summary of analysis

Source	**d.f.**	**s.s.**	**m.s.**	**v.r.**	**F pr.**
Regression	4	0.209656	0.0524141	70.02	<.001
Residual	10	0.007486	0.0007486		
Total	14	0.217142	0.0155102		
Change	-3	-0.082561	0.0275203	36.76	<.001

Percentage variance accounted for 95.2
Standard error of observations is estimated to be 0.0274.

Estimates of parameters

Parameter	estimate	s.e.	t(10)	t pr.
Constant	1.0084	0.0356	28.31	<.001
log_p_After_Shear	-0.2179	0.0165	-13.21	<.001
Sample HB71	0.0076	0.0193	0.40	0.701
Sample HB72	0.1974	0.0209	9.44	<.001
Sample HB73	0.0725	0.0193	3.75	0.004

Response variate: Void_ratio
Fitted terms: Constant + log_p_After_Shear + Sample + log_p_After_Shear.Sample

Summary of analysis

Source	d.f.	s.s.	m.s.	v.r.	F pr.
Regression	7	0.2162654	0.0308951	246.60	<.001
Residual	7	0.0008770	0.0001253		
Total	14	0.2171424	0.0155102		
Change	-3	-0.0066089	0.0022030	17.58	0.001

Percentage variance accounted for 99.2
Standard error of observations is estimated to be 0.0112.

Estimates of parameters

Parameter	estimate	s.e.	t(7)	t pr.
Constant	0.9376	0.0270	34.70	<.001
log_p_After_Shear	-0.1825	0.0133	-13.76	<.001
Sample HB71	0.0052	0.0375	0.14	0.894
Sample HB72	0.4376	0.0393	11.14	<.001
Sample HB73	0.1382	0.0399	3.46	0.011
log_p_After_Shear.Sample HB71	0.0013	0.0184	0.07	0.947
log_p_After_Shear.Sample HB72	-0.1197	0.0191	-6.25	<.001
log_p_After_Shear.Sample HB73	-0.0330	0.0196	-1.69	0.136

Parameters for factors are differences compared with the reference level:

Factor	Reference level
Sample	HB42

5. Intercepts of NCL vs OC for both Broadbalk and Hoosfield soils

Response variate: Y Intercept of the NCL
Fitted terms: Constant + total OC (g/g)

Summary of analysis

Source	d.f.	s.s.	m.s.	v.r.	F pr.
Regression	1	0.23467	0.234669	30.05	<.001
Residual	7	0.05466	0.007809		
Total	8	0.28933	0.036166		

Percentage variance accounted for 78.4
Standard error of observations is estimated to be 0.0884.

Estimates of parameters

Parameter	estimate	s.e.	t(7)	t pr.
Constant	0.7524	0.0615	12.23	<.001
total OC (g/g)	1.720	0.314	5.48	<.001

Response variate: Y Intercept of the NCL
Fitted terms: Constant + total OC (g/g) + Sample

Summary of analysis

Source	d.f.	s.s.	m.s.	v.r.	F pr.
Regression	2	0.26275	0.131377	29.66	<.001
Residual	6	0.02658	0.004429		
Total	8	0.28933	0.036166		
Change	-1	-0.02808	0.028085	6.34	0.045

Percentage variance accounted for 87.8
Standard error of observations is estimated to be 0.0666.

Estimates of parameters

Parameter	estimate	s.e.	t(6)	t pr.
Constant	0.7352	0.0468	15.70	<.001
total OC (g/g)	1.512	0.250	6.04	<.001
Sample HB 42	0.1191	0.0473	2.52	0.045

Response variate: Y Intercept of the NCL
Fitted terms: Constant + total OC (g/g) + Sample + total OC (g/g).Sample

Summary of analysis

Source	d.f.	s.s.	m.s.	v.r.	F pr.
Regression	3	0.27282	0.090941	27.55	0.002
Residual	5	0.01651	0.003301		
Total	8	0.28933	0.036166		
Change	-1	-0.01007	0.010070	3.05	0.141

Percentage variance accounted for 90.9

Standard error of observations is estimated to be 0.0575.

Estimates of parameters

Parameter	estimate	s.e.	t(5)	t pr.
Constant	0.7984	0.0543	14.71	<.001
total OC (g/g)	1.074	0.331	3.25	0.023
Sample HB 42	-0.0115	0.0852	-0.13	0.898
total OC (g/g).Sample HB 42	0.763	0.437	1.75	0.141

Parameters for factors are differences compared with the reference level:

Factor	Reference level
Sample	BK FYM

6. Intercepts of CSL vs OC for both Broadbalk and Hoosfield soils

Response variate: Intercept of the CSL
Fitted terms: Constant + total OC (g/g)

Summary of analysis

Source	d.f.	s.s.	m.s.	v.r.	F pr.
Regression	1	0.24799	0.247985	27.46	0.001
Residual	7	0.06321	0.009029		
Total	8	0.31119	0.038899		

Percentage variance accounted for 76.8
Standard error of observations is estimated to be 0.0950.

Estimates of parameters

Parameter	estimate	s.e.	t(7)	t pr.
Constant	0.6362	0.0662	9.61	<.001
total OC (g/g)	1.768	0.337	5.24	0.001

Response variate: Intercept of the CSL
Fitted terms: Constant + total OC (g/g) + Sample

Summary of analysis

Source	d.f.	s.s.	m.s.	v.r.	F pr.
Regression	2	0.30093	0.150467	88.01	<.001
Residual	6	0.01026	0.001710		
Total	8	0.31119	0.038899		
Change	-1	-0.05295	0.052948	30.97	0.001

Percentage variance accounted for 95.6
Standard error of observations is estimated to be 0.0413.

Estimates of parameters

Parameter	estimate	s.e.	t(6)	t pr.
Constant	0.6127	0.0291	21.05	<.001
total OC (g/g)	1.482	0.155	9.53	<.001
Sample HB 42	0.1635	0.0294	5.57	0.001

Response variate: Intercept of the CSL

Fitted terms: Constant + total OC (g/g) + Sample + total OC (g/g).Sample

Summary of analysis

Source	d.f.	s.s.	m.s.	v.r.	F pr.
Regression	3	0.307123	0.1023742	125.83	<.001
Residual	5	0.004068	0.0008136		
Total	8	0.311191	0.0388988		
Change	-1	-0.006190	0.0061897	7.61	0.040

Percentage variance accounted for 97.9
Standard error of observations is estimated to be 0.0285.

Estimates of parameters

Parameter	estimate	s.e.	t(5)	t pr.
Constant	0.6622	0.0269	24.58	<.001
total OC (g/g)	1.139	0.164	6.94	<.001
Sample HB 42	0.0611	0.0423	1.45	0.208
total OC (g/g). Sample HB 42	0.598	0.217	2.76	0.040

Parameters for factors are differences compared with the reference level:

Factor	Reference level
Sample	BK FYM

7. Void ratio in NCL at 200 kPa vs OC
Response variate: Void Ratio in NCL (200 kPa)

Fitted terms: Constant, OC g/g

Summary of analysis

Source	d.f.	s.s.	m.s.	v.r.	F pr.
Regression	1	0.07201	0.072011	50.35	<.001
Residual	7	0.01001	0.001430		
Total	8	0.08202	0.010253		

Percentage variance accounted for 86.1

Standard error of observations is estimated to be 0.0378.

Estimates of parameters

Parameter	estimate	s.e.	t(7)	t pr.
Constant	0.4538	0.0259	17.51	<.001
OC g/g	9.43	1.33	7.10	<.001

Regression analysis for Uniaxial Compression

Response variate: CI
Fitted terms: Constant, OC

Summary of analysis

Source	d.f.	s.s.	m.s.	v.r.	F pr.
Regression	1	0.01286	0.012859	5.78	0.037
Residual	10	0.02225	0.002225		
Total	11	0.03511	0.003192		

Percentage variance accounted for 30.3
Standard error of observations is estimated to be 0.0472.

Estimates of parameters

Parameter	estimate	s.e.	t(10)	t pr.
Constant	0.2292	0.0294	7.80	<.001
OC	0.390	0.162	2.40	0.037

CI	SOM
0.391	0.2978
0.2476	0.117
0.3014	0.1227
0.1787	0.1289
0.2801	0.1148
0.3508	0.1284
0.2884	0.0904
0.2877	0.0972
0.2477	0.1454
0.3425	0.365
0.2591	0.0991
0.3265	0.2181

Statistical analysis for other properties of soils

1. Particle density (one-way ANOVA)

Broadbalk soils

Variate: Particle density (g/cc)

Source of variation	d.f.	s.s.	m.s.	v.r.	F pr.
Sample_name	8	0.061050	0.007631	2.73	0.037
Residual	18	0.050337	0.002797		
Total	26	0.111388			

Tables of means

Grand mean 2.669

Sample name	BK FYM	BK N1	BK N2	BK N3	BK N4	BK N5	BK N6
	2.573	2.673	2.626	2.696	2.734	2.711	2.651

Sample name	BK Nil	BK PKMg
	2.646	2.710

Standard errors of differences of means

Table	Sample name
rep.	3
d.f.	18
s.e.d.	0.0432

Hoosfield soils

Variate: Particle density (g/cc)

Source of variation	d.f.	s.s.	m.s.	v.r.	F pr.
Sample_name	3	0.089414	0.029805	7.29	0.011
Residual	8	0.032698	0.004087		
Total	11	0.122112			

Tables of means

Grand mean 2.649

Sample_name	HB 42	HB 71	HB 72	HB 73
	2.756	2.680	2.518	2.641

Standard errors of differences of means

Table	Sample name

rep.	3
d.f.	8
s.e.d.	0.0522

Regression analysis for particle density vs OC

Broadbalk soils

Response variate: Particle density (g/cc)

Fitted terms: Constant, OC (g/g)

Summary of analysis

Source	**d.f.**	**s.s.**	**m.s.**	**v.r.**	**F pr.**
Regression	1	0.013005	0.013005	10.31	0.015
Residual	7	0.008827	0.001261		
Total	8	0.021832	0.002729		

Percentage variance accounted for 53.8

Standard error of observations is estimated to be 0.0355.

Estimates of parameters

Parameter	**estimate**	**s.e.**	**t(7)**	**t pr.**
Constant	2.7609	0.0286	96.40	<.001
OC (g/g)	-6.36	1.98	-3.21	0.015

Hoosfield soils

Response variate: Particle density (g/cc)

Fitted terms: Constant, OC (g/g)

Summary of analysis

Source	**d.f.**	**s.s.**	**m.s.**	**v.r.**	**F pr.**
Regression	1	0.0290819	0.0290819	80.47	0.012
Residual	2	0.0007228	0.0003614		
Total	3	0.0298047	0.0099349		

Percentage variance accounted for 96.4

Standard error of observations is estimated to be 0.0190.

Estimates of parameters

Parameter	**estimate**	**s.e.**	**t(2)**	**t pr.**
Constant	2.8238	0.0217	129.96	<.001
OC (g/g)	-8.471	0.944	-8.97	0.012

Regression analysis of Particle density vs SOC

Response variate: Particle density (g/cc)

Fitted terms: Constant, OC (g/g)

Summary of analysis

Source	**d.f.**	**s.s.**	**m.s.**	**v.r.**	**F pr.**
Regression	1	0.04186	0.041859	38.22	<.001
Residual	11	0.01205	0.001095		
Total	12	0.05391	0.004492		

Percentage variance accounted for 75.6

Standard error of observations is estimated to be 0.0331.

Message: the following units have large standardized residuals.

Unit	Response	Residual
9	2.626	-2.21

Message: the following units have high leverage.

Unit	Response	Leverage
2	2.518	0.58

Estimates of parameters

Parameter	estimate	s.e.	t(11)	t pr.
Constant	2.7770	0.0198	140.07	<.001
SOC g/100g	-0.0694	0.0112	-6.18	<.001

2. Regression analysis for TG data

Broadbalk soils

Response variate: value labile SOM

Fitted terms: Constant, OC (g/g)

Summary of analysis

Source	d.f.	s.s.	m.s.	v.r.	F pr.
Regression	1	0.02256	0.022559	12.88	0.002
Residual	16	0.02803	0.001752		
Total	17	0.05058	0.002976		

Percentage variance accounted for 41.1
Standard error of observations is estimated to be 0.0419.

Estimates of parameters

Parameter	estimate	s.e.	t(16)	t pr.
Constant	0.1272	0.0239	5.33	<.001
OC (g/g)	5.93	1.65	3.59	0.002

Hoosfield soils

Response variate: value labile SOM

Fitted terms: Constant, OC (g/g)

Summary of analysis

Source	d.f.	s.s.	m.s.	v.r.	F pr.
Regression	1	0.03352	0.033522	6.86	0.026
Residual	10	0.04884	0.004884		
Total	11	0.08236	0.007488		

Percentage variance accounted for 34.8

Standard error of observations is estimated to be 0.0699.

Estimates of parameters

Parameter	estimate	s.e.	t(10)	t pr.
Constant	0.1396	0.0461	3.03	0.013
OC (g/g)	5.25	2.00	2.62	0.026

3. Regression analysis for Plastic limit with OC

Broadbalk soils

Response variate: PL (%)

Fitted terms: Constant, OC (g/g)

Summary of analysis

Source	d.f.	s.s.	m.s.	v.r.	F pr.
Regression	1	25.947	25.9468	112.90	<.001
Residual	7	1.609	0.2298		
Total	8	27.556	3.4444		

Percentage variance accounted for 93.3

Standard error of observations is estimated to be 0.479.

Estimates of parameters

Parameter	estimate	s.e.	t(7)	t pr.
Constant	17.481	0.387	45.22	<.001
OC (g/g)	284.3	26.8	10.63	<.001

Hoosfield soils

Response variate: PL (%)

Fitted terms: Constant, OC (g/g)

Summary of analysis

Source	d.f.	s.s.	m.s.	v.r.	F pr.
Regression	1	25.5378	25.5378	110.52	0.009
Residual	2	0.4622	0.2311		
Total	3	26.0000	8.6667		

Percentage variance accounted for 97.3

Standard error of observations is estimated to be 0.481.

Estimates of parameters

Parameter	estimate	s.e.	t(2)	t pr.
Constant	17.806	0.549	32.41	<.001
OC (g/g)	251.0	23.9	10.51	0.009

Statistics for Plastic limit (PL) and other parameters (Regression analysis)

1. Void ratio at plastic limit vs at 100 kPa in CSL

Response variate: Void ratio of CSL at 100 kPa

Fitted terms: Constant, void ratio at PL

Summary of analysis

Source	d.f.	s.s.	m.s.	v.r.	F pr.
Regression	1	0.05772	0.057716	28.19	0.002
Residual	6	0.01228	0.002047		
Total	7	0.07000	0.010000		

Percentage variance accounted for 79.5

Standard error of observations is estimated to be 0.0452.

Estimates of parameters

Parameter	estimate	s.e.	t(6)	t pr.
Constant	-0.124	0.137	-0.91	0.400
void ratio at PL	1.178	0.222	5.31	0.002

2. Water content at PL and inflection point in WRC

Response variate: water content at pF 2.477 (cm^3/cm^3)

Fitted terms: Constant, water content at PL (cm^3/cm^3)

Summary of analysis

Source	d.f.	s.s.	m.s.	v.r.	F pr.
Regression	1	0.0017367	0.00173666	27.36	0.001
Residual	7	0.0004443	0.00006347		
Total	8	0.0021810	0.00027262		

Percentage variance accounted for 76.7

Standard error of observations is estimated to be 0.00797.

Estimates of parameters

Parameter	estimate	s.e.	t(7)	t pr.
Constant	-0.0189	0.0239	-0.79	0.456
water content at PL (cm^3/cm^3)	0.559	0.107	5.23	0.001

Statistics for Impedance tube measurement

One-sample t-test

1. Sand samples

Variate: absorption coef.

Summary

Sample	Size	Mean	Variance	Standard deviation	Standard error of mean
absorption coef.	7	0.1864	0.009089	0.09534	0.03603

95% confidence interval for mean: (0.09826, 0.2746)

Test of null hypothesis that mean of absorption coef. is equal to 0

Test statistic t = 5.17 on 6 d.f.

Probability = 0.002

2. 4 cm thick Air-dry soils with same packing density of 1.3 g/cc

Variate: absorption coef.

Summary

Sample	Size	Mean	Variance	Standard deviation	Standard error of mean
Absorption coef.	4	0.1806	0.001668	0.04084	0.02042

95% confidence interval for mean: (0.1156, 0.2456)

Test of null hypothesis that mean of absorption coef. is equal to 0

Test statistic t = 8.84 on 3 d.f.

Probability = 0.003

3. Air-dry soil samples packed at 10 kPa pressure

Variate: absorption coef.

Summary

Sample	Size	Mean	Variance	Standard deviation	Standard error of mean
Absorption coef.	4	0.1238	0.0003396	0.01843	0.009214

95% confidence interval for mean: (0.09443, 0.1531)

Test of null hypothesis that mean of absorption coef. is equal to 0

Test statistic t = 13.43 on 3 d.f.

Probability < 0.001

4. Soil samples with moisture content at -300 kPa matric potential and packed to 1.3 g/cc

Variate: absorption coef.

Summary

Sample	Size	Mean	Variance	Standard deviation	Standard error of mean
Absorption coef.	3	0.07000	0.0007000	0.02646	0.01528

95% confidence interval for mean: (0.004276, 0.1357)

Test of null hypothesis that mean of absorption coef. is equal to 0

Test statistic t = 4.58 on 2 d.f.

Probability = 0.044

5. FYM soil samples with different packing and moisture conditions

Variate: absorption coef.

Summary

Sample	Size	Mean	Variance	Standard deviation	Standard error of mean
Absorption coef.	4	0.09875	0.001173	0.03425	0.01712

95% confidence interval for mean: (0.04425, 0.1532)

Test of null hypothesis that mean of absorption coef. is equal to 0

Test statistic t = 5.77 on 3 d.f.

Probability = 0.010

Appendix 2 (Impedance tube measurement)

Images for measurement

Figure A2.1: *10 cm diameter (ID) aluminium sample holder with rigid back*

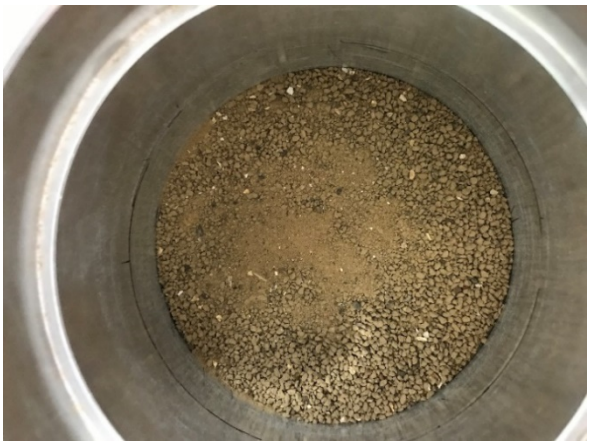

Figure A2.2: *Air-dried soil sample repacked in sample holder for impedance measurement.*

Figure A2.3: *Impedance tube measurement by using single microphone in two different positions.*

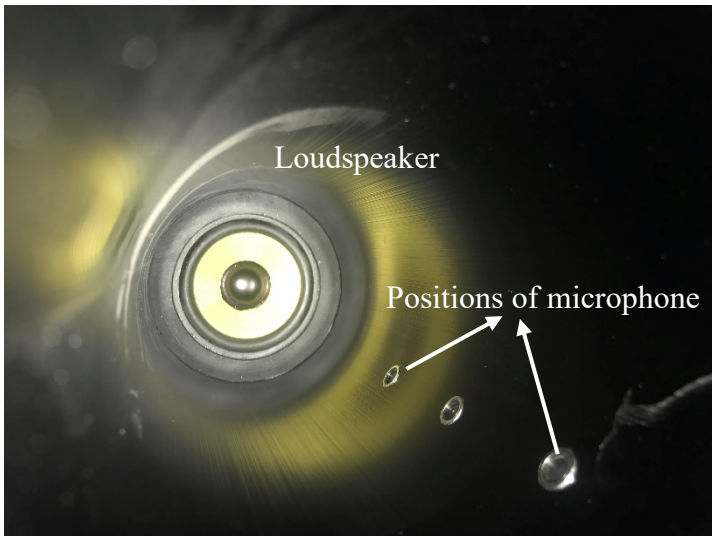

Figure A2.4: *Position of loudspeaker and microphone assembling ports of BK impedance tube.*

MatLab script used in the measurement
Script for data acquisition

```
clear all
close all
% Data Acquisition using NI-USB 6212

fName = 'BKFYM_10kPa_4cm_300kPa_1a.mat';

daq.sec = 20; %recording seconds
daq.amp = 5; %amplitude (max = 10)

daq.AI_range = [10,5]; %choose from 0.2, 1, 5 or 10 (V)
%=========================================================================
=======
daq.Dev = 1; %NI-DAQ Device number
daq.ch_AO = 0; %Output channel: only 0 or 1

daq.ch_AI = [0,1]; %Input channels: single or only two from 0 to 7.
% daq.AI_range = [10,5]; %choose from 0.2, 1, 5 or 10 (V)

daq.Fs = 2e4; %(Hz) sampling frequency

% signal type
% daq.signal = 'sin';  %sine wave
daq.signal = 'white'; %white noise
switch daq.signal
    case 'sin'
        daq.sin_fq = 500; %(Hz)
end

data = daq_ImpTube(daq);

n=size(data,1);
figure
```

```
% subplot(211),plot(1:n,data(:,1)),ylabel('Ch 1')
% subplot(212),plot(1:n,data(:,2)),ylabel('Ch 2')
subplot(211),plot(1:n,data(:,1),[1,n],daq.AI_range(1)*[1 1],'r',...
   [1,n],daq.AI_range(1)*[-1 -1],'r'),ylabel('Ch 1')
subplot(212),plot(1:n,data(:,2),[1,n],daq.AI_range(2)*[1 1],'r',...
   [1,n],daq.AI_range(2)*[-1 -1],'r'),ylabel('Ch 2')

xlabel('Samples')

save(fName)
```

Script for data analysis

```
clear all
close all
addpath('data')

C = 26; %(degree celsius)

fName0 ='BKFYM_10kPa_4cm_300kPa_3';
load([fName0 'a.mat']); data1=data; clear data  % mic. close to sample
load([fName0 'b.mat']); data2=data; clear data  % mic. close to loud-speaker

df = 10; %(Hz) fq resolution

thick=0.0389;
% thick=0.04566;
dm = 0.072-thick;

fq_valid = [50, 1600]; %(Hz)

Fs = daq.Fs;
nfft = round(Fs/df);
wnd = blackman(nfft);
nOlap = round(nfft/2);

m1 = dm+0.1; %(m) distance from sample to near-microphone
m2 = dm+0.2; %(m) distance from sample to far-microphone

c = 331.6*sqrt(1 + C/273); %speed of sound in air

t_range = Fs:size(data1,1);

[H1,fqs] = tfestimate(data1(t_range,1),data1(t_range,2),wnd,nOlap,nfft,Fs);
[H2,fqs] = tfestimate(data2(t_range,1),data2(t_range,2),wnd,nOlap,nfft,Fs);

H = H2./H1;

k = 2*pi*fqs/c; % Wavenumber

R = ( exp(1j*k*m2) - H.*exp(1j*k*m1) )./( H.*exp(-1j*k*m1) - exp(-1j*k*m2) ); %
Reflection coefficient

A = 1 - abs(R).^2; % Absorption coefficient
```

```
Z = (1+R)./(1-R); % Normalised surface impedance

figure
subplot(211),plot(fqs,abs(R),'r',fqs,A,'b'),xlim(fq_valid),ylim([0 1]),grid
legend('|R|','A')
title('|R| & Absorption coef')

subplot(212),plot(fqs,real(Z),'r',fqs,imag(Z),'b'), xlim(fq_valid), grid
legend('real','imag')
xlabel('Frequency (Hz)')
title('Normalised surface impedance')

clear wnd H1 H2
```

Appendix 3 (Neutron tomography)

Introduction:

In this study, neutron imaging of the soil samples to predict the spatial distribution of SOM were conducted at the IMAT beamline (Figure A3.1), ISIS neutron spallation source, Rutherford Appleton Laboratory, UK.

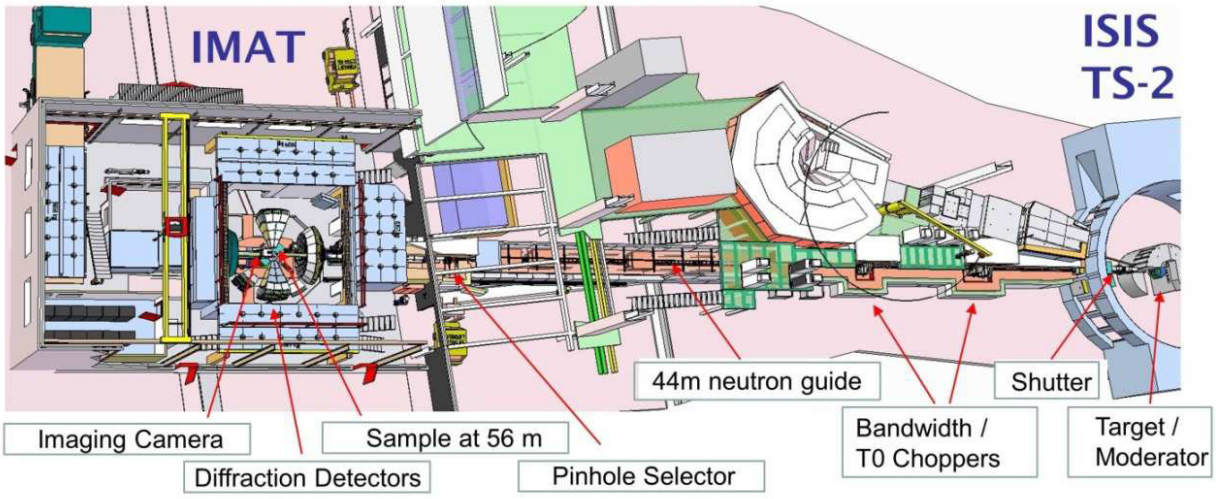

Figure A3.1: *IMAT design outline at ISIS facilities, UK [www.isis.stfc.ac.uk accessed on 24 October 2018].*

Neutron imaging facility in Science and Technology Facilities Council (STFC), UK:

Neutrons at ISIS are produced by nuclear spallation reactions induced by a high energy proton burst impinging on a tungsten target. This process produces neutrons that have a mean energy of about 2 MeV from spallation of 800 MeV protons, very far away from the suitable energy range, particularly relevant for Bragg edge neutron imaging, with cold neutron wavelengths up to 10 Å. This slowing-down process requires time and affects the resolution function of time-of-flight (TOF) methods typically applied at pulsed sources. The source characteristics are one of the crucial points for any TOF based instrument and requires a characterization of the energy dependent pulse width. Equally important neutron beam properties for the envisaged materials science applications are affected by the neutron transport components from source to sample. One pulse of neutrons travels down the IMAT

(Imaging and Materials Science & Engineering) instrument in a neutron supermirror guide, passes through a pinhole before continuing through flight tubes to the sample position at a distance of 56 m from the moderator centre, where they either interact with the sample or are transmitted. The fraction of transmitted neutrons is finally detected in a neutron camera [58].

Method of Scanning:

The core soil samples were placed on the rotating platform placing one after another vertically into a cylindrical aluminium sample holder fixed on an aluminium rod at the distance L = 10 m from the beam aperture (pinhole) and at the distance d = 15 mm from the scintillator screen. The selected diameter of the beam aperture (pinhole) was D = 40 mm that defines an L/D ratio of 250 and ensures a neutron flux of $6 \cdot 10^6$ n cm^{-2} s^{-1} [15]. The detection system consisted of a 16-bit sCMOS camera (ZYLA 4.2 Plus) with 2048 × 2048 pixels coupled with optical lenses and ^{6}LiF/ZnS based scintillators with thickness 60 µm. The focal length was 135 mm and the aperture f = 2. The field-of-view (FOV) was set to 59.5 × 59.5 mm^2 to image the whole phantom. The resulting pixel size was 29 µm.

The exposure time for each projection was 30 s. A stack of 20 open beam images were taken as well before and after each tomographic scan for normalization purposes and 20 dark field projections has been taken after each day measurement [59].

Images for measurement:

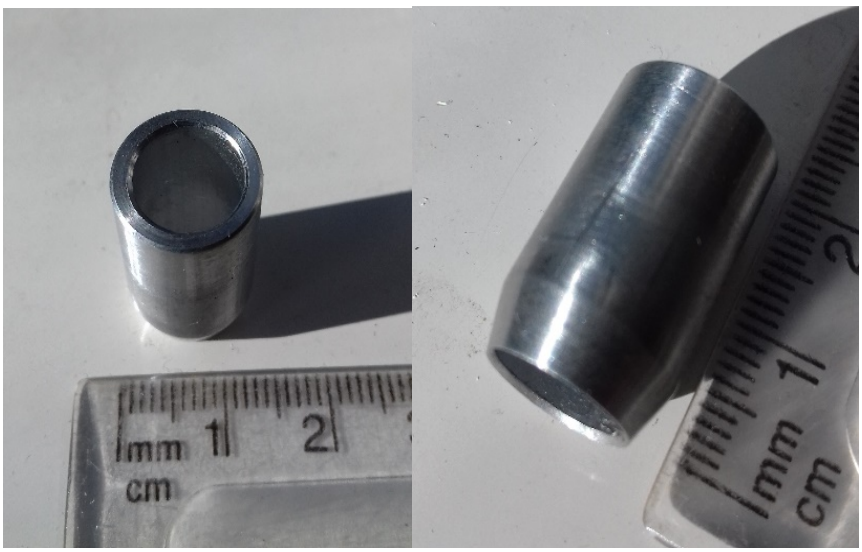

Figure A3.2: *Aluminium core (ID 10 mm and height 20 mm) used for soil sampling for neutron tomography.*

Figure A3.3: *Arrangement of three randomly chose soil sample in a cylindrical aluminium sample holder for the scanning.*

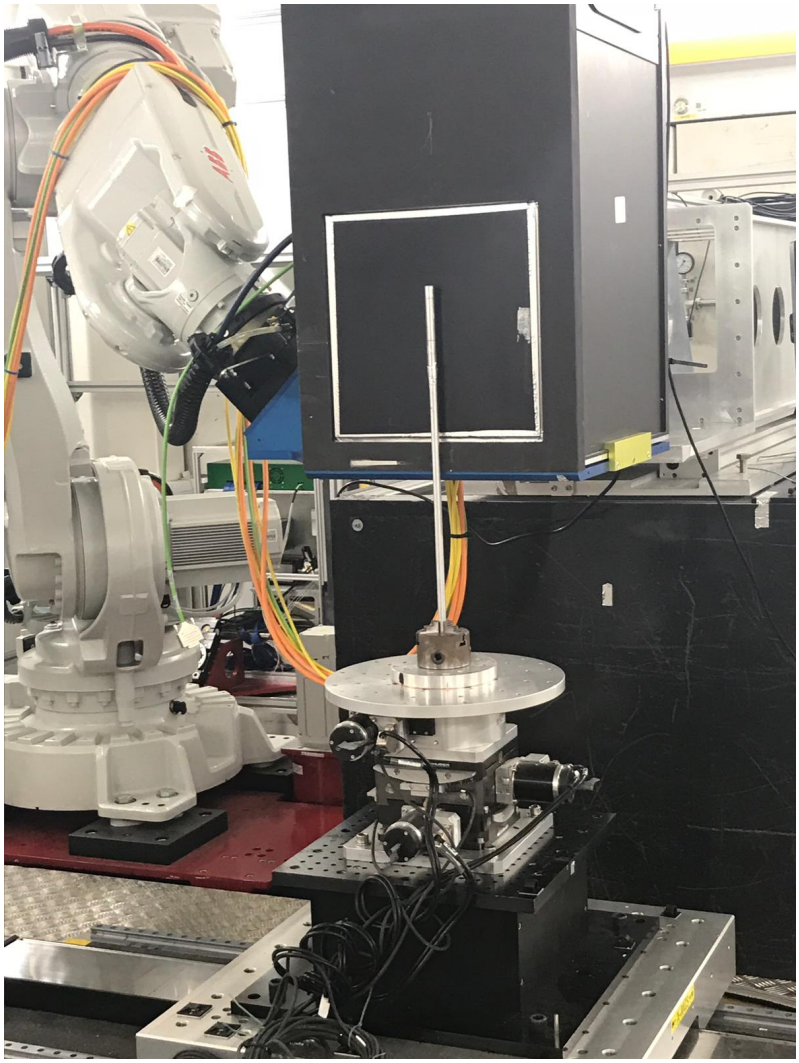

Figure A3.4: *Samples set up at IMAT for scanning.*

Genie python script to scan 10 mm diameter soil cores:

```
def  CMOS_Zyla_RB1820412_AndyGregory():
        #Prototipe function to perform multiple radiographyes, Author TM, 08/10/2017
        # CMOSradio(image_type, n_radio, expo_time, x, y, z, rot, RBnumber, runno,
ctitle, data_type)
        # image_type = 0 --> dark field       image_type = 1 --> radiography
        # n_radio --> number of radiographies
        # expo_time --> exposition time for each radiography
        # x, y, z --> SPS coordinates
        # rot --> position of the rotation stage
        # RBnumber --> assigned RB number of the experiment
        # runno --> run number of the experiment. It is automatically get from the DAE.
Do not need to modify !!!
        # ctitle --> title of the experiment
        # data_type --> type of data, for example "sample" or "open beam" or "dark"
        # CMOSradio(image_type, n_radio, expo_time, x, y, z, rot, RBnumber, runno,
ctitle, data_type)
        #Disable fifo
        #os.system(r"c:\users\spudulike\fifo_off.bat")
        #Open Fast Shutter
        cset("ATTN_OPEN", 1)
        #Run number of the experiment. It is automatically get from the DAE. Do not need
to modify !!!
        runno = get_runnumber()
#       PH40
#  jaws_set(40,80)
#  default choppers
        # #start IMAT instrument (get IMAT ready)
        begin(paused=True)
# #  Alignment
        # #Alignment Set 1 (lower)
        # CMOS_Zyla_radio_log(1, 1, 10, 4000, 450.0, -13.0, -199.0, 0.0, "RB1820412",
runno, "Set_28_30_31_60um", "Alignment")
        # #Alignment Set 2 (upper)
        # CMOS_Zyla_radio_log(1, 1, 10, 4000, 450.0, -13.0, -149.5, 0.0, "RB1820412",
runno, "Set_25_26_27_60um", "Alignment")
# #  Tomo Set 1 (lower)
        cset(x=300); waitfor_move();
        cset(y=300); waitfor_move();
        # # # Flat Field before tomography with log file
        # # # CMOS_Zyla_radio_log(image_type, n_radio, expo_time, monitor_thresh, x,
y, z, rot, RBnum, runno, ctitle, data_type)
        CMOS_Zyla_radio_log(1, 20, 30, 4000, 300.0, 300.0, -199.0, 0.0, "RB1820412",
runno, "Set_28_30_31_60um", "Flat_Before")
        cset(y=-13.0); waitfor_move();
        cset(x=450.0); waitfor_move();
        # # # Tomography bottom with log file
        # # # CMOS_Zyla_tomo_log(image_type, n_radio, expo_time,  monitor_thresh, x,
y, z, start_angle, stop_angle, step_angle, RBnum, runno, ctitle, data_type)
        CMOS_Zyla_tomo_log(1, 1, 30, 4000, 450.0, -13.0, -199.0, 0.0, 360.0,
0.66298,"RB1820412", runno, "Set_28_30_31_60um", "Tomo")
        # # Tomography High res with log file - 180 deg projection
```

```
        # # CMOS_Zyla_radio_log(image_type, n_radio, expo_time, monitor_thresh, x, y,
z, rot, RBnum, runno, ctitle, data_type)
        CMOS_Zyla_radio_log(1, 1, 30, 4000, 450.0, -13.0, -199.0, 180.0, "RB1820412",
runno, "Set_28_30_31_60um", "180deg")
        # cset(x=300); waitfor_move();
        # cset(y=300); waitfor_move();
        # # # # Flat Field after tomography with log file
        # # # # CMOS_Zyla_radio_log(image_type, n_radio, expo_time, monitor_thresh,
x, y, z, rot, RBnum, runno, ctitle, data_type)
        # CMOS_Zyla_radio_log(1, 20, 30, 4000, 300.0, 300.0, -199.0, 0.0, "RB1820412",
runno, "Set_28_30_31_60um", "Flat_After")
# #  Tomo Set 2 (upper)
        # cset(y=-13.0); waitfor_move();
        # cset(x=450.0); waitfor_move();
        # # # # Tomography bottom with log file
        # # # # CMOS_Zyla_tomo_log(image_type, n_radio, expo_time,  monitor_thresh,
x, y, z, start_angle, stop_angle, step_angle, RBnum, runno, ctitle, data_type)
        # CMOS_Zyla_tomo_log(1, 1, 30, 4000, 450.0, -13.0, -149.5, 0.0, 360.0,
0.66298,"RB1820412", runno, "Set_25_26_27_60um", "Tomo")
        # # # # Tomography High res with log file - 180 deg projection
        # # # # CMOS_Zyla_radio_log(image_type, n_radio, expo_time, monitor_thresh,
x, y, z, rot, RBnum, runno, ctitle, data_type)
        # CMOS_Zyla_radio_log(1, 1, 30, 4000, 450.0, -13.0, -149.5, 180.0,
"RB1820412", runno, "Set_25_26_27_60um", "180deg")
        # cset(x=300); waitfor_move();
        # cset(y=300); waitfor_move();
        # # # # Flat Field after tomography with log file
        # # # # CMOS_Zyla_radio_log(image_type, n_radio, expo_time, monitor_thresh,
x, y, z, rot, RBnum, runno, ctitle, data_type)
        # CMOS_Zyla_radio_log(1, 20, 30, 4000, 300.0, 300.0, -149.5, 0.0, "RB1820412",
runno, "Set_25_26_27_60um", "Flat_After")
# #  Dark
        # Dark
        # CMOS_Zyla_radio_log(0, 20, 30, 4000, 300.0, 300.0, -149.5, 0.0, "RB1820412",
runno, "Set_25_26_27_60um", "Activation_After")
        # CMOS_Zyla_radio_log(0, 20, 30, 4000, 300.0, 300.0, -149.5, 0.0, "RB1820412",
runno, "Set_25_26_27_60um", "Dark_After")
        cset("ATTN_OPEN", 0)
        end()
```

Results obtained:

Neutron transmission through soil samples is shown in Table A 3.1 and Figure A 3.4

represents an example of 2D view of scanned soil samples.

Table A 3.1: Neutron transmission data (mean value) with some selected properties of soil

Site	Treatment	SOC, g/100g	Air dry water content, g/100g	Density (estimated), g/cc	Mean Neutron Transmission (151*151 pixel) for 200 slices of image
Broadbalk	Nil	0.904	1.105	1.226	31355
	PKMg	0.971	0.989	1.235	34998
	FYM	2.978	1.308	1.034	23788
	N1 (P)KMg	1.089	1.098	1.137	39120
	N2 (P)KMg	1.17	1.122	1.137	23499
	N3 (P)KMg	1.227	1.037	1.143	36940
	N4 (P)KMg	1.289	1.252	1.170	28596
	N5 (P)KMg	1.148	0.870	1.278	27500
	N6 (P)KMg	1.284	0.891	1.228	31688
Hoosfield	(FYM) 1852-71	1.454	1.475	1.434	23373
	FYM 1852-	3.650	1.337	1.041	31890
	FYM 2001-	2.181	1.051	1.124	25341
	N(P)K(Mg)	0.991	0.874	1.177	31039

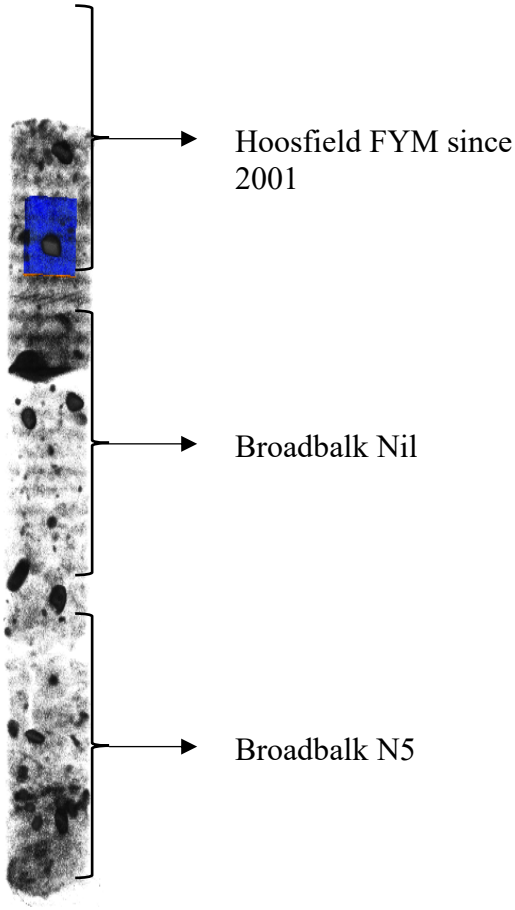

Figure A3.4: *2D view of three soil samples obtained from neutron tomography.*